The University of Maine
DigitalCommons@UMaine

Electronic Theses and Dissertations | Fogler Library

2003

Fatigue Behavior of FRP-Reinforced Douglas-Fir Glued Laminated Bridge Girders

Matthew Ritchie
University of Maine - Main

Follow this and additional works at: http://digitalcommons.library.umaine.edu/etd

Part of the Civil and Environmental Engineering Commons

Recommended Citation
Ritchie, Matthew, "Fatigue Behavior of FRP-Reinforced Douglas-Fir Glued Laminated Bridge Girders" (2003). *Electronic Theses and Dissertations*. 124.
http://digitalcommons.library.umaine.edu/etd/124

This Open-Access Thesis is brought to you for free and open access by DigitalCommons@UMaine. It has been accepted for inclusion in Electronic Theses and Dissertations by an authorized administrator of DigitalCommons@UMaine.

FATIGUE BEHAVIOR OF FRP-REINFORCED DOUGLAS-FIR GLUED LAMINATED BRIDGE GIRDERS

By

Matthew C. Richie

B.S. University of Maine, 2001

A THESIS

Submitted in Partial Fulfillment of the

Requirements for the Degree of

Master of Science

(in Civil Engineering)

The Graduate School

The University of Maine

December, 2003

Advisory Committee:

William Davids, Assistant Professor of Civil and Environmental Engineering, Advisor

Eric Landis, Associate Professor of Civil and Environmental Engineering

Roberto Lopez-Anido, Assistant Professor of Civil and Environmental Engineering

FATIGUE BEHAVIOR OF FRP-REINFORCED DOUGLAS-FIR GLUED LAMINATED BRIDGE GIRDERS

By Matthew C. Richie

Thesis Advisor: Dr. William Davids

An Abstract of the Thesis Presented
in Partial Fulfillment of the Requirements for the
Degree of Master of Science
(in Civil Engineering)
December, 2003

The use of composites in engineered wood products has recently led to the use of fiber-reinforced polymers (FRP) as a reinforcing for glued-laminated (glulam) beams. Bridge girders are among the more common applications of FRP-reinforced glulam beams and therefore the beam is subject to millions of load cycles as well as moisture fluctuations. Significant flexural strength can be gained through the use of such reinforcing, however, the behavior of the wood composite when subject to repeated load cycles and hygrothermal effects is not well understood.

In this study, eighteen glulam beams were reinforced in tension with 1.93% E-glass/epoxy reinforcing (defined as the volume of reinforcing fiber divided by the volume of wood) and tested in flexural fatigue at stress levels corresponding to $1.0F_b$ and $1.3F_b$, where F_b is the allowable flexural capacity. Both full length and partial length reinforced specimens were tested. The FRP sheet was terminated at the theoretical cut off point (or the point at which the reinforcing is no longer needed to sustain the applied loads) with

the partial length reinforcing and was explored with and without end restraints on the reinforcing. Unrestrained terminations were beveled to alleviate peeling stresses while restrained terminations were confined by a steel plate and lag screws.

Fatigue testing of all specimens cycled the beams in four-point bending for a total of two million cycles with static bending tests performed periodically to track changes in stiffness. Specimens were then broken in static bending to determine residual strength. Loading at $1.0F_b$ fatigued the specimens at a stress ratio of R=0.333 while loading at $1.3F_b$ produced a stress ratio of R=0.255. Load heads were spaced to produce flexural stress-to-shear stress ratios consistent with those seen by typical in-service timber bridge girders. However, the flexural capacity of the reinforced beams was over-estimated due to lower than expected lamstock properties and the use of a transformed section modulus where the wood section modulus was required. The cumulative effect of this resulted in a conservative testing program where the specimens fatigued at $1.0F_b$ were actually stressed to $1.52F_b$ and the specimens fatigued at $1.3F_b$ were actually stressed at $1.98F_b$.

The results of these tests showed that the full length reinforced beams fatigued at $1.0F_b$ were not prone to fatigue failures. At the higher stress level of $1.3F_b$, specimens failed prematurely and exhibited fatigue failures causing bending stiffness losses. The results also showed that with adequate confinement of the FRP terminations, partial length reinforcing may be structurally feasible. Beams with unconfined terminations fared poorly in fatigue.

In addition, the effects of hygrothermal stresses in combination with mechanical fatigue are of particular concern. To better understand the effect, both finite difference and finite element modeling was done to quantify the stresses due to hygrothermal

fluctuations that are typical over the life span of a timber bridge girder. A kiln schedule was designed to subject beams to extreme high and low moisture contents to reproduce the cumulative damage occurring over a 50 year life span of a timber bridge girder in a New England environment.

ACKNOWLEDGEMENTS

The author would like to express his sincere gratitude to the following people: Dr. Bill Davids for his help and guidance during the past two years; all of the staff at the Advanced Engineered Wood Composites Center whose assistance was much appreciated; the author's family; and Julie Altenhoff for her love and support.

This research was funded by the Federal Highway Administration under the direction of Sheila Duwadi (FHWA Contract No. DTFH61-99-C-00064). The author is grateful for this financial support.

TABLE OF CONTENTS

ACKNOWLEDGEMENTS ii

LIST OF TABLES ix

LIST OF FIGURES x

Chapter

1. INTRODUCTION 1

1.1 Background 1

1.2 Objective 3

1.3 Scope of Work 3

1.4 Organization 4

2. LITERATURE REVIEW 6

2.1 Introduction 6

2.2 FRP-Glulam Technology 7

2.3 Durability Issues 10

2.3.1 Background on Fatigue Testing 11

2.3.2 Mechanical Fatigue of Wood and FRP-Reinforced Glulam Beams 12

2.3.2.1 Full Length Reinforcing 14

2.3.2.2 Partial Length Reinforcing 15

2.3.3 Hygrothermal Effects in FRP-Reinforced Glulam Beams 15

3. DESIGN OF MECHANICAL FATIGUE TESTING PROGRAM 18

3.1 Introduction 18

3.2 Specimen Properties 18

3.2.1 Unreinforced Glulam Beams 18

3.2.2 FRP-Reinforced Glulam Beams 20

3.2.3 Gordon Composites FRP 21

3.3 Fatigue Testing Program 22

3.3.1 Flexural Stress Calculations 23

3.3.2 Development of Loads and Load Head Positions 23

3.4 Testing Facility 27

3.5 Equipment 27

3.5.1 Testing Frame and Actuators 28

3.5.2 End Supports and Lateral Bracing 28

3.6 Data Acquisition 29

3.6.1 Instrumentation of Specimen 30

3.6.2 LabVIEW Program 31

3.7 Test Protocol 31

3.7.1 Fatigue Cycling Frequency 32

3.7.2 Periodic Static Tests 34

3.8 Summary 34

4. CONSTRUCTION OF FRP-REINFORCED GLUED LAMINATED SPECIMENS 36

4.1 Introduction 36

4.2 Fabrication of FRP-Reinforced Beams 36

4.2.1 HMR Pretreatment 37

4.2.2 FPL 1A Epoxy Adhesive 38

4.2.3 FRP Preparation 39

4.2.4 Cold Press 40

4.2.5 Treatment of Defects 41

4.2.6 Storage of Specimens 41

4.3 Full-Length Reinforced Specimens 42

4.4 Partial Length Reinforcing 42

4.4.1 Partially Reinforced Specimens, Unrestrained Terminations 43

4.4.2 Partially Reinforced Specimens, Mechanically Restrained Terminations 44

4.5 Summary 46

5. MECHANICAL FATIGUE TESTING OF FRP-REINFORCED GLUED LAMINATED BRIDGE GIRDERS 48

5.1 Introduction 48

5.2 Fatigue Testing Program 50

5.3 Fatigue Testing at 1.0 F_b 52

5.3.1 Fully Reinforced Specimens, 1.0 F_b 52

5.3.1.1 Specimens S1, S2, and S3 (Fully Reinforced, 1.0 F_b) 53

5.3.1.2 Specimens S4, S5 and S6 (Fully Reinforced, 1.0 F_b) 56

5.3.2 Partially Reinforced Specimens, 1.0 F_b 58

5.3.2.1 Specimens S7, S8, and S9 (Partially Reinforced, 1.0 F_b) 59

5.3.2.2 Specimens S10, S11, and S12 (Partially Reinforced, 1.0 F_b) 63

5.4 Fatigue Testing at 1.3 F_b 68

5.4.1 Fully Reinforced Specimens, 1.3 F_b 68

5.4.1.1 Specimens S13, S14 and S15 (Fully Reinforced, 1.3 F_b) 68

5.4.2 Partially Reinforced Specimens, 1.3 F_b 71

5.4.2.1 Specimens S16, S17 and S18 (Partially Reinforced/Restrained, 1.3 F_b) 71

5.5 Summary of Fatigue Testing Results 75

6. EVALUATING THE EFFECTS OF HYGROTHERMAL FLUCTUATIONS 78

6.1 Introduction 78

6.2 Evaluating In-Service Hygrothermal Conditions 79

6.2.1 One-Dimensional Moisture Transport Model 79

6.2.2 Annual Weather Data 81

6.2.3 Convergence of Diffusion Model 83

6.2.3.1 Convergence for the Number of Cross-Sectional Divisions 83

6.2.3.2 Convergence for the Number of Time Steps 85

6.2.3.3 Initial Conditions 86

6.2.3.4 Boundary Conditions 87

6.2.3.5 Establishing an Equilibrium Point for In-Service Beams 87

6.3 Kiln Conditioning Limits 90

6.4 ANSYS Modeling 92

6.4.1 Model Properties and Assumptions 93

6.4.2 Finite Element Modeling Procedure 94

6.4.3 Results of ANSYS Finite Element Model 96

6.5 Defining Stress History 101

6.5.1 Stress History Method 1 102

6.5.2 Stress History Method 2 103

6.5.3 Stress History Method 3 103

6.6 Kiln Schedule 105

6.7 Summary 106

7. SUMMARY AND CONCLUSIONS 108

7.1 Introduction 108

7.2 Summary of Testing Program 108

7.3 Summary of Specimen Construction 109

7.4 Summary of Mechanical Fatigue Testing 110

7.5 Summary of Hygrothermal Fatigue Evaluation 112

7.6 Conclusions 113

7.7 Design Recommendations 114

7.8 Recommendations for Future Work 115

REFERENCES 117

APPENDICES 124

Appendix A - Data Sheets from Periodic Static Tests 124

Appendix B - Calculations 130

Appendix C - Matlab Code for 1D Moisture Diffusion Model 151

BIOGRAPHY OF THE AUTHOR 153

LIST OF TABLES

Table 3.1 Allowable Flexural Stress (F_b) of reinforced and unreinforced glulam beams 20

Table 3.2 Gordon Composites FRP material properties 21

Table 3.3 Typical dead load to live load ratios 25

Table 3.4 Ratios of applied stress to design stress 26

Table 3.5 Calculated values for load head spacing 27

Table 3.6 Cycling plan for reinforced specimens 32

Table 4.1 Formula for HMR coupling agent 38

Table 4.2 Formula for FPL 1A epoxy adhesive 39

Table 5.1 Summary of the results of the mechanical fatigue tests 49

Table 6.1 Temperature, RH and EMC data for Caribou, Maine (Conway, 1990) 82

Table 6.2 Model Properties for ANSYS finite element model..... 93

Table A.1 Data sheets for specimens S1-18..... 124

LIST OF FIGURES

Figure 3.1 Typical cross section of an unreinforced glulam beam specimen..... 19

Figure 3.2 Cross section of the timber bridge used in the design example..... 25

Figure 3.3 A typical test specimen in the testing frame..... 29

Figure 3.4 Top view of beam showing the instrumentation scheme of a typical specimen..... 30

Figure 3.5 Load cell and actuator load versus time for a frequency of 2.0 Hz 33

Figure 4.1 A 6700 mm Beam in cold press..... 40

Figure 4.2 The left side of the picture shows a knot, right side shows the same knot filled with epoxy..... 41

Figure 4.3 Typical partially reinforced beam 43

Figure 4.4 Beveled end detail for partial length reinforcing..... 44

Figure 4.5 Mechanical restraint used to confine the FRP terminations of partial length reinforcing, shown here on an inverted beam..... 45

Figure 4.6 Relationship between averaged torque and pressure for ten lag screws..... 46

Figure 5.1 A 6,700 mm specimen in the testing apparatus..... 50

Figure 5.2 Stiffness vs Time plot for specimens S1, S2 and S3..... 54

Figure 5.3 Load vs Displacement plot for specimens S1, S2 and S3..... 54

Figure 5.4 Failure at a finger joint near midspan in specimen S1..... 55

Figure 5.5 Stiffness vs Time plot for specimens S4, S5 and S6..... 57

Figure 5.6 Load vs Displacement plot for specimens S4, S5 and S6..... 57

Figure 5.7 View shows typical end restraint for partially-reinforced specimens 59

Figure 5.8 Stiffness vs Time plot for specimens S7, S8 and S9 60

Figure 5.9 Debonding failure of Specimen S7 during fatigue 61

Figure 5.10 Compression failure in specimen S9 62

Figure 5.11 Load vs Displacement plot for specimen S9 63

Figure 5.12 Stiffness vs Time plot for specimens S10, S11 and S12 64

Figure 5.13 Compression failure in top lamination of specimen S10 65

Figure 5.14 Load vs Displacement plot for specimens S10, S11 and S12 65

Figure 5.15 Shear failure in specimen S11 67

Figure 5.16 Shear failure in specimen S13 (shear crack highlighted by two horizontal marker lines) 69

Figure 5.17 Stiffness vs Time plot for specimens S14 and S15 70

Figure 5.18 (a) Local tension failure near midspan at 953845 cycles. (b) The same local tension failure after ultimate failure of specimen at 953845 cycles 72

Figure 5.19 Stiffness vs Time plot for specimen S16 73

Figure 5.20 Specimen S17, post-failure 74

Figure 5.21 Block shear failure of termination of partial length reinforcing 75

Figure 6.1 (a) Plot of Diffusion Coefficient for Moisture Content range of 0-100% (b) Plot of Diffusion Coefficient for Moisture Content range of 5-15% 81

Figure 6.2 Plot of annual EMC fluctuation 83

Figure 6.3 Convergence of cross-sectional divisions, Δx 85

Figure 6.4 Convergence of time step value, time_step 86

Figure 6.5 Moisture Profile for month of January after 1, 2, 4, 5, and 8 years 88

Figure 6.6 Plot of moisture profile for 12 months data after initial 4 years 89

Figure 6.7 Extreme kiln limits overlaid on in-service high and low conditions 92

Figure 6.8 Mesh Convergence for Hygrothermal Finite Element Model 95

Figure 6.9 Mesh used for finite element model. The darker color on the bottom represents FRP, the lighter color represents the wood. Close-up of bottom quarter of cross section 96

Figure 6.10 (a) Tensile stresses for annual high moisture profile, in-service conditions. (b) Tensile stresses for cyclic high moisture profile, kiln conditions Close-up of bottom left corner of cross section 97

Figure 6.11 (a) XY-shear stresses for annual high moisture profile, in-service Conditions. (b) XY-shear stresses for cyclic high moisture profile, kiln conditions 98

Figure 6.12 (a) Tensile stresses for annual low moisture profile, in-service conditions. (b) Tensile stresses for cyclic low moisture profile, kiln conditions Close-up of bottom left corner of cross section 99

Figure 6.13 (a) XY-shear stresses for annual low moisture profile, in-service Conditions. (b) XY-shear stresses for cyclic low moisture profile, kiln conditions 100

Figure B.1 Specimen with boundary conditions 132

Figure B.2 Transformed section 137

Chapter 1

INTRODUCTION

1.1 Background

In spite of the many improvements and advancements in concrete and steel construction, timber remains a popular construction material because of its relatively low cost, ease of construction, and low maintenance after construction. A significant portion of the timber construction market belongs to the glued-laminated (glulam) beam industry. Glulam beams are manufactured from smaller pieces of wood, called lamina, which are glued and laminated together to form larger dimension beams. The main advantage of a glulam beam is that defects in the laminations are dispersed throughout the beam, which significantly lessens their effect on beam strength. By laminating the thinner pieces, the one large defect that might weaken a piece of solid sawn lumber will be cut up and spread out over the entire beam in the form of smaller defects. Because of this laminating effect, the strength of glulam beams can be more than twice as high as conventional timber strength values. Other advantages of glulam include the availability in large dimensions, dimensional stability, its high strength-to-weight ratio, chemical resistance because it does not rust or corrode and fire resistance due to a slow char rate.

One method of improving the strength of a glulam beam is to reinforce the beam with fiber reinforced polymer (FRP) to decrease member size and enable the use of lower grade wood. A relatively small amount of FRP is needed (usually 1%-3% of the beam volume for various types of FRP) when reinforcing for tension capacity and this fiber reinforcing can be easily bonded to the wood to provide a significant strength gain. The

fibers are typically unidirectional, and help make efficient use of materials since the required depth of the beam will be much shallower with the addition of reinforcing. Taking this concept one step further, higher grade wood can be strategically located to provide extra capacity in only the places where it is needed, while lower grade wood can be substituted in areas where the reinforcing provides the strength.

Although the reinforced glulam holds much potential, there is still little known about how this innovative material will perform in-service under repetitive loading. One issue concerning the applications of reinforced glulam beams is their behavior in fatigue. This is especially true for bridge structures, which are subjected to millions of live load cycles over their design life. In structural design, glulam strength is generally assumed to be unaffected by fatigue. However, by laminating FRP to a glulam, the allowable flexural capacity is greatly increased but the allowable shear capacity remains the same as the unreinforced beam. Unreinforced glulam bridge girders are unintentionally over-designed in shear in order to meet flexural capacity requirements. In contrast, an FRP-wood composite beam can have both the shear and tensile stresses very close to allowable capacity under live load conditions. Shear failures due to fatigue may therefore be a concern, since under repeated loading, the fatigue performance of an FRP-reinforced glulam under these conditions is unknown.

Another area of concern is the fatigue performance of the wood-FRP bond line. This is especially critical when partial-length FRP reinforcing is used, i.e. the FRP is terminated somewhere in the clear span. A third area of concern is the behavior of the wood and FRP under hygrothermal fluctuations. The two materials react very differently to changes in moisture content. The wood shrinks and swells with respect to the changes

in ambient moisture content. FRP, on the other hand, exhibits relatively little shrinkage or swelling, if any at all. A glulam beam exposed to exterior conditions will exhibit cyclical shrinkage and swelling annually with the changing weather patterns. This will induce stresses on the bond line between the FRP and wood. The magnitude of these stresses and how they will affect the performance of the reinforcing is of particular concern. These stresses pose the potential to cause debonding over time and separate the FRP from the wood, introducing delaminations. Obviously, this problem is coupled with the fatigue performance of the wood-FRP bond line, and warrants investigation.

1.2 Objective

The objective of this research is to evaluate the fatigue durability of FRP-reinforced glued laminated bridge girders and help determine the effectiveness of FRP as a reinforcing material. Preliminary research on this matter had been conducted which provided a good basis to form a plan of action for conducting the fatigue tests (Gamache 2001).

1.3 Scope of Work

The focus of this research is centered on the fatigue behavior of structural-scale FRP-reinforced bridge girders. The research focused on mechanical fatigue due to vehicular loading as well as the combined effect of stress cycling due to hygrothermal fatigue from environmental fluctuations in temperature and relative humidity. Effects of preservative treatment were not included in this research and the specimens used were untreated.

To explore the mechanical fatigue behavior of the FRP-reinforced girder, a program was developed to repeatedly load the specimens in a configuration that closely replicates the stresses due to a design live and dead loads on a bridge girder. Eighteen glulam specimens reinforced with 1.93% E-glass FRP by volume were fatigued at two different stress levels and the results analyzed. The details of this portion of the research are presented in chapters 3-5.

The second portion of the research focused on developing a process to replicate the effects of hygrothermal cycling experienced by an FRP-reinforced glulam bridge girder over its design life. This required both finite-difference and finite-element modeling to produce moisture movements and resultant shrinkage- and swelling-induced stresses at the wood-FRP bond line. A quantitative stress history parameter is proposed, and a kiln schedule was developed to reproduce the cumulative damage caused by in-service hygrothermal fluctuations over a 50 year girder life span in a period of 54 days.

1.4 Organization

The remainder of this thesis consists of six chapters. Chapter 2 is a literature review discussing research and publications relevant to the topic of research. Chapter 3 presents the design and details of the testing program developed for mechanical fatigue. Chapter 4 discusses the construction of the specimens and Chapter 5 presents the results of the mechanical fatigue tests. Chapter 6 details the development of the hygrothermal weathering program and the kiln schedule for evaluation of hygrothermal fatigue. Finally, Chapter 7, gives a summary of the work completed, conclusions and recommendations for future work. References used in this study are listed at the end of

Chapter 7. Supporting data and calculations are presented in the three appendices at the end of the thesis.

Chapter 2

LITERATURE REVIEW

2.1 Introduction

The increasingly scarce supply of high-grade structural wood and competition from steel and concrete has forced the wood industry to engineer more marketable wood products (MDA 2003). The many forms of engineered wood products include wood I-joist, oriented strand board, plywood, rim board, parallel strand lumber, laminated veneer lumber and glued laminated lumber and are used in many aspects of construction (APA 2003). In recent years, efforts have been made to improve upon these products through the use of non-wood materials.

From these efforts, a new field of study has emerged which focuses on wood composites, which are wood products which benefit in some way from non-wood components. Since the early 1990s there has been significant interest in developing wood composites. Research on development of these wood composites has focused on making a product with more desirable properties than those of either material alone, including increased structural properties, reduced labor costs or more efficient use of materials (Youngquist 1995).

Most recently, developments in the engineered wood products sector include the use of fiber reinforced polymers (FRP) composites. In structural applications, FRP typically refers to composites made of glass, carbon, graphite, and aramid. FRP fiber orientations come in a variety of configurations including continuous rovings, woven rovings, textiles and chopped stand mats. Some recent innovations in FRP-wood hybrid

composites include FRP-overlaid plywood (APA 1998), FRP-wood guardrails and rail posts (Dickson 1996), FRP-composite wood piles (Lopez-Anido et al 2003), FRP-glulam ocean piers (Coger 1997; Dagher and Bragdon 2001), FRP-glulam panels for bridge decks (Lopez-Anido and Xu 2002), and also FRP-glulam bridge girders (Dagher and Lindyberg 2003).

The specific focus of this chapter is to present an overview of some of the past research pertaining to reinforced glulam beams and the durability issues surrounding them. The glulam industry has been operating on a commercial basis since the early 1900s but has just recently expanded to include benefits of composite technology. Research with glulam technology has recently focused on improving strength capacity through the use of composites. Composite reinforcing materials, specifically FRP, have shown promise for significantly strengthening glulam and making it a more competitive product.

Mention must be made here that the literature review builds on that done by Christopher Gamache in his MS thesis (Gamache 2001).

2.2 FRP-Glulam Technology

A glulam beam is a structural component constructed from individual lengths of lumber, called laminations, that are bonded together to form deeper members. The individual lengths are typically finger-jointed to form longer members. The glulam beam excels over solid-sawn lumber by making possible longer, deeper and wider members with cambered, curved and tapered configurations not possible with solid sawn lumber (APA 2003). The beams are also engineered with efficient use of wood by organizing

lower grade laminations in areas of lower stress (APA 1998) where the strength of the higher quality lumber is not needed.

One of the most interesting advantages of using glulam comes from a case study performed by Petersen and Solberg (2002). The study compared the environmental benefits of using glulam over structural steel in the construction of a new airport outside of Oslo, Norway Taking into account the differences in the manufacturing process and construction with the two materials, the report showed that, depending on the method of waste handling, the greenhouse gas (GHG) emissions are 6-12 times as high as with steel than glulam. Converting the avoided GHG emissions into dollar amounts using the price of the CO_2-tax on gasoline in Norway, glulam was found to be the economical choice when the initial cost of glulam was no more than 1-6% more expensive than steel.

Perhaps the most important advantage with glulam, though, is the increased strength over solid sawn lumber due to the laminating effect. Serrano (1997) described this laminating effect as stemming from a dispersion of defects as well a reinforcing of defects. When cut into laminates, the large defects present in a piece of solid sawn lumber become smaller defects that are dispersed throughout the glulam, lessening their effect. The clear wood in adjacent laminations then reinforces the surrounding defects by redistributing the induced stresses. The combined effect is an increase in the capacity of the cross section. The outer laminations on the top and bottom, however, benefit from this defect-reinforcing phenomenon on only one side (Falk and Colling 1995). Building on this reinforcing idea, composites have most recently been used as a reinforcement material for engineered wood products.

Galloway et al (1996a) noted that in a glulam beam tested in static bending, the ultimate strength becomes more dependent on tensile strength, rather than compressive strength, as the grade of wood decreases. Martinez and Calil (2002) state that glulam beams are most prone to failure modes in the form tensile ruptures in the outer-most tensile lamination. They also noted that these ruptures initiated at a finger joint or defect, which is also consistent with findings published by Dagher and Lindyberg (2003) and Romani and Blaß (2001). Therefore, the use of FRP reinforcing would be beneficial in the tensile stress region of the beam. In this case, not only would the reinforcing act to increase the ultimate strength by providing added tensile strength but would also act to reinforce defects present in the critical tensile region.

Using an FRP reinforcing for structural wood components has been studied by many researchers (Plevris and Triantafillou 1992; Triantafillou and Desovic 1992; Kimball 1995; Galloway 1996a; Galloway 1996b; Davids 2000; Dagher et al 1998; Romani and Blaß 2001; Dagher and Bragdon 2002; Lopez-Anido and Xu 2002; Dagher and Lindyberg 2003; Lopez-Anido Michael and Sanford 2003). Commonly used reinforcing materials include E-glass (Dagher and Lindyberg 2003), Kevlar/aramid (Galloway et al 1996a), and carbon fiber (Meierhofer 1995). FRP-glulam products are even being produced on a commercial basis by companies such as American Laminators (American Laminators 2003).

The most notable advantage of reinforced glulam beams is the gain in flexural strength from tensile reinforcing. Previous testing has shown that flexural strength can be increased by 50-100% over the unreinforced strength with the use of tensile reinforcing (Plevris and Triantafillou 1992; Kimball 1995; Dagher et al 1998). The use of FRP

reinforcing can also decrease variation in modulus of elasticity and strength by reducing the effect of defects (Lindyberg 2000).

In addition to the increased strength and decreased material property variability, other notable advantages have been documented. Tingley et al (1996) cited several advantages noted in the case of a FRP-reinforced glulam bridge built over the Clallam River in near Sekiu, WA. The beams used in this bridge utilized lower grade wood which also lead to reduced costs, lower treatment costs, and decreased dead weight for easier construction. Dagher et al (1996) also found that FRP tensile reinforcing can be used to produce higher strength glulam beams using under utilized species such as Eastern Hemlock.

2.3 Durability Issues

With all the desirable advantages pushing reinforced glulam technology to the forefront, several issues restrain it from more widespread use, the most prominent of which is durability. The long term durability of the product raises many concerns (Dagher et al 1996). The FRP and the wood have very different material properties, but are dependent on a strong bond between two for full composite action. The effects of repeated loading and fluctuating environmental conditions on the wood-FRP bond line are not well understood.

Fatigue, in reference to structural applications, is a term used to describe the permanent changes that occur in a material as result of fluctuating or cyclic applied stress and strain conditions (ASTM 1987). Mechanical fatigue, combined with the effects of temperature and moisture fluctuations could lead to wood-FRP bond line failures. The

long term durability of structural components is typically determined from mathematical models that are derived from long-term testing (Liu, Zahn and Schaffer 1994), thus to develop accurate models to predict life spans, fatigue testing of FRP-glulam beams must be performed.

2.3.1 Background on Fatigue Testing

Fatigue testing is designed to determine the maximum number of load cycles a component can sustain under a given stress before failing. However, changes in material properties in specimens are rarely noted during fatigue testing and therefore failures often occur suddenly without warning. Fatigue properties cannot be reliably determined from other mechanical properties and can only be quantified through direct testing. Furthermore, it is commonly accepted that full-scale testing is necessary to ensure accurate results and even then results can vary significantly (Bodig and Jayne 1982).

Fatigue testing of wood and other materials is performed under a number of conditions. With the advent of computers and feedback loops, more sophisticated and accurate testing is now available and most fatigue testing is done under constant load amplitude. Equipment limitations required that early fatigue tests be run at constant displacement amplitude where creep and fatigue would reduce the applied stresses over time (Tsai and Ansell 1990).

The type of loading is usually defined as either "low-cycle-fatigue" or "high-cycle-fatigue". In low-cycle-fatigue, higher loads are applied for number of load cycles typically between 10-100,000 cycles. High-cycle-fatigue is just the opposite, characterized by lower loads over a period of greater than 100,000 cycles. The most

common method of loading in both cases is sinusoidal, however loading can be in the form of square waves, triangular waves, saw-tooth, etc. (MSC 2003).

Typical fatigue testing programs seek to establish *S-N* curves, or plots of stress, *S*, versus the logarithm of the number of cycles to failure, *N*. These curves are used to establish a fatigue limit or fatigue strength specific to a material. The fatigue limit is the maximum stress that can be applied over an infinite number of cycles and is taken as the stress at the point when the *S-N* curve becomes horizontal (Bagdahn et al 2003). Stress levels below the fatigue limit can be applied for an infinite number of cycles with no failures. The fatigue strength is the failure stress at a given number of cycles (Gere and Timoshenko 1997).

The stress ratio, or *R*, is most commonly used to characterize the type of fatigue loading. The stress ratio is defined as the ratio of the minimum applied load to the maximum applied load (Bodig and Jayne 1982). A positive *R* indicates that the loading in non-reversed, i.e. the specimen is only loaded in compression or tension. A negative stress ratio would indicate reversed loading, i.e. the specimen is loaded in compression and then tension, or vice versa, in the same cycle (Paepegem and Degrieck 2002).

2.3.2 Mechanical Fatigue of Wood and FRP-Reinforced Glulam Beams

Fatigue in wood is not a well defined parameter. With less than fifty publications on the matter from 1940-1990 (Tsai & Ansell 1990), there is an evident lack of research regarding on this matter. Tsai and Ansell (1990) call attention to the fact that other design factors such as deflection and creep tend to control design to the point where fatigue in wood is a non-issue. However, with the use of tensile reinforcing, the flexural

capacity of the glulam beam is significantly increased while the shear capacity remains unchanged from the capacity of the unreinforced section (Dagher & Lindyberg 2003). Increasing the applied flexural stress will simultaneously increase the applied shear stress. The effects of fatigue loading on beams with high shear stress is not well understood. In addition, the durability of the wood-FRP bond line is also a concern for glulams subjected to fatigue loadings.

Martinez and Calil (2003) reported that the fatigue strength of wood is largely characterized by the species and origin of the wood, the dimensions of the specimen, the temperature and moisture content, and type of loading. Chemical treatments, the bonding adhesives used, and the type of joints can also affect the fatigue performance of wooden members. Gong and Smith (2000) found that failure in wood specimens loaded cyclically parallel-to-grain were caused by kinks in the cell walls. This phenomenon was also noted by Hoffmeyer (1993) and Scurfield et al (1972).

Past research has shown conflicting finding about the fatigue properties of softwood glulam and solid sawn wood. Studies have concluded that the low material variability of laminated wood products improves fatigue performance (Marusceac and Verdes 1984), while others concluded that laminated wood does not perform better than solid sawn in under fatigue loading (Bond and Ansell 1998). Hansen (1991) stated that the species of wood plays a vital role in fatigue performance while Tsai and Ansell (1990) give a refuting opinion that species does not matter when test data is normalized by static strength.

Establishing full S-N curves can entail applying millions of fatigue cycles at a variety of stress levels, which is a long and costly process. This makes running the test at

a higher frequency desirable. The loading frequency at which the fatigue test is run also produces conflicting opinions. However, Martinez and Calil (2003) noted that the higher frequency increased the number of fatigue cycles to failure in individual horizontally finger jointed laminations. But, with metals, it has been shown that the frequency was independent of crack growth rate (Singh et al 2001) that could cause fatigue failure. Liu et al. (1994) modeled the effects of cyclic loading of wood as independent of the loading frequency. Liu and Ross (1996) reported that for Douglas Fir, for a given mean stress, fatigue life increases with a decrease in stress amplitude.

Despite the contradictions, studies have provided important insight into the fatigue behavior of wood. Lewis (1960) noted, that in his study of laminated beams, static and fatigue failure occurred exclusive of the bond line. Lewis (1962) also reported that quarter-scale bridge stringer specimens of Southern Pine and Douglas Fir loaded to 55% of the static strength survived two million fatigue cycles without failure. Elmendorf (1918) found that the fatigue strength for reversed loading of wood specimens was approximately 25% of the static strength. Tingley et al (1996) found no appreciable creep or fatigue effects with FRP-reinforced bridge girders in a bridge in Sekiu, WA after a year of traffic loading.

2.3.2.1 Full Length Reinforcing

Full length reinforced beams have been tested and shown to have benenficial properties. In-service uses have also showed promise (Tingley et al 1996; Dagher and Lindyberg 1999). The FRP reinforcing in full length reinforced beams is confined at its terminations by the supports. The force exerted by the supports and by extension of the reinforcing to regions of low moment in simply supported structures helps to reduce any

peeling stresses and other fatigue effects. Partial length reinforcing, however, does not share in this advantage.

2.3.2.2 Partial Length Reinforcing

The FRP terminations of partially reinforced beams undergo complex stress states of shear and tension which can produce delamination (Chawla 1987), and therefore a moment must be applied to counteract the peeling stresses (Cheng et al 1991). Kirlin (1996) found that thicker tensile reinforcing resulted in higher stress concentrations at the FRP terminations. Work done by Hong (2003) with FRP-wood composites has shown that single-lap shear joints, such as the detail at the partial length reinforcing termination, are prone to fatigue failures. Possible methods used to compensate for the stress concentrations include beveled terminations (AASHTO 1996) and extending the reinforcing beyond the point where it is no longer necessary (American Laminators 2003).

Other areas of related work have been done on steel plate reinforcing bonded to the soffits of concrete beams. Hamoush and Ahmad (1990) and Oehlers (1992) have published data which helps define failure modes that exist due to the peeling forces at the plate ends. Saadatmanesh and Ehsani (1990) reported that steel and FRP reinforcing display very similar behavioral characteristics with regard to flexural loading.

2.3.3 Hygrothermal Effects in FRP-Reinforced Glulam Beams

The movement of water through wood is governed by diffusion. A surface emission coefficient and a diffusion coefficient are generally held as the two factors that

characterize movement of a substance through a material (Liu and Simpson 1996). Moisture diffusion through a material with a constant diffusion coefficient is governed by the following a partial differential equation in the form:

$$\frac{\delta C}{\delta t} = D\frac{\delta^2 C}{\delta x^2} \qquad \text{Eqn 1.1}$$

In the above equation, C is the moisture content, t is time, D is the diffusion coefficient and x is the space coordinate (Siau 1996). A consideration when dealing with wetting and drying of wood is that the rate of moisture absorption in wood is always less than the rate of drying (Forest Products Laboratory 1999). This process is referred to as hysteresis (Stamn and Loughborough 1935). With FRP, behavior under fluctuating moisture conditions is very different. The moisture absorption rate is on the order of 85% of the drying rate.

A major concern involving the use of FRP-reinforced glulam beams in long term structural applications is the effects of hygrothermal stresses on the wood-FRP bond line and their interaction with mechanically-induced fatigue stress (Dagher et al 1996; Tascioglu et al 2003). Hygrothermal stresses are a direct result of a difference in coefficients of moisture expansion between the FRP reinforcing and the wood. These stresses are induced because the expansion and contraction of the wood far exceeds that of the FRP. The FRP restrains the wood from expanding and contracting along bond line and produces stress conditions that could compromise the reinforcing (Sanchez 2002). Modeling done by Gamache (2001) and Sanchez (2002) have shown that high stress conditions can occur at the outer edge of the wood-FRP interface where moisture penetration is highest.

When compared to wood, the dimensional changes in FRP with regard to moisture changes are negligible, however, composites are not completely immune to moisture. Carbon, for example is prone to moisture absorption and subsequent dilatational expansion in humid conditions (Vaddadi et al 2003). This fact does not affect the hygrothermal stresses in FRP-glulam beams and dimensional changes in the FRP are therefore ignored. The hygrothermal effects combined with long term loading, such as in the case of bridge girders, pose a threat to the durability of FRP-glulam beams and need to be better quantified.

Chapter 3

DESIGN OF MECHANICAL FATIGUE TESTING PROGRAM

3.1 Introduction

In this study, eighteen glulam beams were reinforced on their tension side with an E-glass Fiber Reinforced Plastic (FRP) and tested in fatigue to determine the fatigue durability of FRP reinforced glulam when used as bridge girders. All testing was done using hydraulic actuators to repeatedly load the specimens. This chapter discusses the facility, environmental conditions, and equipment used for this research, the material properties of the FRP-reinforced glulam specimens, and the development of the fatigue testing program. Detailed calculations of the quantities presented in this chapter are located in Appendix B. Chapter 4 describes the process of reinforcing the glulam specimens and Chapter 5 presents the results of the fatigue tests.

3.2 Specimen Properties

Material properties for the unreinforced and reinforced glulam beams and the FRP reinforcing are given in the following sections.

3.2.1 Unreinforced Glulam Beams

The specimens tested in fatigue were a combination of fully and partially reinforced 6,700 mm and 11,278 mm long Douglas-Fir glued laminated beams of a custom lay-up fabricated by Willamette Industries, Inc. based in Albany, OR. The glulam combination was made up of visually graded L1 compression laminations in the

upper twenty-five percent of the cross section and a random mix of L2/L3 laminations in the bottom seventy-five percent of the cross-section. Figure 3.1 shows the layup of the unreinforced glulam beam.

The L1 and L2/L3 laminations are grades of visually inspected wood reserved for use in glulam applications. According to the Wood Handbook (1999) published by the Forest Products Laboratory, the specific grade given to the individual lamination is characterized by maximum allowable knot size, grain slope and wane. An L1 lamination cannot have knots larger than one-quarter the width of the lamination, an L2 lamination has knots no larger than one-third the lamination width, and an L3 lamination has a maximum allowable knot size of one-half the width of the lamination. Since the multiple laminations in a glulam reduce the effects of edge knots, the locations of the knots within the lamination have no bearing on the grade.

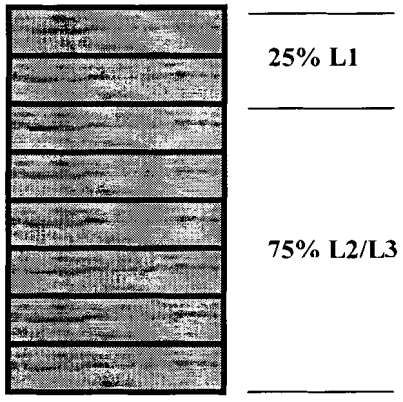

Figure 3.1 Typical cross section of an unreinforced glulam beam specimen.

In a typical unreinforced glulam beam, lower grade laminations would not be used in the tension region of the beam. In the case of reinforced glulam, the FRP provides the majority of the tensile strength, and therefore the lower grade L2/L3 is

economical on the tension side. As the tensile capacity of the beam is increased through the use of FRP, the compressive stresses in the top laminations are also increased when the beam is loaded to capacity. The L1 laminations were used in the top to provide extra compressive strength where there was no reinforcing.

3.2.2 FRP-Reinforced Glulam Beams

All of the specimens tested were reinforced with Gordon Composite, Inc. unidirectional E-glass using an epoxy adhesive. The allowable stress and modulus of rupture (MOR) of the FRP-reinforced glulam beams was predicted using the ReLAM program (Lindyberg, 2000). ReLAM is a software program that returns glulam design strengths and modulus of rupture based on the size, strength, loading characteristics and lay-up of the laminations (Lindyberg and Dagher 2000). The design strengths used to develop the testing program are given in Table 3.1 below.

Table 3.1 Allowable Flexural Stress (F_b) of reinforced and unreinforced glulam beams.

Beam Size and Type	***F_b*** **Original / Updated Lamstock Database (MPa)**	***MOR*** **Original / Updated Lamstock Database (MPa)**
6700 mm Unreinforced	10.7 / 10.3	-
6700 mm Reinforced	23.6 / 17.5	56.9 / 45.6
11278 mm Unreinforced	10.2 / 10.3	-
11278 mm Reinforced	24.8 / 17.7	58.2 / 44.2

The table also includes a the strengths based on updated lamstock data. The lamstock data used by ReLAM to generate the design strength values for the reinforced specimens was based on testing done on an earlier sample of lamstock. A second sample of lamstock from which the specimens used in this research were fabricated was taken

directly from the glulam assembly line. This sample was tested and found to be of significantly lower average strength. The fact that the actual strengths were lower than originally thought resulted in a more conservative testing program. The updated lamstock design strengths, which are almost 26% less than the older strengths, are a more accurate representation of the strength of the specimens tested because they were sampled directly from the wood used to fabricate the beams tested. However, the testing program had already been developed and several specimens had been tested when this was realized, therefore the test protocols were not changed to reflect the lower lamstock strengths.

3.2.3 Gordon Composites FRP

The FRP used to reinforce the all of the glulam beams tested was a unidirectional E-glass barstock from Gordon Composites, Inc. in Colorado (product designation GC-67-UB). The individual pieces of reinforcing were cut to fit the required length and measured 120.6 mm x 6.35 mm width and thickness for the 6700 mm beams and 120.6 mm x 12.7 mm for the 11278 mm beams. A few of the physical and mechanical properties are listed below in Table 3.2. These and several other material properties and physical characteristics can be found on the Gordon Composites website (http://www.gordoncomposites.com).

Table 3.2 Gordon Composites FRP material properties.

Glass Content by Weight	67%
Density	1.86×10^{-4} N/mm^3
Modulus of Elasticity	41230 MPa
Poisson's Ratio	0.30

3.3 Fatigue Testing Program

The original work plan for this research required the development of full *S-N* curves for a sample of structural-scale FRP-reinforced glulam beams. Developing a full *S-N* curve involves fatiguing specimens until failure at a number of different stress levels to determine number of cycles to failure at a given stress level. However, based on preliminary investigations done by Gamache (2001), this was not feasible and the plan was revised to evaluate the durability of the reinforcing over a shortened fatigue testing period. Instead, the fatigue tests were changed to reflect a loading schedule consistent with a full life cycle of an in-service timber bridge girder and were loaded for two million cycles, or until failure, at 100% and 130% of the allowable design stress, F_b. It is commonly accepted that two million fatigue cycles at the allowable flexural stress of a specimen is a good representation of the damage due to vehicular loads over the life span of a bridge girder. An in-service girder would see far more than two million cycles of fatigue, however, most cycles do not stress the girder to its allowable design strength. This method has been employed by other fatigue researchers such as Senthilnath et al (2001) who studied fatigue of CFRP strengthened reinforced concrete bridge beams and also by Fieder et al (2003) who studied the fatigue of carbon shell composite bridge panels.

The fatigue tests conducted were a modified ASTM D198 procedure (ASTM 2000), and designed to load the beams at two different stress levels, $1.0F_b$ and $1.3F_b$. The stress ratio, R, for the tests was derived from live load to dead load ratios for typical timber bridges. Load head spacing was design to produce an applied shear to applied moment ratio the same as that seen in typical timber bridge girders.

Mention should be made here that the testing program used specimens that were not preservative treated. Glulam beams used in-service have preservative treatment which could have detrimental effects on the reinforcing and/or the wood-FRP bond line. Very few treatments are acceptable for wood laminates and research done by Tascioglu et al (2002) found that water-borne preservative treatment reduced the tensile strength and interlaminar shear strength of E-glass/phenolic composites.

3.3.1 Flexural Stress Calculations

A significant mistake was made regarding the calculations of flexural stress which resulted in an unintentionally conservative testing program. The flexural stress calculation presented here were based on a transformed section that included the FRP reinforcing whereas ReLAM is designed to be used with just the wood cross section modulus. This mistake, coupled with the low lamstock properties discussed in Section 3.3.2, resulted in the application of a flexural stress 52% higher than the allowable stress for the beams fatigued at $1.0F_b$ and 98% higher for the beams fatigued at $1.3F_b$. However, the desired shear stress to flexural stress ratio of 0.81 (discussed later in this chapter) was still produced in the specimens fatigued at $1.0F_b$.

3.3.2 Development of Loads and Load Head Positions

The position of the load heads on the specimens was based on a four-point bending setup that would cycle the beams between an appropriate minimum and maximum load. The maximum load was designed to produce a flexural stress of either $1.0F_b$ or $1.3F_b$ as discussed earlier. The minimum load represented a typical dead load

for a typical in-service timber bridge girder equivalent to the specimen tested, and was calculated based on ratios of dead load to dead-plus-live load.

Defining the stress ratio, R, was necessary to determine the minimum fatigue load. Load head spacing for a four point bending test more commonly places the load heads at the third points of the beam. However, using typical moment-to-shear ratios is more conservative and would more accurately represent in-service bridge girder loading.

To determine the required R, a timber bridge girder design example found in the Timber Bridge Design Manual (Ritter, 1990) was used as a guideline for designing a beam with the properties of the unreinforced and FRP-reinforced glulam beams being tested. The example was followed as it appears in the manual with two exceptions: the live load was increased to HS-25-44 loading instead of the HS-20-44 loading, and the glulam allowable flexural stress values were replaced with the values for the unreinforced and reinforced test specimens given in Table 3.1 (original lamstock data). Then beam was then redesigned once using the unreinforced section properties and once for the reinforced section properties. Both the unreinforced and reinforced allowable stress values were reduced by the same 32% as the glulam section in the design example to account for allowable stress design reduction factors due to duration of load, wet use, etc. Using values from the two resized sections, the live load to dead load ratios were then calculated for applied shear and moment.

Figure 3.2 shows a cross section of the timber bridge used in the design example. The example in the manual followed the design of a simply supported girder with a span of 14,630 mm center-to-center of bearings. The bridge was designed to carry one lane of traffic with a 4,268 mm roadway width. The required girder depth was determined using

a fixed width of 130 mm and subjecting it to loading from an AASHTO HS-20-44 design truck.

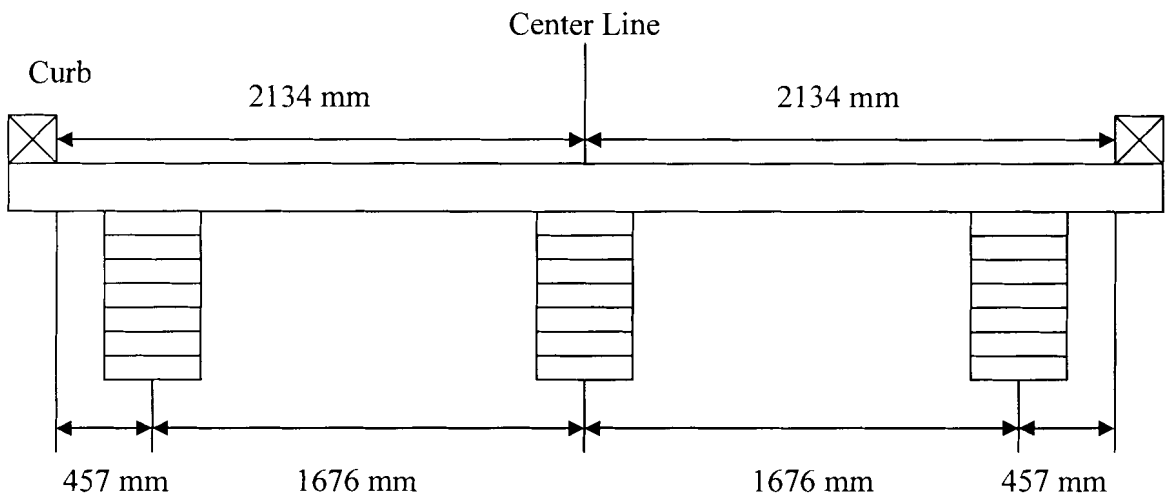

Figure 3.2 Cross section of the timber bridge used in the design example.

The live load moments in the example were taken from a table of design values for maximum moment due to a wheel line and the appropriate distribution factor applied. The distribution factor was also applied to the maximum shear. The worst-case live load to dead load ratios for moment (M_{LL}/M_{DL}) and shear (V_{LL}/V_{DL}) were then calculated for unreinforced and reinforced girders. These values, presented in Table 3.3, show that a live-to-dead load ratios of 2:1, for both moment and shear, is a reasonable approximation. Thus an R of 0.333 was used determine the stress range for fatigue cycling at a stress level of $1.0F_b$.

Table 3.3 Typical dead load to live load ratios.

	M_{LL}/M_{DL}	V_{LL}/V_{DL}
Reinforced	2.27	1.70
Unreinforced	1.97	1.55

In addition, the combined live load plus dead load (LL+DL) ratio for applied flexural stress to unfactored allowable flexural stress, f_b/F_b, was determined. This ratio was calculated as the value of the applied stress under worst case DL+LL conditions divided by the unfactored allowable reinforced strength. In the same manner, the applied shear stress to unfactored design shear stress ratio f_v/F_v, and the ratio $(f_v/F_v)/(f_b/F_b)$ were also determined for the reinforced section designed with the timber bridge example. These values, listed in Table 3.4, show that the applied shear stress is increased significantly for the reinforced girders. The ratio f_b/F_b in the table is not 1.0 because the unreduced allowable flexural stress, F_b, is used in the calculations. Further, for the reinforced girder, 81% of the allowable shear stress is produced by the DL + LL, versus the 56% for the unreinforced girder. This increase in shear stress must be accounted for in the fatigue testing program.

Table 3.4 Ratios of applied stress to design stress.

	f_v/F_v	f_b/F_b	$(f_v/F_v)/(f_b/F_b)$
Reinforced	0.54	0.67	0.81
Unreinforced	0.37	0.66	0.56

From the ratio of total shear to total moment, the load heads were positioned to produce 81% of the design allowable shear stress simultaneously with 100% of the design allowable flexural stress. At the higher stress level of $1.3F_b$, the same load head distances as with the $1.0F_b$ tests were used, which produced 104% of the allowable shear stress. The load head spacing calculated for the 6,700 mm and 11,278 mm long specimens are given below in Table 3.5. Detailed calculations of these values are given in Appendix B.

Table 3.5 Calculated values for load head spacing.

Beam Length (mm)	Distance from End of Specimen to Load Head (mm)
6700	1986
11278	3553

3.4 Testing Facility

All structural testing and specimen construction for the fatigue durability research was conducted in the structural testing laboratory at the Advanced Engineering Wood Composites (AEWC) Center. The testing frames and actuators are located on the 376 m^2, 356 mm thick concrete reaction floor. The reaction floor contained anchor points on a 610 mm grid which allows a number of different configurations for the testing frames and actuators which can load specimens from either above or below the floor. Each individual anchor point has a capacity of 1,717 kN.

The structural testing area of the laboratory is an uncontrolled environment subject to relative humidity changes due to weather fluctuation. During the winter months the relative humidity in the laboratory ranged from 20-30% and the temperature was consistently between 20-24°C. In the summer, the relative humidity fluctuated between 40% and 60% and the temperature ranged from 21-31°C.

3.5 Equipment

The testing apparatus consisted of a testing frame, actuator, end supports, a spanner beam with load heads and lateral bracings. Each item is discussed in more detail below.

3.5.1 Testing Frame and Actuators

The equipment used to load the specimens was a steel frame which housed a vertically mounted hydraulic actuator. The frames were custom built for the University of Maine and designed according to the use and capacity of the actuators (Gamache 2001).

There were two different actuators used to load the specimens, an Instron 244 kN dynamic and 490 kN dynamic actuator. The 6,700 mm beams were tested with both the 244 kN and 490 kN actuators while the 11,278 mm beams were tested only in the 490 kN actuator because their ultimate capacity was close to that of the 244 kN actuator.

3.5.2 End Supports and Lateral Bracing

The specimens were simply supported at each end, with a pinned connection at one support and roller connection at the other. These connections were mounted on concrete pedestals and the centerline of the reaction was located 152 mm from the end of the beam. Figure 3.4 shows a typical beam with boundary conditions in the testing set-up.

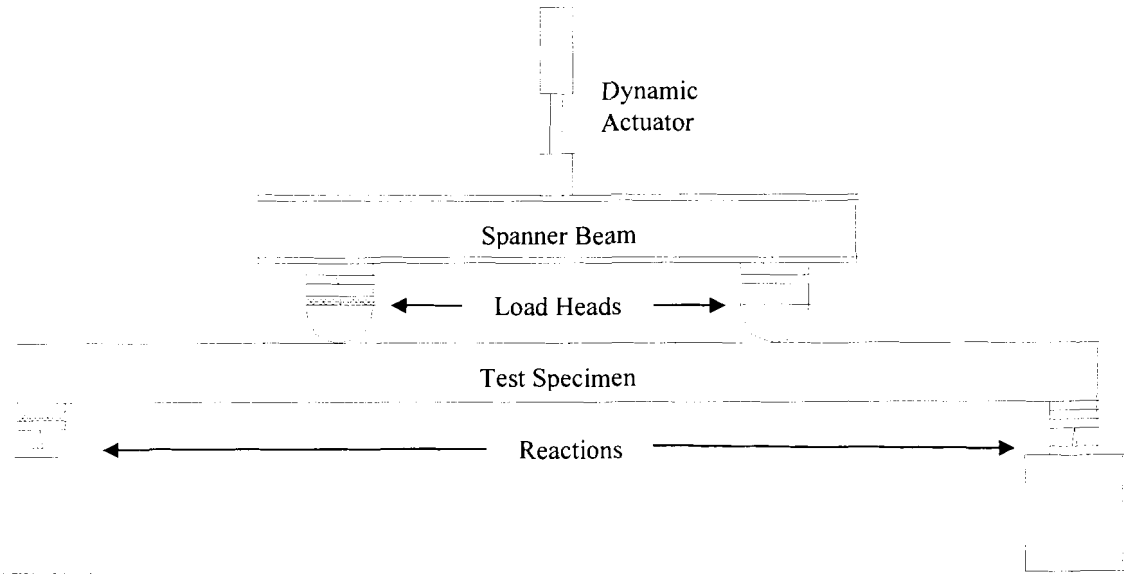

Figure 3.3 A typical test specimen in the testing frame.

During fatigue, the beams were supported against lateral torsional buckling by steel bracing anchored to the floor. Lateral bracing was placed near the third points of the beam and a system of casters attached to the lateral bracing provided low-friction contact between the bracing and the sides of the beam.

3.6 Data Acquisition

Data was acquired during the periodic static tests (discussed later in this chapter) where the load cycling was stopped and the beam was loaded to its design strength at a slow rate. During the static test, deflection data was recorded via LVDTs and load data was recorded via the load cell on the actuator. Only data regarding the number of elapsed cycles was recorded while the beams were cycling.

3.6.1 Instrumentation of Specimen

The instrumentation scheme for the static tests is shown in Figure 3.4. A total of six Linear Variable Differential Transformers (LVDTs) measured displacement on the specimen. Two LVDTs were located at center span to measure maximum deflection while two LVDTs located at the centerline of the reactions at each end of the beam measured uplift. The LVDTs at center span (LVDT 3 and 4 in Figure 3.3) had a range of +/- 125 mm for a total range of 250 mm and the four LVDTs at the ends of the beam (LVDT 1, 2, 5, and 6) had a range of +/- 12 mm for a total range of 25 mm. All six LVDTs recorded displacement from the specimens at the neutral axis.

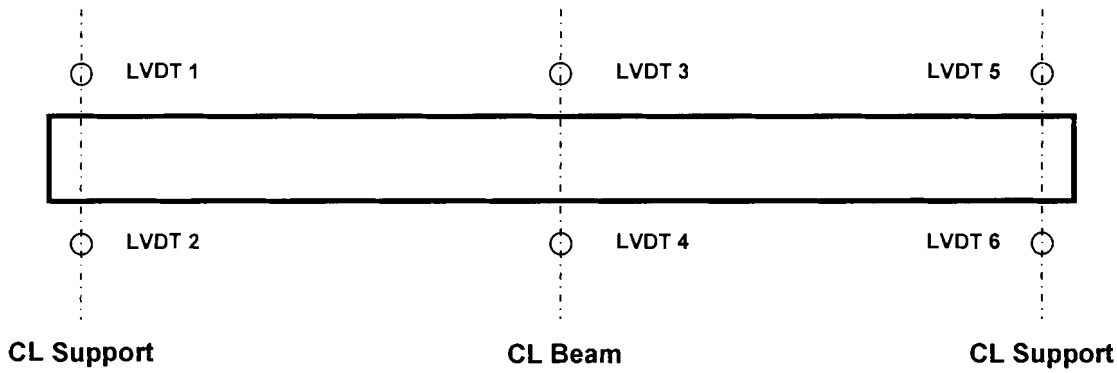

Figure 3.4 Top view of beam showing the instrumentation scheme of a typical specimen.

All LVDTs used had a maximum linearity error of 0.25% of their full range and were calibrated to ensure accurate readings. Each LVDT was calibrated at the end of each fatigue test before the next test was performed. Calibration was performed in accordance with AEWC work instructions on a calibration table fabricated specifically for LVDTs.

3.6.2 LabVIEW Program

Deflection and load data was recorded using the program LabVIEW 5.0.1 (National Instruments, 1998). LabVIEW is a software program designed for data acquisition and comes with several preprogrammed applications that can be customized to the user's individual needs. The specific LabVIEW program used was the built-in "simple data logger" application that is provided with the software package. The data logger read a total of seven channels of input, one channel for the applied load and six channels from the LVDTs. The was recorded in the form of a voltage and was then converted to load and displacement readings using the appropriate conversion coefficients obtained from calibration.

3.7 Test Protocol

The specimens were fatigued in four-point bending according to ASTM D198 (ASTM 2000), with a minor modification. The standard calls for a radius of curvature for the load heads to be between two and four times the depth of the beam, however, the load heads used for this research had a radius of curvature of 1.33 times the depth of the beam.

Two different loading schedules were developed for the testing. The first loading schedule stressed the beam to the design bending strength ($1.0F_b$) based on the ReLAM simulations (Lindyberg 2001). The second was developed to study the durability of the beams as they would be loaded by trucks heavier than the design truck. In this case the live load was increased by 130% ($1.3F_b$), a value used to represent an extreme loading case. Table 3.6 below shows the loading schedules for tests run at stress levels of $1.0F_b$

and $1.3F_b$. As a conservative approach, the minimum fatigue cycling value was unchanged from the $1.0F_b$ to $1.3F_b$, giving a stress ratio of R=0.255 at the highest load level. The positon of the load heads also remained unchanged which produced a shear of 104% of the allowable shear strength.

Table 3.6 Cycling plan for reinforced specimens.

Stress Level	Beam Size (1.93% FRP)	Dead Load (kN)	Dead + Live Load (kips)
$1.0F_b$	6700 mm	19.6	58.7
$1.0F_b$	11278 mm	34.7	103.2
$1.3F_b$	6700 mm	19.6	76.5

3.7.1 Fatigue Cycling Frequency

Before starting the fatigue tests, it was necessary to determine the maximum frequency the beams could be cycled at without introducing dynamic effects and exceeding the capacity of the hydraulic system. The goal was to run the beams at the highest possible frequency to decrease the testing time for each specimen. The cycling rate was governed by the hydraulic demand and the capacity of the pumps driving the actuator.

To determine the upper limit on the cycling rate, a load cell was placed under one of the reactions and load was recorded from both the load cell and dynamic actuator while the beam cycled at different frequencies. The two data series were then plotted to see that the two curves were in phase and that the load cell was consistently reading half the load from the actuator.

For the 6,700 mm long beams, frequencies of 1.0, 1.5, 2.0, 2.5 and 3.0 Hz were checked in the 244 kN actuator. At the higher frequencies of 2.5 and 3.0 Hz, the actuator could not fully meet the demands of the required loading and the peak load was not

reached. The maximum rate at which the tests could be run without sacrificing accuracy was 2.0 Hz. The actuator and the load cell loads are plotted against time in Figure 3.5 for a frequency of 2.0 Hz. The maximum and minimum loads were being met with reliable accuracy and therefore the slight distortion in the peak of the actuator loads was acceptable. As can be seen, the plot from the load cell is in phase and half that of the actuator load. All of the 6,700 mm beams were fatigued at a frequency of 2.0 Hz in the 244 kN actuator. Testing was run 24-hours per day constantly and each test took approximately 13 days to complete.

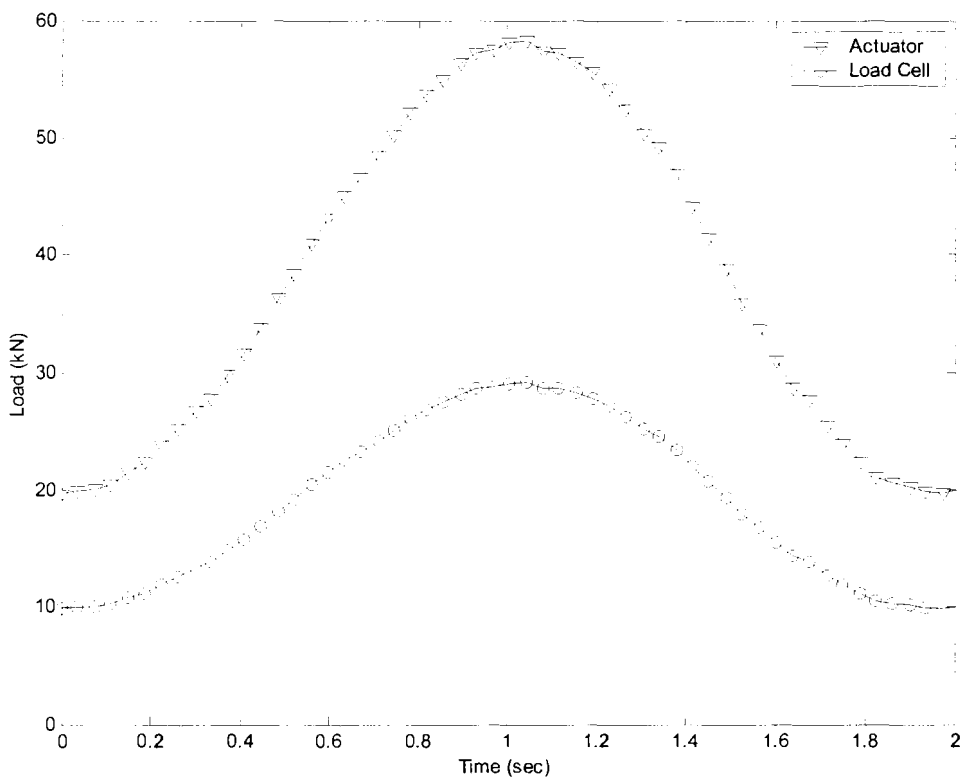

Figure 3.5 Load cell and actuator load versus time for a frequency of 2.0 Hz.

The same procedure was performed before fatiguing the larger 11,278 mm long beams in the 490 kN actuator, checking frequencies of 0.5 Hz to 2.0 Hz in increments of 0.1 Hz. The larger deflection from the longer specimens combined with the larger piston in the 490 kN actuator required a significant increase the volume of hydraulic flow and limited the rate of cycling to 1.0 Hz. Frequencies higher than 1.0 Hz created too much demand on the hydraulic system and the pumps could not meet the desired amplitude. All of the 11,278 mm beams were fatigued at a frequency of 1.0 Hz in the 490 kN dynamic actuator. Testing was run 24-hours per day constantly and each test took approximately 24 days to complete.

3.7.2 Periodic Static Tests

At every 150,000 to 250,000 cycles during the fatigue tests, load cycling was stopped and the specimen was loaded to its allowable flexural capacity in a static test to track stiffness degradation. Data acquisition equipment recorded the load-deflection plots for each test and the deflection at the design load for each test was used to plot the stiffness over time.

3.8 Summary

A testing program was developed to evaluate the fatigue durability of structural scale FRP-reinforced glulam beams. The test involved cycling specimens in four-point bending for a total of two million cycles, or until failure. Specimens were cycled between a minimum and maximum load at two different stress levels: $1.0F_b$ and $1.3F_b$. Loading at $1.0F_b$ fatigued the specimens at a stress ratio of R=0.333, which was based on

a typical value for in-service timber bridge girders. For the stress level of $1.3F_b$, the minimum load was held constant while the maximum load was increased to 130% of the allowable flexural stress. This produced a stress ratio of R=0.255.

Load heads were spaced to produce a shear stress to flexural stress ratio consistent with that seen in in-service timber bridge girders. This spacing yielded 81% of the allowable shear stress at $1.0F_b$ and 104% at $1.3F_b$.

The cycling frequency was limited by the capacity of the actuators used to apply the loads and was found to be 2.0 Hz for the 6,700 mm long beams and 1.0 Hz for the 11,278 mm long beams.

An important note in the design of the testing program is that the lamstock data used to generate an estimate of the reinforced strength of the specimens was significantly higher than that of the lamstock used in the glulam specimens tested. In the future, more accurate allowable strength data needs to be established for designing with this visually graded lamstock to avoid this sort of problem. Also, the transformed section properties of the specimens were erroneously used in place of the wood section properties to calculate flexural stress. The cumulative effect of these inconsistencies resulted in a conservative testing program, where the specimens fatigued at $1.0F_b$ were in reality being stressed at $1.52F_b$, while the specimens fatigued at $1.3F_b$ were being loaded to $1.98F_b$.

Chapter 4

CONSTRUCTION OF FRP-REINFORCED GLUED LAMINATED SPECIMENS

4.1 Introduction

The FRP-glulam specimens used in this research were reinforced in the AEWC laboratory. The procedure involved priming the surface of the glulam with a bonding agent and gluing the FRP reinforcing with an epoxy. A cold press applied pressure to the bond line while the epoxy cured. Beams with both full length and partial length reinforcing were constructed.

A total of nine full length reinforced specimens were constructed, six of which measured 130 mm x 305 mm x 6700 mm and three measured 130 mm x 533 mm x 11278 mm. A second set of nine specimens were constructed with partial length reinforcing all of which measured 130 mm x 305 mm x 6700 mm. Three of the partial length reinforced specimens were constructed with a beveled FRP termination and six were constructed with a mechanical restraint to confine the FRP terminations. The construction procedure along with the equipment used is discussed in greater detail in the following sections. The testing program is discussed in detail in Chapter 3, and the results of the fatigue tests are presented in Chapter 5 of this thesis.

4.2 Fabrication of FRP-Reinforced Beams

Although the FRP and unreinforced glulam beams were purchased from Willamette Industries, the process of reinforcing the specimens had to be performed at the AEWC laboratory. Reinforcing the glulam beams with the FRP was a relatively

straightforward process, which consisted of preparing the wood application surface with a coupling agent, applying the epoxy and clamping the FRP-glulam beam in a set of cold clamps and allowing the epoxy to cure. The glulam beams and FRP were purchased from manufacturers, while the coupling agent and epoxy were made in-house.

4.2.1 HMR Pretreatment

The first step in reinforcing the beams was to apply a coupling agent to the wood surface. Approximately eighteen to twenty-four hours prior to lay-up, all of the glulam beams were treated with a hydroxymethylated-resorcinol (HMR) coupling agent on the side that the E-glass was to be applied. The purpose of the HMR is to prime the beam surface and facilitate a better bond between the wood and the epoxy adhesive. Typically, epoxies are not used as structural adhesives. While the shear strength of epoxies under dry conditions can exceed the shear strength in the wood, epoxy bonds are very prone to delamination under shrinkage and swelling induced by variable hygrothermal conditions (Vick, et al 1997). HMR was developed by the Forrest Products Laboratory and is an organic compound which enhances the durability of wood-FRP bonds exposed to exterior or wet conditions (Christiansen and Vick 2000). One side of the compound forms a strong bond with the wood while the other side bonds well with the epoxy. When the epoxy is spread on and the FRP applied, the end result is a more durable bond between the two materials (Tascioglu 2001).

The HMR treatment required painting the surface of the beam with the solution for a number of applications using entire quantity of HMR. The application rate for the HMR was 463 g/m^2, which yielded a batch size of 404 g for the 6,700 mm full-length

reinforced specimens, 296 g for the 6,700 mm long partial-length reinforced specimens and 679 g for the 11,278 mm long full-length reinforced specimens. Once the HMR was applied, the beam was stored for eighteen to twenty-four hours to allow all the water to evaporate from the application surface. The HMR solution was mixed according to the standard operating procedures on file in the AEWC. The formula used to mix the HMR is given in Table 4.1.

Table 4.1 Formula for HMR coupling agent.

Indgedient	Percent by Weight
Water, deionized	90
Resorcinol, crystalline	3.3
Formaldehyde, 37% formalin	3.8
Sodium Hydroxide, 3 Molar	2.4
Dodecyl Sulfate Sodium Salt	0.5

4.2.2 FPL 1A Epoxy Adhesive

After the water was allowed to evaporate from the HMR, the FRP was ready to be bonded the glulam. FPL 1A Epoxy Resin was used as the bonding agent. Both the HMR and FPL 1A Epoxy Resin were developed by Dr. Charles B. Vick of the Forest Products Lab. Testing done by Vick and Okkonen (1997) on four different species of aircraft wood showed this epoxy formulation fared the best out of three common epoxies and was tested for resistance to delamination shear and deformation under ASTM D2559. This formula, detailed in Table 4.2 has also been used with good success in the past on several other applications at the AEWC, where the fatigue testing for this project took place (Dagher and Lindyberg 2003; Hong 2003).

Table 4.2 Formula for FPL 1A epoxy adhesive.

Indgedient	Percent by Weight
DGEBA Resin (Diglycidyl ether of bisphenol A)	79.3
Benzyl Alcohol	9.9
Hydrophobic Fumed Silica	2.0
Triethylenetetramine Hardener	8.8

Using a plastic spatula, the FPL 1A was then spread evenly by hand to the bottom of the glulam beam on the HMR treated surface. The FRP was put in place on the beam and the two were clamped together in the cold press and allowed to cure for a minimum of 12 hours. The beams were clamped at a pressure of 0.345 MPa. The optimum clamping pressure was determined experimentally through earlier testing done by Lindyberg (2002). The FPL 1A has a useable pot life of between thirty and forty minutes. This time constraint and the limited number of available workers kept the maximum number of beams laid-up to two at a time. The beams that were not in use were stored in the laboratory at ambient conditions until they were reinforced for testing. The FPL 1A was mixed according to the standard operating procedures on file in the AEWC. The application rate for FPL 1A is 538 g/m^2, which yielded a batch size of 470 g for the 6,700 mm full-length reinforced specimens, 344 g for the 6,700 mm long partial-length reinforced specimens and 790 g for the 11,278 mm long full-length reinforced specimens.

4.2.3 FRP Preparation

The E-glass reinforcing was cut to the desired length and cleaned with acetone on the bonding side. Because the beams were slightly wider than the reinforcing, special attention was paid during fabrication to ensure that the FRP stayed centered on the beam.

In most cases, duct tape was used to secure the FRP on the beam by taping the FRP to the side of the glulam while the epoxy cured.

4.2.4 Cold Press

The last step in reinforcing the beams was to clamp the FRP and glulam together to apply pressure to the bond line. The cold press used to clamp the FRP to the glulam was a large I-beam with threaded rods spaced evenly through the top flanges of the beam. The glulam beam was then placed between the treaded rods and clamped to a pressure of 0.345 MPa. Figure 4.1 shows a reinforced beam in the cold press. The threaded rods were calibrated using a load cell and torque wrench to obtain a tension value based on applied torque. This was done for a number of rods and the average value was used to calculate the appropriate torque needed in each rod given the number of rods, the rod spacing and the required bond line pressure. The appropriate torque for each rod was determined by the total number of rods used to clamp the specimen.

Figure 4.1 A 6700 mm Beam in cold press.

4.2.5 Treatment of Defects

Several of the beams came from the Willamette plant with knotholes that had not been plugged. Many of the unplugged knots were on the tension side of the beams where the FRP was applied. Before the beams were reinforced, these holes were plugged with an epoxy resin, the same FPL-1 epoxy used to bond the FRP to the glulam. This ensured that there would be at least some bond between the wood and FRP at these knotholes. The pictures in Figure 4.2 show one such knothole, before and after it had been filled with epoxy resin. Defects such as cracks and checking in the beams were not treated. Beams not suitable for partial length reinforcing (as discussed later in this chapter) were used for full-length reinforced tests.

Figure 4.2 The left side of the picture shows a knot, right side shows the same knot filled with epoxy.

4.2.6 Storage of Specimens

Unreinforced specimens were stored in the laboratory under ambient conditions until they were reinforced. Reinforced specimens that were removed from the cold press were stored for a period of at least five days prior to testing to allow the epoxy to fully cure to maximum strength.

4.3 Full-Length Reinforced Specimens

Twelve of the eighteen specimens tested were full-length reinforced beams. With full length reinforcing, the FRP ends are confined by the supports and therefore no special FRP-termination treatment was necessary. The FRP was cut at 90 degrees to the same overall length as the specimen. The reinforcing was bonded to the wood as previously described previously.

4.4 Partial Length Reinforcing

A total of nine partially reinforced beams were tested in fatigue. All nine partially reinforced beams were pretreated with HMR and bonded with FPL 1A epoxy resin in the same manner as the fully reinforced beams. Three of the nine beams were partially reinforced with no restraints on the FRP terminations and three had mechanical restraints to confine the FRP-terminations.

Several full length specimens had been tested before the partial length reinforcing was designed and, from the results, it was noted that there was little or no bond between the wood and FRP at knots and certain grain defects. Therefore, during lay-up of the partially reinforced beams, special care was taken to ensure no knots, defects or potentially detrimental grain deviations were present within 150 mm of the FRP termination. Clear grain at the FRP termination would help clarify whether peeling of the FRP, if it occurred, was a result of the stress concentrations that exist at the FRP ends and not a result of poor bond at the terminations.

The FRP reinforcing was terminated at the theoretical cut off point (TCOP), approximately 900 mm from each end of the beam as shown in Figure 4.3 and discussed

in Chapter 3. This gave the maximum possible savings in reinforcing material, 26.8% for the 6700 mm specimens, without sacrificing the specimen's flexural strength. However, this also created the most critical situation for evaluating durability of partial length reinforcing. Typically, as in the case of reinforced concrete, tensile reinforcing is extended a certain distance beyond the point where it is theoretically no longer required (American Concrete Institute 1999). This is done to help minimize the effect of stress concentrations at the transition point. Terminating the FRP reinforcing at the TCOP would magnify any problems that might exist at the unconfined terminations and provide a better insight into the behavior of the FRP at unrestrained terminations.

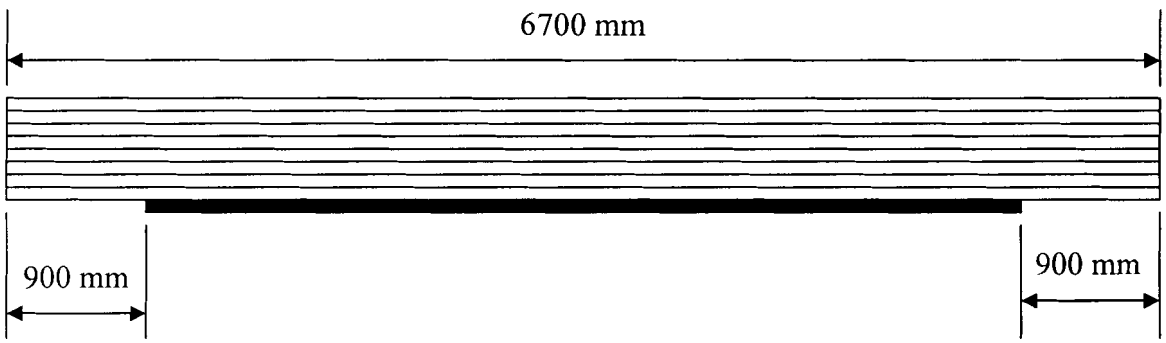

Figure 4.3 Typical partially reinforced beam.

4.4.1 Partially Reinforced Specimens, Unrestrained Terminations

For the three beams with no end restraints, the terminations of the FRP were beveled to an angle of 30 degrees with the horizontal (see Figure 4.4). Earlier research done by Gamache (2001) showed that higher stress concentrations exist at the FRP terminations of partially reinforced beams with 90 degree edges. The beveled edge of the FRP was used as one method of reducing the effects of the stress concentrations. The angle at which the FRP was beveled was chosen based on the Standard Specifications for Highway Bridges (AASHTO 1996), which specifies that steel cover plates welded to

steel beams must be beveled at an angle no more than 30 degrees with the horizontal at their terminations. The beveled portion of the FRP was beyond the TCOP as shown in Figure 4.4.

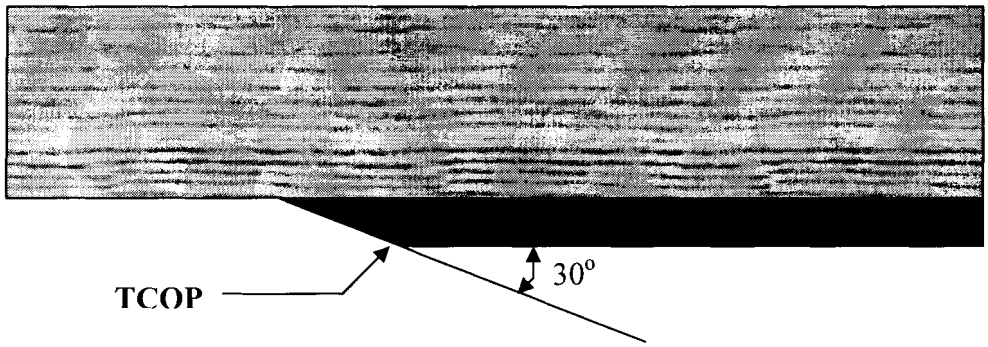

Figure 4.4 Beveled end detail for partial length reinforcing.

4.4.2 Partially Reinforced Specimens, Mechanically Restrained Terminations

The unrestrained ends of the specimens tended to debond at the FRP terminations and cause subsequent failure in the wood (see Chapter 5). Additionally, previous research done by Hong (2003) using the same materials as tested here also showed that small scale single-lap shear joints were prone to fatigue failures. Given this insight, the remaining six beams were fabricated with mechanical restraints to confine the FRP terminations and prevent peeling.

The restraints used to confine the FRP terminations, shown in Figure 4.5, were fabricated from A36 steel plates measuring 130 mm x 75 mm x 9.5 mm, a neoprene pad of the same dimensions to provide better surface contact, and two 152 mm x 12.7 mm lag screws. This was an inexpensive and easily constructed detail that could be applied with common tools and no special experience.

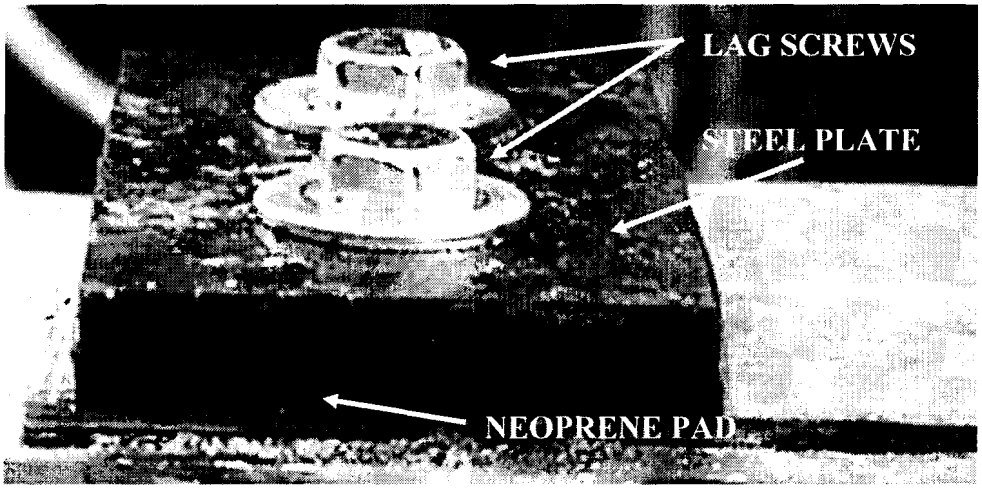

Figure 4.5 Mechanical restraint used to confine the FRP terminations of partial length reinforcing, shown here on an inverted beam.

To determine the ultimate torque that could be applied to the lag screws in the Douglas-Fir glulam beams, ten lag screws were calibrated using a torque wrench, pieces of old glulam specimens and a load cell. Placing the doughnut-shaped load cell between the lag screw and wood, the lag screws were tightened with a torque wrench until they stripped the wood. Plots of tensile force versus torque for the ten lag screws were produced, and each lag screw was calibrated in wood cut from a different section of several different specimens.

The average of these plots was a nearly linear relationship shown in Figure 4.6 with the best-fit line through (0, 0). Each point on the plot represents an average value and this relationship was used to determine clamping force given the applied torque. All of the lag screws began to strip the wood at a torque greater than 108 kN-mm, and the average toque at stripping was 115 kN-mm. The maximum allowable torque, for the purpose of restraining the FRP terminations, was taken as 80% of the minimum torque at pull-out, or 86.4 kN-mm. Therefore, the clamping force in each lag screw used confine

the FRP termination was approximately 18.1 kN. The thickness of the steel plate was designed so that at the applied clamping force, the stress in the cantilever portion of the plate (the portion from the center of the lag screw to the outer edge of the plate) would be half of the yield stress of the steel. While the specimens were being fatigued, the torque in the lag screws was checked during the periodic static tests, and re-torqued to 86.4 kN-mm if necessary as discussed in Chapter 5.

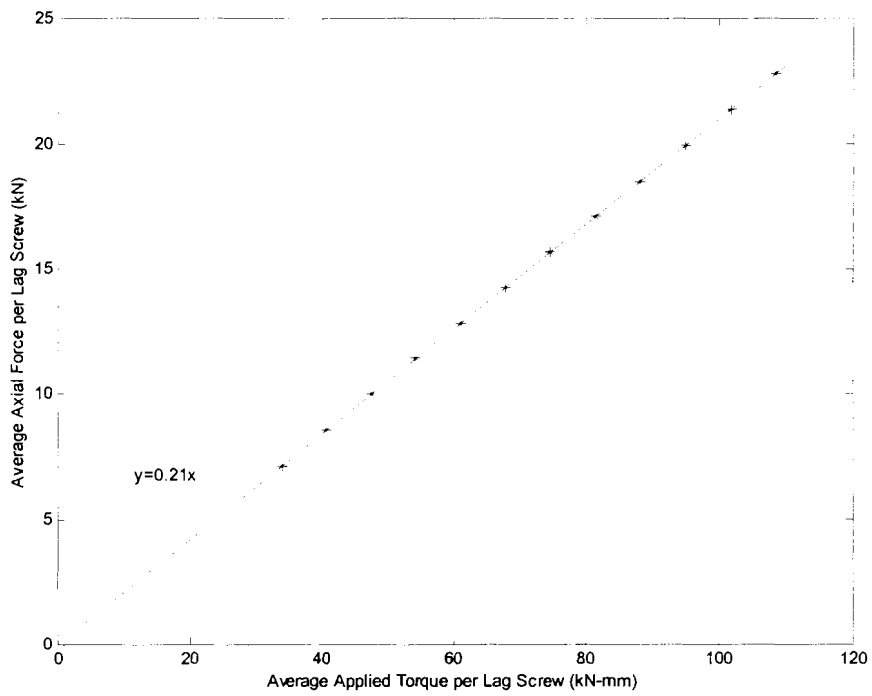

Figure 4.6 Relationship between averaged torque and pressure for ten lag screws.

4.5 Summary

A total of eighteen glulam beams were reinforced on the flexural tension side with an E-glass fiber reinforced polymer (FRP) for the purpose of fatigue testing. The glulam beams were purchased from a manufacturer and reinforced at the AEWC laboratory. Full length reinforcing was used on twelve beams while the remaining six were partially

reinforced. Partial-length reinforcing was designed with and without restraints at the FRP terminations.

For both the full-length and partial length reinforcing, the FRP was bonded to the glulam beams using the same procedure. Three of the partially reinforced specimens had unrestrained FRP terminations with a 30 degree bevel on the FRP to alleviate peeling stress that occur at the end of partial length reinforcing. The other set of six partially reinforced specimens utilized steel plates and lag screws to mechanically confine the terminations and prevent failure at this location.

Chapter 5

MECHANICAL FATIGUE TESTING OF FRP-REINFORCED GLUED LAMINATED BRIDGE GIRDERS

5.1 Introduction

A total of eighteen structural scale bridge girders were tested to evaluate the fatigue durability of Gordon Composites, Inc. unidirectional E-glass FRP as a reinforcing for glulam bridge girders. The specimens were tested at two different stress levels and with both full-length and partial-length reinforcing. This chapter outlines the results of the fatigue tests performed on the 18 FRP-reinforced glulam beam specimens. The results are grouped into full and partial length reinforcing and further broken into subgroups based on stress level, beam size and type of FRP termination restraints. More detailed descriptions of the testing program can be found in Chapter 3, and an account of the construction of the specimens is located in Chapter 4 of this thesis.

A summary of the characteristics of all fatigue specimens is given in Table 5.1 on the following page. The specimens are designated S1-S18 and the table includes information on ultimate failure of the specimen as well as whether or not failures occurred during fatigue. Throughout the chapter, plots of beam stiffness versus number of fatigue cycles are given as a relative measure of stiffness changes. In these cases, stiffness is presented in the form of midspan displacement.

Table 5.1 Summary of the results of the mechanical fatigue tests.

Specimen Number	Reinforcing Type	Applied Load	Number of Cycles	Failure During Cycling?		Failure Mode (Failure During Fatigue)	Residual Strength (kN)	Ultimate Deflection (mm)	MOR (MPa)
				Yes	No				
$1.0F_b$									
S1	Full	$1.0F_b$	2000000		x	Static Bending -Tension	149.6	126.0	68.0
S2	Full	$1.0F_b$	2000000		x	Static Bending -Tension	121.4	100.5	55.2
S3	Full	$1.0F_b$	2000000		x	Static Bending -Tension	121.6	110	55.3
S4	Full	$1.0F_b$	2000000		x	Static Bending -Tension	199.30	161.5	54.9
S5	Full	$1.0F_b$	2000000		x	Static Bending -Tension	169.2	172.6	46.6
S6	Full	$1.0F_b$	2000000		x	Static Bending -Tension	176.1	163.7	48.5
S7	Partial/Unrestrained	$1.0F_b$	1061377	x		Bond - FRP Termination	N/A	N/A	N/A
S8	Partial/Unrestrained	$1.0F_b$	592311	x		Bond - FRP Termination	N/A	N/A	N/A
S9	Partial/Unrestrained	$1.0F_b$	2000000	x		Static Bending (Compression)	96.0	81.3	43.70
S10	Partial/Restrained	$1.0F_b$	2000000	x		Static Bending (Compression)	112.3	149.6	51.10
S11	Partial/Restrained	$1.0F_b$	2000000		x	Static Bending -Tension	101.4	88.7	46.10
S12	Partial/Restrained	$1.0F_b$	2000000		x	Static Bending -Tension	110.3	96.1	50.2
$1.3F_b$									
S13	Full	$1.3F_b$	31487	x		Horizontal Shear	N/A	N/A	N/A
S14	Full	$1.3F_b$	1272585	x		Compression	N/A	N/A	N/A
S15	Full	$1.3F_b$	1109229	x		Compression	N/A	N/A	N/A
S16	Partial/Restrained	$1.3F_b$	953845	x		Tension Failure	N/A	N/A	N/A
S17	Partial/Restrained	$1.3F_b$	101647	x		Shear & Tension Failure	N/A	N/A	N/A
S18	Partial/Restrained	$1.3F_b$	19722	x		Tension Failure	N/A	N/A	N/A

5.2 Fatigue Testing Program

All fatigue tests were run for 2 x 10^6 cycles, or until failure, and then broken in static bending. The fatigue testing program was a modified ASTM D198 (ASTM 2000) four-point bending setup that cycled the beams between an appropriate minimum load and maximum load. The support length was 300 mm and lateral bracing was placed at the beam's third points. A picture of a 6,700 mm specimen in the testing appartatus can be seen in Figure 5.1. The dead load to live load ratios were calculated using typical unreinforced timber bridge design values, but substituting the flexural strengths of the reinforced beams. These FRP-reinforced design values were obtained from ReLam (Lindyberg, 2001), a computer program which returns glulam strengths based on lamstock data and probabilistic moment-curvature analysis.

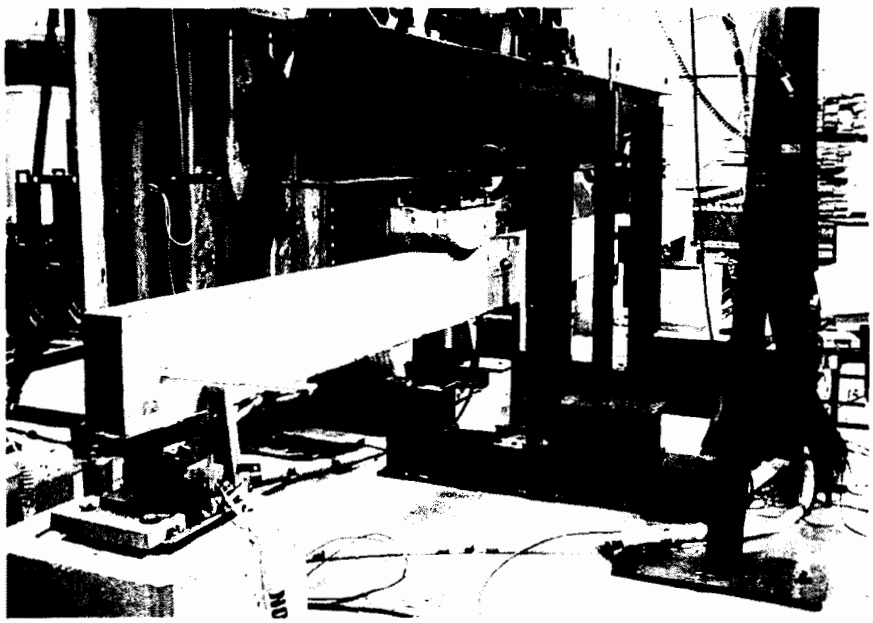

Figure 5.1 Picture shows a 6,700 mm specimen in the testing apparatus.

The beams were cycled two different peak flexural stresses: $1.0F_b$ and $1.3F_b$. For a typical in-service timber bridge girder, the dead load is about 1/3 the total service dead

load plus live load. Design examples from the Timber Bridges: Design, Construction and Maintenance Manual (Ritter, 1990) were checked to verify this ratio as discussed previously in Chapter 3. Thus, for the beams loaded to $1.0F_b$, a stress ratio of R=0.33 was used for the fatigue tests. For the beams loaded to $1.3F_b$, the minimum load was held constant, giving an R=0.25.

As discussed in Chapter 3, for the beams fatigued at $1.0F_b$, the load heads were positioned on the beam to produce 100% of the allowable flexural design strength, F_b, simultaneously with 81% of the shear strength. These percentages were also derived from design examples given in the Timber Bridge: Design, Construction and Maintenance manual (Ritter, 1990). As a conservative approach, the load head spacing was unchanged for the beams fatigued at $1.3F_b$, yielding 130% of the design moment capacity simultaneously with 104% of the shear capacity. Shear strength used in all calculations was obtained from the NDS (NDS 1997) and the Wood Handbook (Forest Products Laboratory 1999) as discussed in Chapter 3.

Specimens were tested in subgroups of three with both full length and partial length reinforcing. The fully reinforced group of specimens consisted of two subgroups of 6,700 mm long beams (6,400 mm span) tested at stress level of $1.0F_b$, and $1.3F_b$ and one subgroup of 11,278 mm long (10,973 mm span) specimens to help identify size effects. The partially-reinforced group of specimens were tested both with and without mechanical restraints on the FRP terminations, however only the specimens with restraints were tested at the higher stress level of $1.3F_b$.

During all fatigue tests, the cycling was stopped at increments of between 150,000 to 250,000 cycles and a static bending test was performed to track stiffness changes over the

testing period. During these periodic static tests, the beam was loaded to its allowable load based on design flexural stress while data acquisition equipment was set up to record the applied load and midspan deflection to give a plot of relative stiffness over time.

5.3 Fatigue Testing at $1.0F_b$

A total of twelve specimens were tested at a stress level of $1.0F_b$ using 1.93% Gordon Composites E-glass reinforcing. Six of the twelve specimens were utilized full length reinforcing; three being 6,700 mm long beams and three 11,278 mm beams. Of the remaining six, three specimens were 6,700 mm long partially reinforced beams with unrestrained FRP terminations and three were 6,700 mm long partially reinforced specimens with mechanically restrained FRP terminations.

5.3.1 Fully Reinforced Specimens, $1.0F_b$

Specimens S1, S2 and S3 were 130 mm x 305 mm x 6,700 mm fully-reinforced beams fatigued at 100% of the design strength. Specimens S4, S5 and S6 were also fatigued at 100% of the design strength, but measured 130 mm x 533 mm x 11,278 mm.

All fully reinforced beams fatigued at $1.0F_b$ survived the 2×10^6 cycles and were broken in static bending. Furthermore, none of the beams showed any significant stiffness loss over the duration of the testing period. The average modulus of rupture for the 6,700 mm specimens was 59.5 MPa (based on the wood section only) with an average maximum midspan deflection of 112 mm. For the 11278 mm specimens, the average modulus of rupture (MOR) was 50.0 MPa with an average maximum midspan deflection of 166 mm.

5.3.1.1 Specimens S1, S2, and S3 (Fully Reinforced, $1.0F_b$)

Specimen S1 was fatigued at 100% of the design strength for 2 x 10^6 cycles and showed no signs damage due to fatigue. Due to an unfortunate incident with the actuator bracing, the beam was loaded to 125.4 kN before the actuator bracing failed. While statically loading the beam to failure, the lateral bracing that held the actuator in place failed and caused the load heads to move sideways and fall off the beam. A static test and visual inspection was performed and there were no visible sign of damage or stiffness loss. Furthermore, the load-deflection plot of the beam up to the point of the bracing failure, showed no nonlinear characteristics, indicating that no permanent damage was done.

Upon fixing the bracing the beam was then loaded again until failure at an ultimate load of 149.6 kN and an ultimate deflection of 126.0 mm. The modulus of rupture for specimen S1 was 68.0 MPa, the highest of any of the 6,700 mm long specimens tested. Figure 5.2 shows the results of the static tests in the form of a plot of midspan deflection at the time (number of cycles) that the test was performed, shows that there was actually a slight decrease in beam stiffness, most notably toward the end of the testing period. However, at an decrease of around five percent, the overall change was negligible. The load-displacement plot of specimen S1 as it was loaded to failure is given in Figure 5.3 below. The mode of failure was a tensile failure at a finger joint near midspan, which pried the FRP reinforcing off the bottom and all the way down one side of the beam. The picture in Figure 5.4 is a close up shot of the tension side of the beam where the failure in specimen S1 initiated.

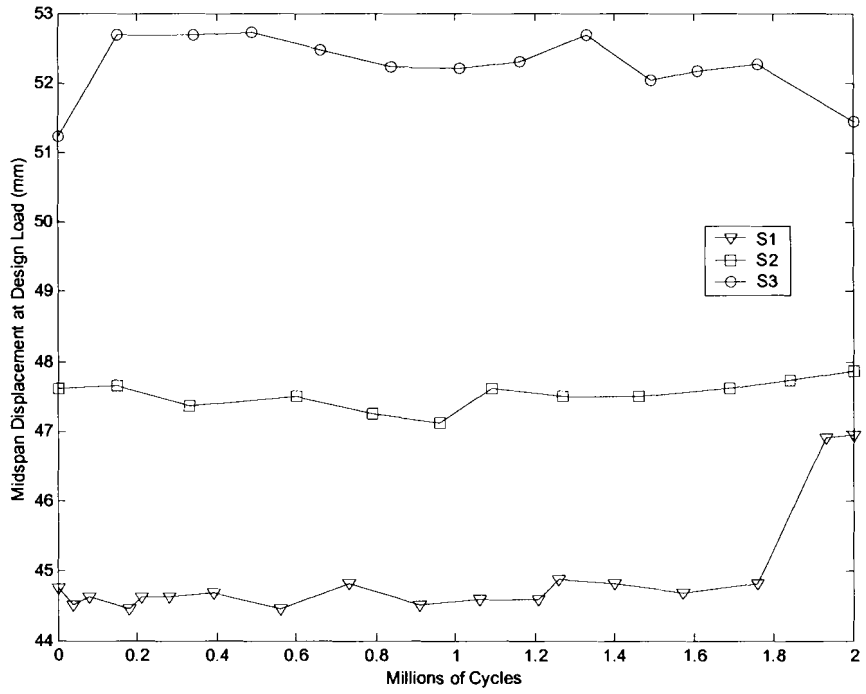

Figure 5.2 Stiffness vs Time plot for specimens S1, S2 and S3.

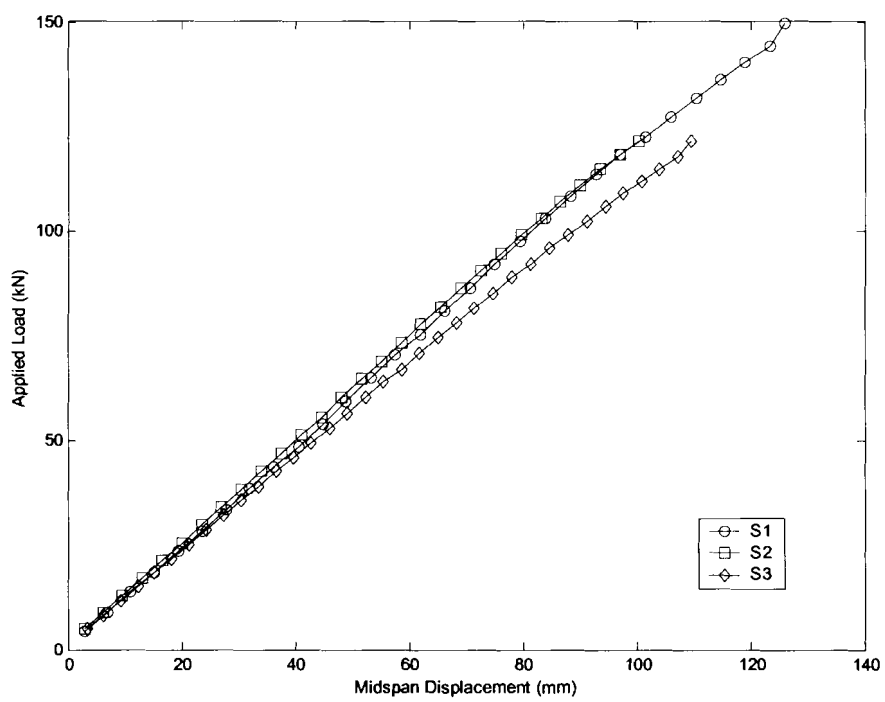

Figure 5.3 Load vs Displacement plot for specimens S1, S2 and S3.

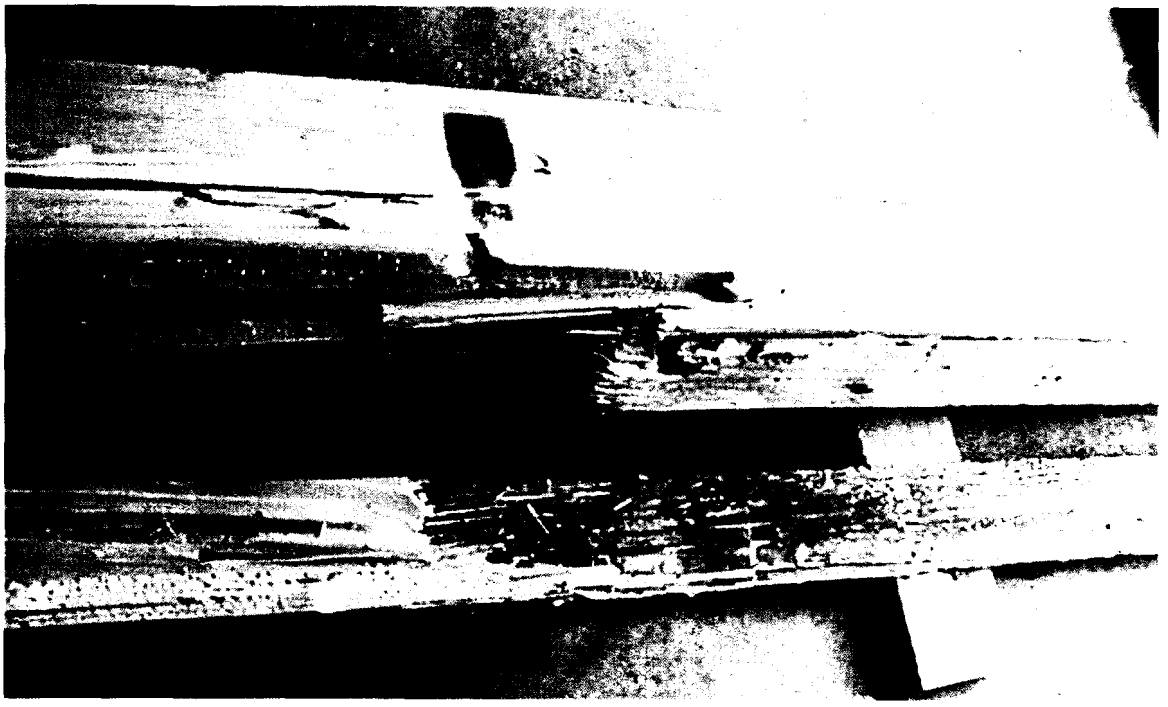

Figure 5.4 Failure at a finger joint near midspan in specimen S1.

Beam S2 failed at a finger joint at an ultimate load of 121.4 kN and a deflection of 100.5 mm. The modulus of rupture for specimen S2 was 55.2 MPa. Beam S3 failed at a knot in the bottom lamination at 121.6 kN at a deflection of 110.0 mm. The modulus of rupture specimen S3 was 55.3 MPa.

Specimens S2 and S3 exhibited very similar behavior to S1. No significant crack formation or propagation was noted during cycling, nor were any failures seen during the fatigue tests. Both beams showed little change in stiffness over the duration of the fatigue test, as can be seen in Figure 5.2, and lasted the full 2 x 10^6 cycles. Beams S2 and S3 failed in tension near midspan at either a finger joint or knot very similar to that of S1 shown in Figure 5.3. These failures were characteristic of static strength testing done by Lindyberg (2003) on beams of the same properties and reinforcing.

The average MOR for the 6700 mm full length reinforced $1.0F_b$ specimens was 59.5 MPa, which differed from the ReLAM predicted MOR by 30.5%.

5.3.1.2 Specimens S4, S5 and S6 (Fully Reinforced, $1.0F_b$)

Specimens S4, S5 and S6 measured 130 mm x 533 mm x 11,278 mm with full-length reinforcing. The behavior during fatigue and also the ultimate failure mode of this group of specimens were very similar to the smaller S1, S2 and S3 specimens. None of the three specimens in this group showed significant stiffness degradation (see Figure 5.5). However, a horizontal shrinkage crack at one end of specimen S5 was noted to be 610 mm long at the start of testing and had propagated to 1,470 mm by the end of the fatigue test. The crack, located in the third lamination from the top, did not have any significant effects on stiffness. No other significant failures or damage were noted during cycling in this or any of the other beams. An interesting phenomenon with specimen S6 was that the initial static test inexplicably showed the beam to be less stiff than all subsequent static tests. No definitive explanation for this is known. For all specimens S4-S6, failure occurred at either a finger joint or knot near midspan and, as seen in Figure 5.6, the load-deformation curves remained linear until failure. The load deformnation plot for specimen S6 shows a slight nonlinearity in the second to last point plotted. This was due to the tensile lamination failing just prior to the FRP being torn from the beam. The beam loses load (second to last point in plot for specimen S6) when the lamination fails and then begins to hold load again as displacement increases. This phenomenon was largely due to the fact that the tests were run in position control and can be seen in several other specimen load-deformation plots.

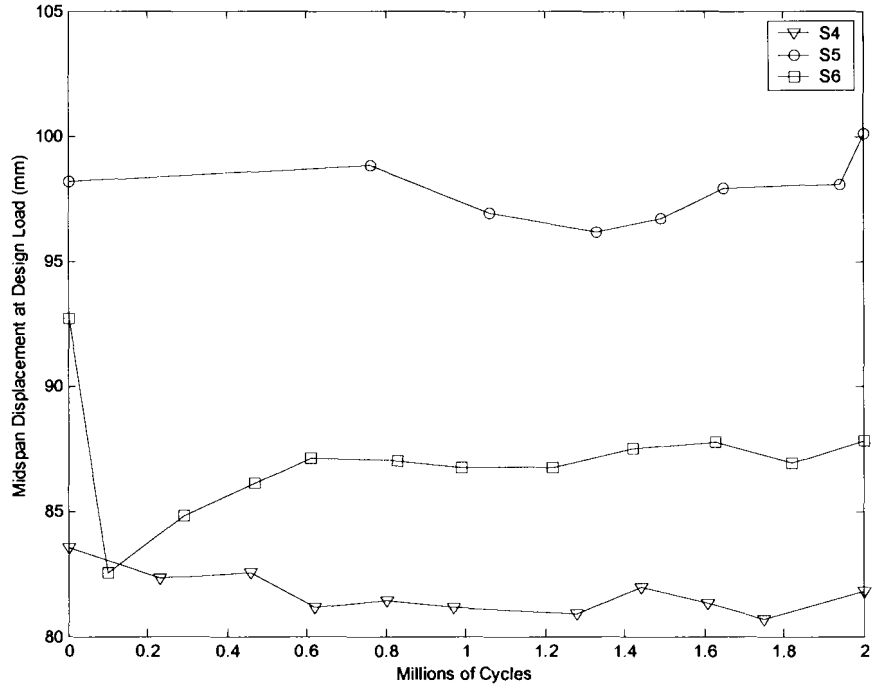

Figure 5.5 Stiffness vs Time plot for specimens S4, S5 and S6.

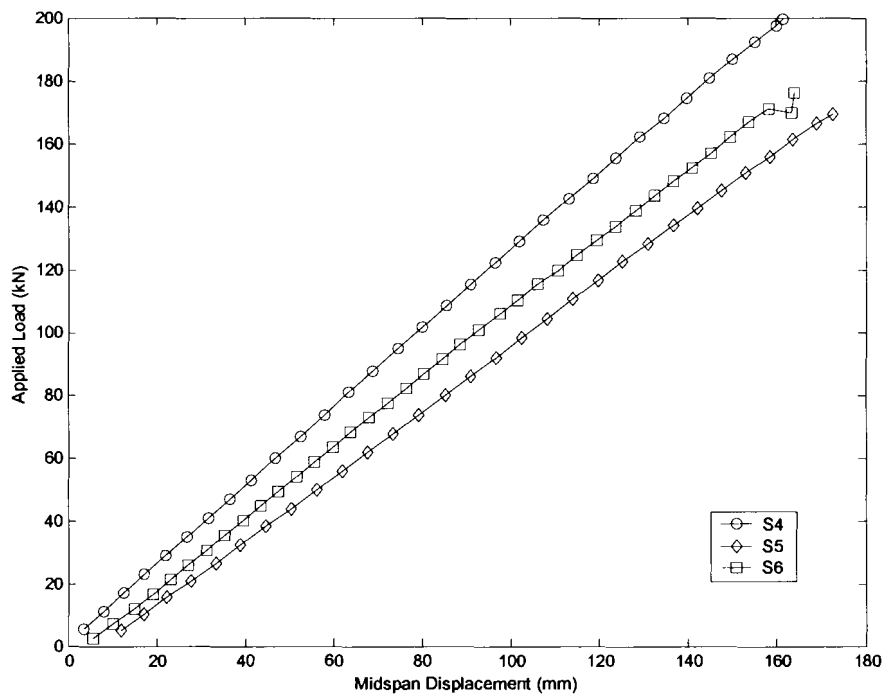

Figure 5.6 Load vs Displacement plot for specimens S4, S5 and S6.

The average MOR for the 11278 mm full length reinforced $1.0F_b$ specimens was 50.0 MPa, which differed from the ReLAM predicted MOR by 13.1%.

5.3.2 Partially Reinforced Specimens, $1.0F_b$

Partial-length reinforcing can be advantageous over full-length reinforcing by reducing the amount of FRP needed, and also has implications for retrofitting existing structures. Partial-length reinforcing is at a disadvantage, however, because the FRP terminations are not confined by the supports as is the case with fully-reinforced girders. Significant stress concentrations can occur at the FRP terminations (Gamache, 2001), which could cause debonding of the reinforcing. In an attempt to prevent debonding at the FRP terminations beveled ends and mechanical restraints were implemented as two possible solutions. The possibility of using partial-length reinforcing was explored in six different beams both with and without FRP end-restraints.

Specimens S7-S9 were tested without restraints on the FRP terminations and S10-S12 were tested with mechanical restraints. In both cases the FRP was cut at the theoretical cutoff point, or the point where the applied moment was equal the moment capacity of the unreinforced specimen. The theoretical cut off point was 900 mm from the end of the 6,700 mm specimens (see Appendix B for calculations). The mechanical restraints for the FRP-terminations consisted of a neoprene pad sandwiched between a 130 mm x 75 mm x 9.5 mm steel plate that was clamped to the beam with two 152 mm x 12.7 mm lag screws (see Figure 5.7). For the specimens tested with mechanical restraints, the torque in the lag screws was checked, and retightened if necessary, at every

periodic static test performed. Torque losses were between 4 and 7 kN-m per static test. Refer to Chapter 4 for more details on the construction of the partially-reinforced beams.

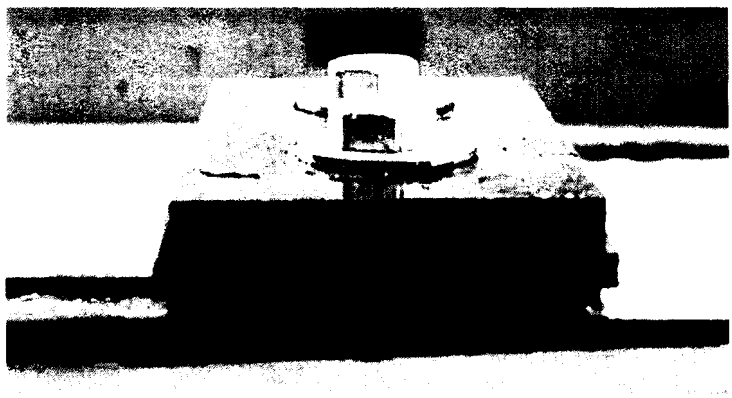

Figure 5.7 View shows typical end restraint for partially-reinforced specimens. Beam is inverted for better perspective.

5.3.2.1 Specimens S7, S8, and S9 (Partially Reinforced, 1.0F_b)

Specimens S7, S8 and S9 were partially-reinforced beams with no end restraints on the FRP. The FRP terminations were beveled to an angle of 30 degrees with the horizontal in order to reduce the peeling stresses that result from the stress concentration at this point.

Specimen S7 was the first partially reinforced beam with unconfined FRP terminations and failed during fatigue after 1.06 million cycles. A plot of the midspan deflection and corresponding cycle number is shown in Figure 5.8. Because the beam failed while cycling some time after the static test, the plot shows only stiffness data up until the time of the last static test. Total stiffness loss during the fatigue test was less than 2% and there were no visible sign of damage. The apparent source of failure for specimen S7 was loss of bond at the FRP termination which caused a subsequent wood failure that propagated the remaining length of the beam. This failure is shown in Figure

5.9 with the beam still in the testing apparatus. The portion of the beam seen lying on the floor is the FRP termination where the failure initiated.

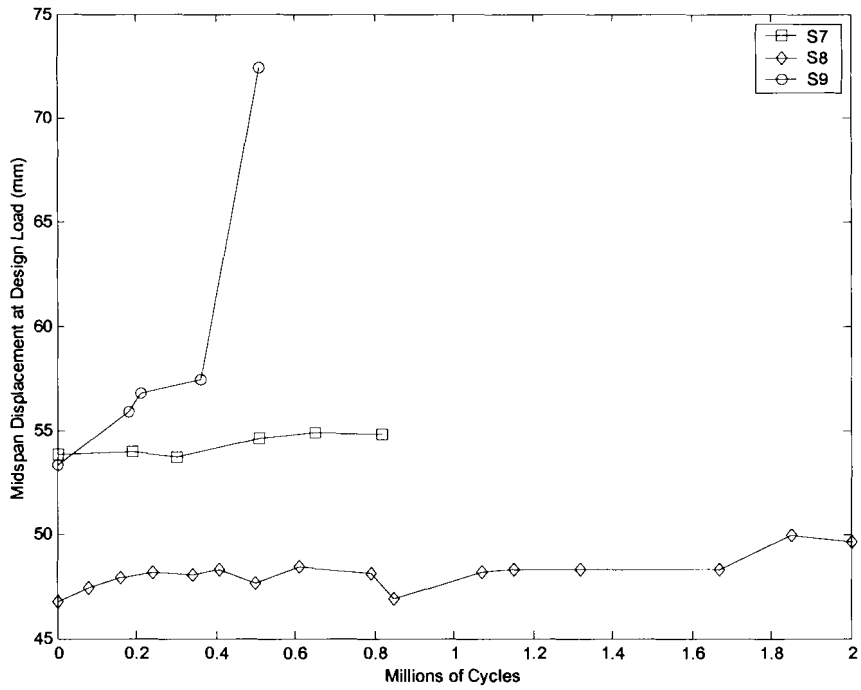

Figure 5.8 Stiffness vs Time plot for specimens S7, S8 and S9.

Specimen S8 lasted only 592,000 cycles and had the most significant stiffness loss of all beams tested. The relative stiffness loss was almost 38%, which can be seen in Figure 5.8. There were no outwardly visible signs of damage occurring in the beam, leading to the conclusion that the significant stiffness loss was due to internal damage that occurred somewhere after 30,000 cycles. The source of failure in specimen S8 was identical to that of S7 and S9, with a loss of bond at the FRP termination leading to a tension failure in the wood.

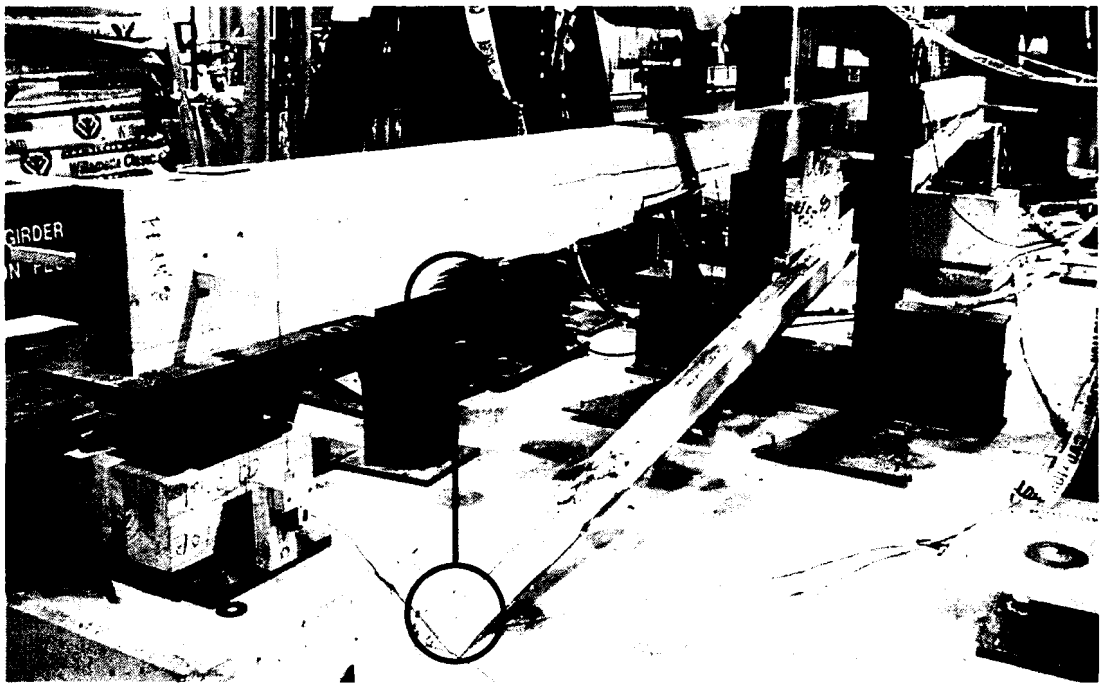

Figure 5.9 Debonding failure of Specimen S7 during fatigue. Circles shows the FRP termination on the floor and the location of the termination before failure. This failure mode was typical of specimen S7, S8 and S9.

Specimen S9 was the only beam of the three partially reinforced specimens to survive the full 2 million fatigue cycles. However, during testing a compression failure in the top lamination was noted around 1.2 million cycles. This compression failure occurred near a knot in the top lamination and was very close to midspan. As can be seen in Figure 5.8, noticeable stiffness loss did not occur until around 1.7 million cycles. The failure was initially seen as a buckling of the wood grain around the knot, shown in the circle in Figure 5.10. The crack, shown by the arrow in the same figure, occurred after the grain buckling and was first seen 1.8 million cycles and propagated significantly during the remainder of the fatigue test.

The compression failures did not seem to affect the linear elasticity of the beam when failed in static bending, although specimen S9 was substantially less stiff than S7 and S8. Figure 5.11 shows that the load-deflection curve stays almost linear until failure

of the specimen. Although the beam did not fail during fatigue, the failure was similar to specimen S7 in that the failure initiated as a loss of bond at the FRP termination and ultimately led to a tension failure in the wood. Failure looked very similar to that of specimen S7 seen in Figure 5.9.

Figure 5.10 Compression failure in specimen S9.

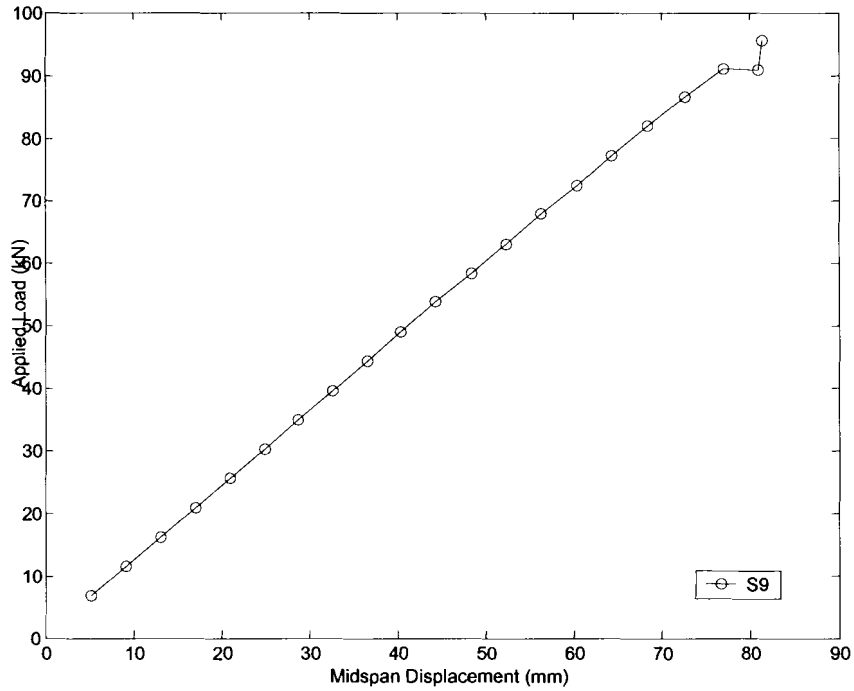

Figure 5.11 Load vs Displacement plot for specimen S9.

The average MOR for the 6700 mm partial length reinforced, unrestraned $1.0F_b$ specimens was 43.7 MPa, which differed from the ReLAM predicted MOR by -4.2%.

5.3.2.2 Specimens S10, S11, and S12 (Partially Reinforced, $1.0F_b$)

Specimen S10 was the first beam to have mechanical restraints used to confine the ends of the partial length reinforcing. A description of these end restraints is given in section 5.3.2 and also in Chapter 4. This specimen was fatigued for 2 million cycles and broken in static bending. The plot of the midspan deflections over time in Figure 5.12 shows a steady and significant decrease in beam stiffness. This decrease in beam stiffness was due to the severe compression failure that appeared early into the first day of fatigue cycling. This compression failure, a picture of which can be seen in Figure 5.13, formed in the full depth of the top lamination. When the failure appeared, it formed

two cracks, separating the top lamination into thirds along the grain and thus substantially reducing the contribution of the top lamination to the beam's stiffness.

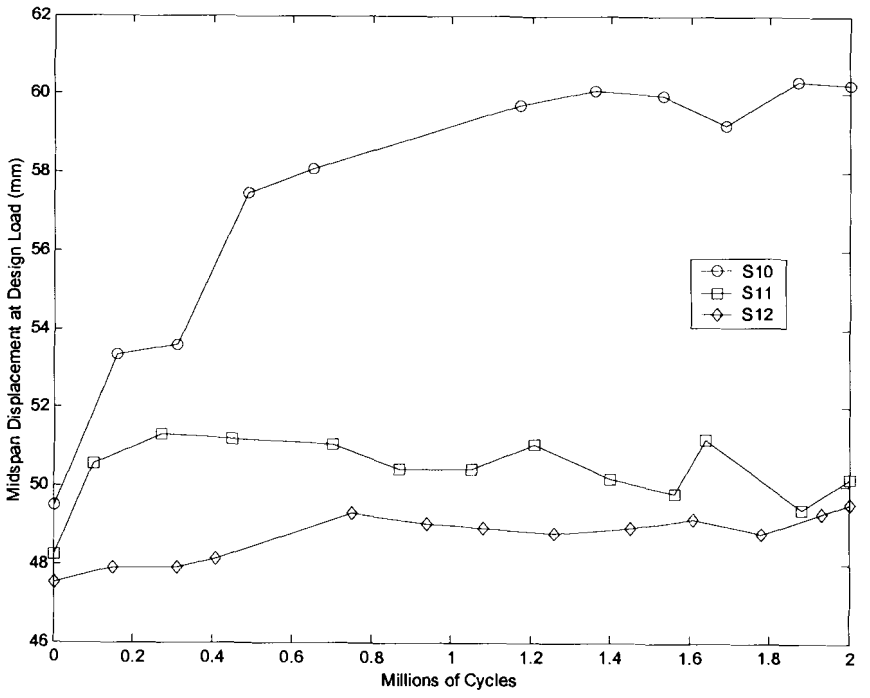

Figure 5.12 Stiffness vs Time plot for specimens S10, S11 and S12.

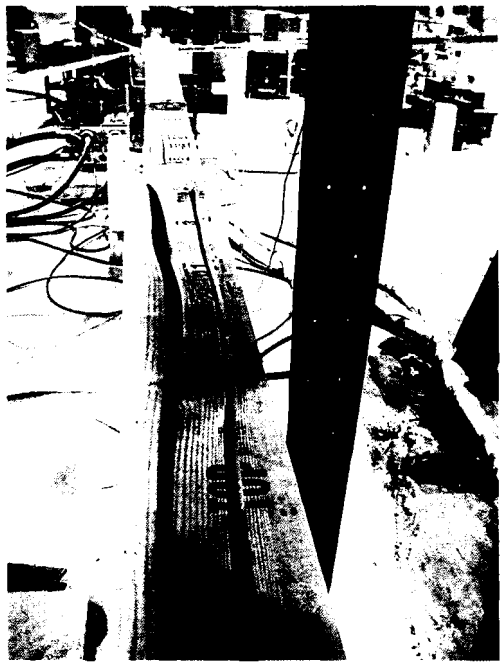

Figure 5.13 Compression failure in top lamination of specimen S10. View is looking down the length of the beam.

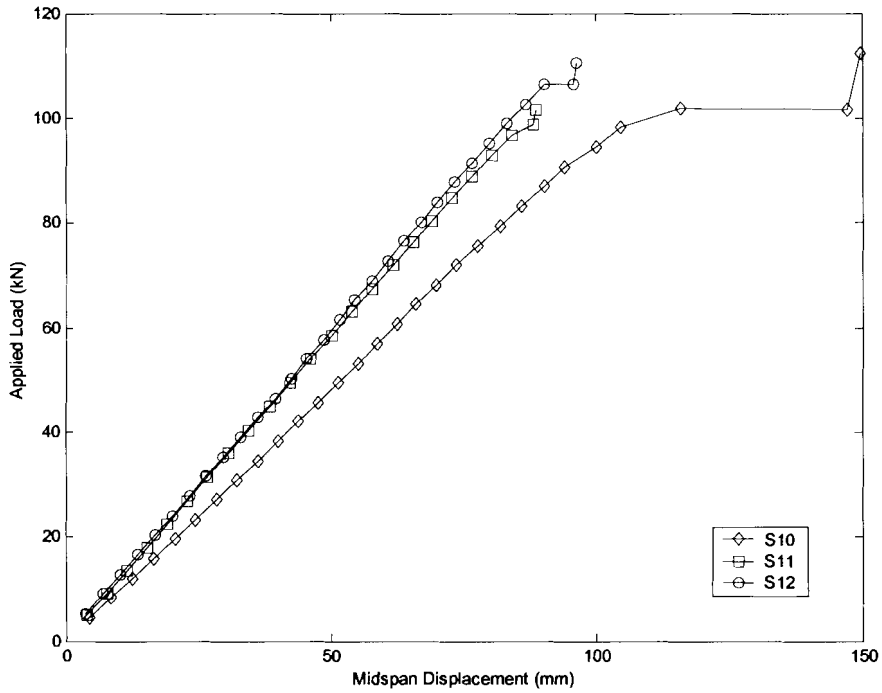

Figure 5.14 Load vs Displacement plot for specimens S10, S11 and S12.

While the beam was being loaded to failure in static bending, there was significant crushing seen in the top laminations. This crushing correlates with the nonlinear portion of the load-deflection curve beginning around 90 kN in Figure 5.14 and was most likely was caused by the compression failure during fatigue. The ultimate mode of failure, however, was in tension at a region in the specimen where the bottom three tension laminations contained a large knot and two finger joints in very close proximity and less than 500 mm from midspan.

Specimen S11 was fatigued for the full 2 million cycles with a stiffness loss of around 6%. This can be seen in the plot of the midspan deflections over time shown in Figure 5.12. There were no visibly notable failures or damage during the fatigue testing.

The beam was loaded to failure in static bending after the fatigue testing was completed. Figure 5.14 shows the load-deflection curve for specimen S11. At failure, the beam developed a horizontal shear failure that ran the entire length of the beam (see Figure 5.15). The shear cracks initiated under the load heads near the neutral axis and propagated down the length of the beam toward the supports. This was the only beam to fail in shear while being broken in static bending.

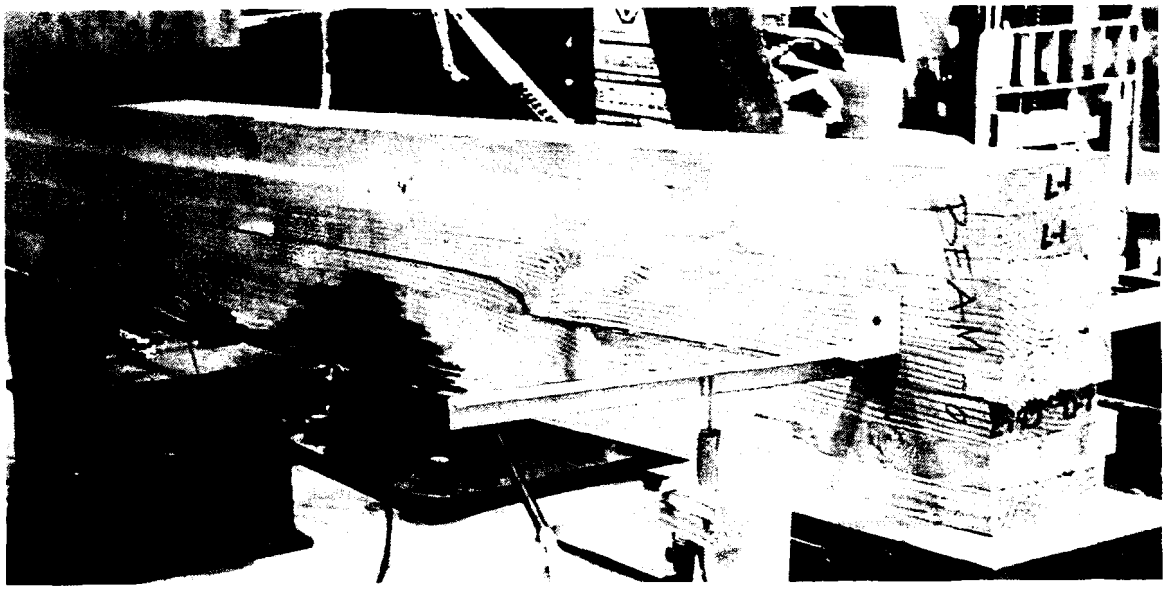

Figure 5.15 Shear failure in specimen S11.

Specimen S12 survived the 2 million cycles and was failed in static bending. There was a steady decrease in beam stiffness of around 4%, seen in Figure 5.12, however there were no outwardly visible sign of damage occurring during the fatigue test.

During the static bending test to failure, Figure 5.14 shows there was a slight loss of stiffness at around 92 kN of applied load. This corresponded to a crushing of the top compression lamination that was observed just prior to failure. The ultimate failure mode for this beam was not in compression, however, but rather was a tensile failure at finger joint near midspan similar to those seen in the fully reinforced specimens fatigued at $1.0F_b$.

The average MOR for the 6700 mm partial length reinforced, mechanically restrained $1.0F_b$ specimens was 49.1 MPa, which differed from the ReLAM predicted MOR by 7.7%.

5.4 Fatigue Testing at $1.3F_b$

The possibility exists that overloaded trucks, and trucks larger than the design truck, may travel the bridge and exceed the girder's design capacity. To understand the effects of overstressing the girder in fatigue, six specimens were fatigued at a higher stress level equivalent to 130% of the allowable moment strength. A complete fatigue cycle in this case started at the same dead load used for the fatigue tests at $1.0F_b$ and cycled up to 130% of the design moment capacity and back to the dead load giving a stress ratio of R=0.25. Three of the six specimens had full length reinforcing and three had partial length reinforcing with mechanical end restraints. Due to the poor performance of the partially-reinforced specimens at $1.0F_b$, none were tested at the higher stress.

5.4.1 Fully Reinforced Specimens, $1.3F_b$

All of the fully reinforced specimens fatigued at $1.3F_b$ failed premature to the intended two million cycles. Local failures during fatigue occurred in the form of both tension and compression failures and were followed by significant stiffness losses and ultimately failure of the specimens.

5.4.1.1 Specimens S13, S14 and S15 (Fully Reinforced, $1.3F_b$)

Specimen S13 was fatigue at 130% of the design strength for less than a full day because of a horizontal shear failure that appeared at 31,487 cycles and ran the entire length of the beam. The shear failure was sudden and split the beam into two pieces very close to the neutral axis location. The failure, shown in Figure 5.16, ran entirely in the

wood and was mostly along the wood-wood bond line of the laminations indicating that it was not a bond line failure, but rather a wood failure. After examining the failed beam, a knot was found on one side of the beam, which had been completely blown out by the shear failure. This knot ran the full depth of the lamination and penetrated approximately 45 mm into the width of the cross section. Because of the very short duration of the fatigue cycling period, only an initial static test was run and therefore there is no record of stiffness change over time.

Figure 5.16 Shear failure in specimen S13 (shear crack highlighted by two horizontal marker lines).

Specimen S14 was fatigued at $1.3F_b$ and broke during testing at 1.27 million cycles. A compression failure was noted in the beam during fatigue between 500,000 and 600,000 cycles. The compression failure occurred in the top lamination and extended

through the entire depth of the lamination. Propagation of the compression failure was noted during the remainder of the fatigue test as the failure more than doubled in size from when it was first noted.

This compression failure corresponds well with what is seen in the plot of midspan deflection versus number of fatigue cycles in Figure 5.17. There is a definite trend of stiffness loss after 400,000 cycles, just before the failure was noticed and this stiffness loss continued as the crack propagated further.

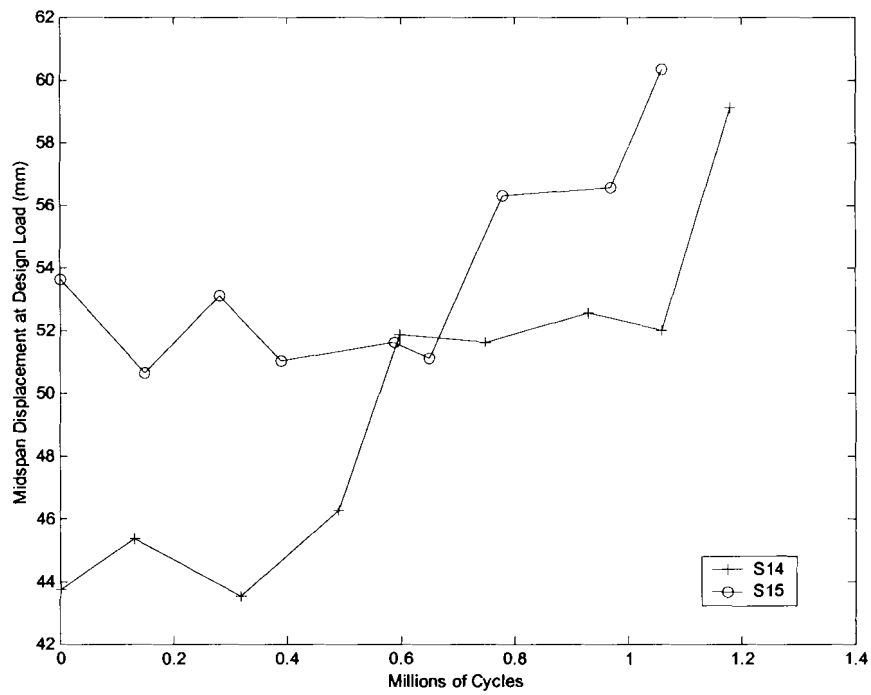

Figure 5.17 Stiffness vs Time plot for specimens S14 and S15.

Also around the same time frame, a tension failure was noted at a knot near mid span, which occurred in the bottom most lamination. The tension crack did not penetrate the entire width of the cross section and did not show any noticeable signs of propagation. However, this tension crack was the ultimate source of failure for S14,

which failed in tension at 1.27 million cycles. Failure in this beam appeared to be similar to those failed in static bending in which the tension failure pries the FRP off the beam along its bondline and there is subsequent wood failure after loss of bond.

Specimen S15 also broke during testing at 1.11 million cycles. Failure characteristics exhibited in S15 were very similar to that of S14. A compression failure much like that of specimen S14 was noted in the beam during fatigue at around 650,000 cycles. After this failure, subsequent static tests revealed significant stiffness loss. This is seen as a sharp increase in midspan deflection shown in Figure 5.17. The compression crack occurred at a knot and penetrated the entire depth of the top lamination. Propagation of the crack was seen throughout the remainder of the test. After 1.1 million cycles a tension failure occurred at a knot near midspan on the bottom lamination.

5.4.2 Partially Reinforced Specimens, $1.3F_b$

The poor performance of the unrestrained partially reinforced specimens led to only the mechanically restrained beams being tested at the higher stress level of $1.3F_b$. Three specimens, S16-S18, were tested and all failed prematurely during fatigue.

5.4.2.1 Specimens S16, S17 and S18 (Partially Reinforced/Restrained, $1.3F_b$)

Specimen S16 developed a significant tension failure around 400,000 cycles. The tensile crack, shown before and after failure in Figure 5.18a and 5.18b, formed around a knot in the wood near midspan, starting out at around 100 mm in length and propagating to over 1200 mm. The crack formed in the tension region of the beam and propagated into the wood along the grain. There was no bond failure between the laminations or

between the wood and the FRP. The beam continued to cycle until ultimately failing at 953,845 cycles due to the local tension failure at the knot. Figure 5.19 shows a significant stiffness loss of almost 14% between the periods when the tensile failure was first noted to when the beam ultimately failed. The same knot where the tensile failure formed was the ultimate source of failure in the beam.

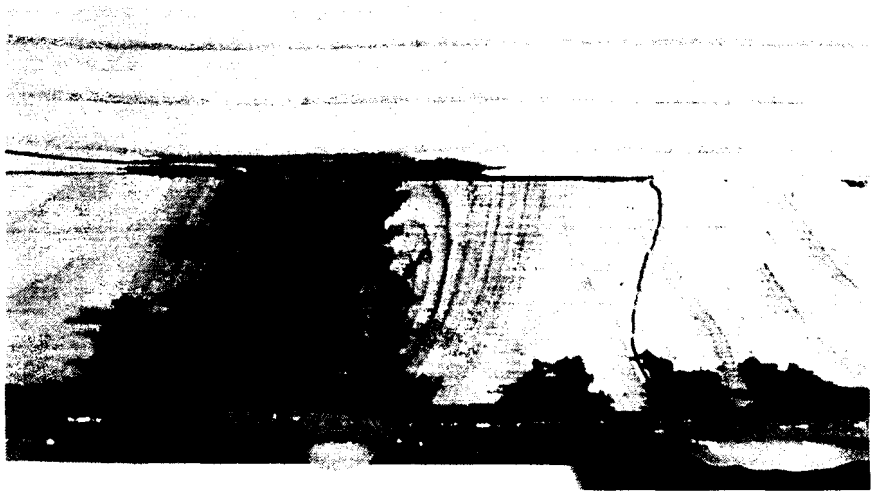

(a)

(b)

Figure 5.18 (a) Local tension failure near midspan at 953845 cycles. **(b)** The same local tension failure after ultimate failure of specimen at 953845 cycles.

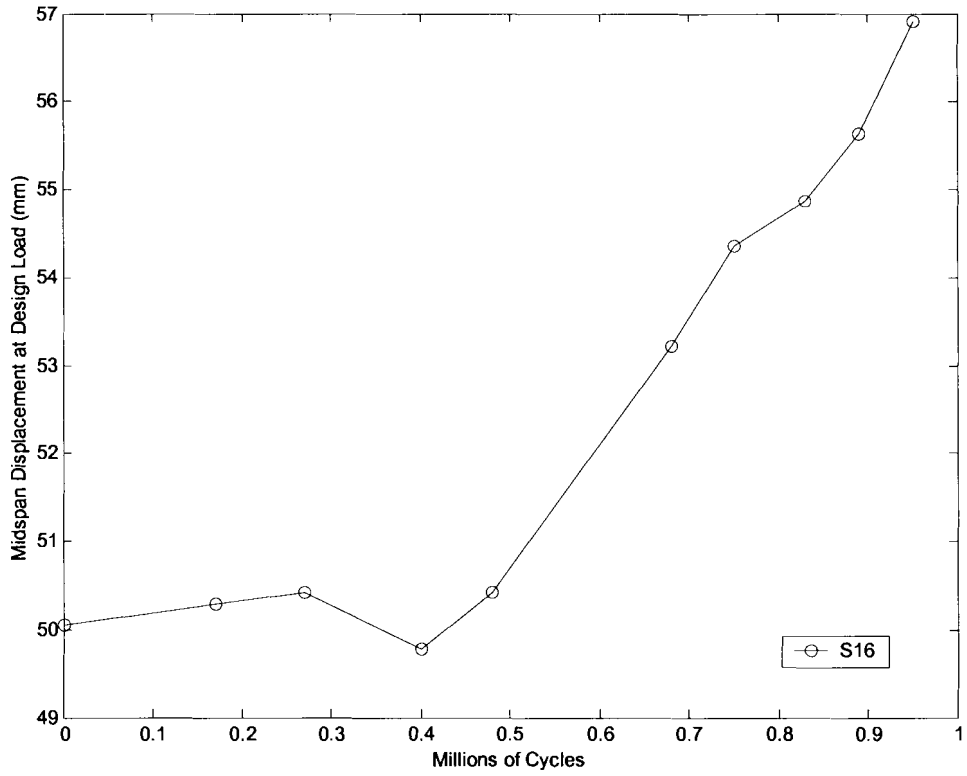

Figure 5.19 Stiffness vs Time plot for specimen S16.

Specimen S17 cycled for 101,000 cycles and failed in fatigue. No one was present to witness the failure, however, the conclusions drawn from examining the broken beam was that the failure initiated as a shear crack under the load head and propagating to the end of the beam. Figure 5.20 shows the beam post-failure, still in the testing apparatus. The cracked section of the beam between the end of the beam and the load head then failed in tension, pulling the lags screws out and cracking the beam in the compression region. Because of the short life span of the beam only an initial static test was performed and therefore there is no plot of stiffness degradation over time.

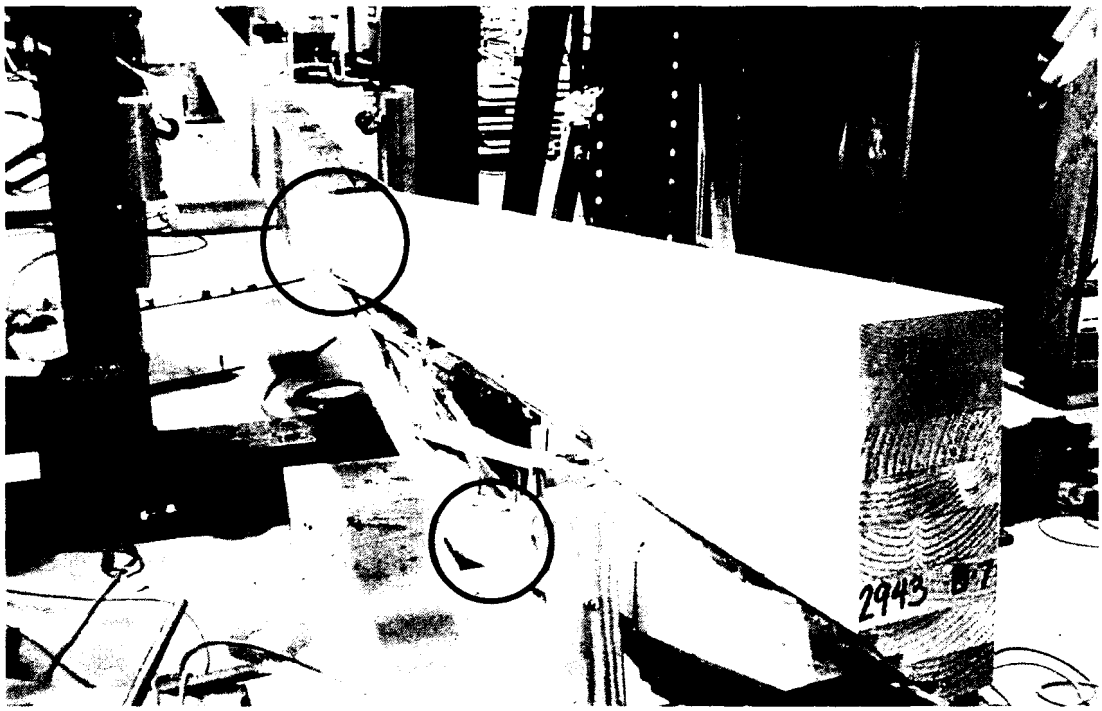

Figure 5.20 Specimen S17, post-failure. Top circle highlights point of initial shear failure and subsequent tensile failure. Bottom circle shows the lag screws.

Specimen S18 failed after only 19,722 cycles, the shortest period of any of the beams tested. The failure was primarily a tension failure at a finger joint which occurred in the second lamination from the bottom near the center span of the beam. The failure caused the FRP to peel off and pull out of the restraints in a block shear fashion (see Figure 5.21). Because of the short life span of the beam only an initial static test was performed and therefore there is no plot of stiffness degradation over time.

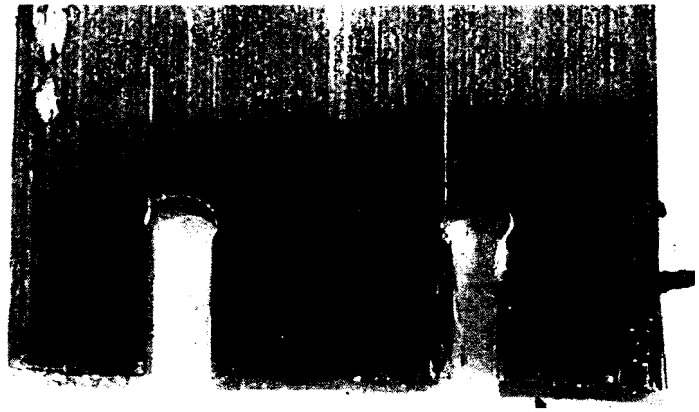

Figure 5.21 Block shear failure of termination of partial length reinforcing

5.5 Summary of Fatigue Testing Results

To evaluate the fatigue durability of FRP as a reinforcing for glulam bridge girders, eighteen structural-scale specimens were tested with varying stress levels and reinforcing lengths. Beams were fatigued at stress levels corresponding to 100% and 130% of the design flexural strength. Twelve beams were tested at $1.0F_b$ with full length reinforcing and six were tested with partial length reinforcing. Of the six beams tested at $1.3F_b$, three were fully reinforced and three were partially reinforced. Table 5.1 gives a summary of the results of all of the fatigue tests performed.

The six specimens that were fatigued at $1.0F_b$ with full-length reinforcing showed good fatigue durability. Three of the specimens tested were 6,700 mm in length (6,400 mm span) and the other three were 11,278 mm long (10,970 mm span). All six specimens were fatigued for the full 2 million cycle regimen with no significant stiffness loss or visible signs of damage. The average modulus of rupture for the three 11,278 mm long specimens was approximately 18% less than the 6,700 mm specimens. However, the average MOR of the 6700 mm specimens is significantly higher due to the

very high failure load of specimen S1. All six specimens failed in tension at a knot or finger joint near midspan.

The six partially reinforced 6,700 mm long beams were tested at $1.0F_b$, three of which had unrestrained FRP terminations and three had mechanically restrained terminations. Only one of the unrestrained specimens lasted the full 2 million cycles and failed at a load almost 28% less than the average capacity of the fully reinforced specimens of the same size. Problems arose with the unrestrained FRP terminations and it was found that the terminations needed to be otherwise confined. The two specimens that failed during fatigue failed due to a loss of bond at the FRP termination which caused a subsequent tensile failure in the beam. The mechanical restraints seemed to solve this problem by adequately confining the terminations during fatigue. All three of the mechanically restrained partially, reinforced specimens lasted the full 2 million cycles and broke at a load 17% less than the fully reinforced specimens of the same size. Compression failures during fatigue were seen in one specimen from each of the unrestrained and restrained groups. In each case the compression failure caused a significant loss of stiffness which worsened with fatigue.

A group of six specimens were tested at a higher stress level of $1.3F_b$ to evaluate the effects of vehicular traffic overloading the bridge girders. Three of the six were fully reinforced and three were partially reinforced beams with mechanically restrained FRP terminations. The three fully reinforced beams all failed in fatigue at an average of 800,000 cycles. Two of the specimens exhibited compression failures during fatigue but ultimately failed in tension, and one failed in horizontal shear. The three partially reinforced specimens fared similarly to their fully reinforced counterparts, but lasted less

than half the time at an average of 360,000 cycles. The three partially reinforced specimens failed in tension with one failing in a combination of shear and then a subsequent tension failure.

Chapter 6

EVALUATING THE EFFECTS OF HYGROTHERMAL FLUCTUATIONS

6.1 Introduction

Temperature and relative humidity fluctuate significantly on an annual basis, affecting the equilibrium moisture content of wood. These naturally occurring hygrothermal (i.e. temperature and moisture related) fluctuations that are seen by in-service bridge girders can change the moisture profile in a glulam beam and cause significant shrinking and swelling in the wood. Due to different material properties, the FRP reinforcing is not subject to the same dimensional changes under variable moisture conditions. The shrinking and swelling of the wood produces peeling and shear stresses along the wood-FRP bond line. The effects of these stresses combined with the repeated loading seen by bridge girders may compromise the bond line of the reinforced glulam beams.

This chapter outlines the development of a study done to evaluate the effects of moisture cycling on the wood-FRP interface due to moisture cycling. Six of the 130 mm x 305 mm x 6700 mm beams using the 1.93% Gordon Composites E-glass reinforcing will be subjected to accelerated moisture and temperature cycling, reproducing the bond line stress history occurring during the design service life of a typical bridge girder. The goal of the cycling will be to evaluate the potential for possible delamination in the FRP-wood interface/bond line. The tests were to be conducted in a kiln with moisture generation capabilities. The beams were to be cycled in the kiln and then subjected to fatigue loading at stress levels corresponding to 100% and 130% of the allowable flexural

strength. The focus of this chapter is on the development of the procedure used to develop the kiln schedule, using coupled moisture transport and finite-element simulations of beam response.

6.2 Evaluating In-Service Hygrothermal Conditions

The first step in developing the kiln schedule was to evaluate the conditions that exist in the real-world for in-service bridge girders. Since there was a lack of previous work done in this area, much time was spent determining how to accurately replicate the moisture changes seen in a typical bridge girder under exterior conditions. These conditions were to be reproduced at an accelerated rate for a typical girder life of 50 years and condensed into the shortest workable time period. This was done by modeling the annual moisture diffusion through the cross section of a typical in-service specimen, using these moisture profiles to evaluate the stresses induced in the wood at the wood-FRP interface and then working those results around the limits of the kiln.

6.2.1 One-Dimensional Moisture Transport Model

A one-dimensional time dependent moisture diffusion model was written in MATLAB to model the change in moisture content in the beam over time. The model followed Fick's Law of Diffusion and returned moisture values at user specified locations along the cross section of the beam. Based on prior analyses done by Gamache (2001), it was determined that for the purposes of these hygrothermal conditioning tests a one-dimensional model would be sufficient to provide the necessary moisture profile data needed to develop a test procedure. This model was used to run simulations on the 130

mm wide cross section using equilibrium moisture contents (EMC) as boundary conditions. Input for the model included width of the cross section, number of divisions of the cross section, time that the model was to be run, number of time steps, the diffusion coefficient, the initial moisture conditions in the beam and the boundary conditions. The model returned a matrix of moisture values at every time step at each division across the width of the beam.

The model was governed by Fick's Law of Diffusion and was a one-dimensional linear solution to the governing partial differential equation (PDE). The governing PDE takes the form of:

$$\frac{\delta C}{\delta t} = D\frac{\delta^2 C}{\delta x^2} \qquad \text{Eqn 6.1}$$

where C is the moisture content, t is time, D is the diffusion coefficient and x is the space coordinate. In reality, the diffusion coefficient is a function of the moisture content. Therefore D in the equation would change for every new value of C, making the problem nonlinear. However, the equation for the diffusion coefficient used in the model was the same equation used by Gamache (2001), which was taken from Toratti (1992) and is given below in Equation 6.2.

$$D = 0.01607[e^{(0.0228C)}] \qquad \text{Eqn 6.2}$$

In the diffusion coefficient equation, C is the moisture content and D is given in units of in^2/day. Because of the significant amount of variability in wood and the variablility in published diffusion coefficients, the accuracy of using a nonlinear model to recalculate D for every new C is questionable. Also, the value of the diffusion coefficient for moisture contents between 5% and 15% varies by at most 12% from the diffusion coefficient at a mean moisture content of 10%. The graph in Figure 6.1a below is a plot

of the diffusion coefficient for moisture contents of 0% to 100% and Figure 6.1b shows the linearity of D between 5% and 15%. For these reasons, a diffusion coefficient of 12.903 mm^2/day, which corresponds to a moisture content of 10%, was used for all simulations.

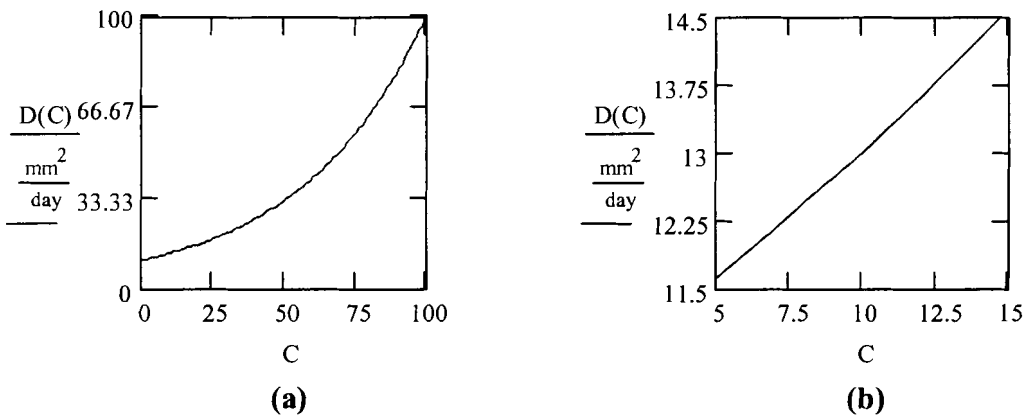

Figure 6.1 **(a)** Plot of Diffusion Coefficient for Moisture Content range of 0-100% **(b)** Plot of Diffusion Coefficient for Moisture Content range of 5-15%.

6.2.2 Annual Weather Data

The annual fluctuations in temperature and relative humidity in several cities in the New England region were examined to determine the most severe conditions a beam would be subjected to under environmental conditions. Values for these properties were obtained from The Weather Handbook (1990). This reference contains average data for the morning and evening relative humidity and the minimum and maximum normal daily temperature among other information. These temperature and relative humidity values were averaged and then converted to equilibrium moisture contents in the beam. The equation for converting a given temperature in Fahrenheit and a given relative humidity was found in the Wood Handbook and is in the form:

$$EMC = \frac{1800}{W}\left(\frac{Kh}{1-Kh} + \frac{K_1Kh + 2K_1K_2K^2h^2}{1+K_1Kh+K_1K_2K^2h^2}\right) \qquad \text{Eqn 6.3}$$

$$W = 330 + 0.453T + 0.00415T^2$$
$$K = 0.791 + 0.000463T - 0.000000844T^2$$
$$K_1 = 6.34 - 0.000775T - 0.0000935T^2$$
$$K_2 = 1.09 + 0.0284T - 0.0000904T^2$$

In the above equation, EMC is the equilibrium moisture content, and h is the relative humidity (%/100). W, K, K_1, and K_2 are constants that vary with temperature, T. According to the Wood Handbook, this relationship is applicable to any wood species.

Severity, in terms of EMC fluctuations, was based on the range of moisture contents throughout the year. The most severe case for the New England area presented in the Weather Handbook (1990) was that of Caribou, Maine where the EMC ranged from 12.5% to 16.1%, and the decision was made to base the procedure on this data set in order to be conservative with the testing. Table 6.1 shows the weather data obtained for Caribou, Maine.

Table 6.1 Temperature, RH and EMC data for Caribou, ME (Conway and Liston, 1990).

	Jan	Feb	Mar	April	May	Jun	Jul	Aug	Sep	Oct	Nov	Dec
RH am	74%	75%	76%	79%	79%	84%	84%	89%	89%	86%	85%	79%
RH pm	66%	63%	61%	57%	53%	56%	58%	59%	60%	62%	72%	71%
Ave RH	70%	69%	69%	68%	66%	70%	71%	74%	75%	74%	79%	75%
Ave Temp	10.7	13	24.3	37.3	50.2	60.3	65.1	62.5	53.6	43.1	31.1	15.7
EMC Ave	13.4	13.2	13.3	13.1	12.5	13.3	13.4	14.3	14.6	14.6	16.1	14.8

Annual fluctuations of this data fit roughly to a sinusoidal function. Figure 6.2 is a plot of the change in equilibrium moisture content over the year. The lowest annual equilibrium moisture content occurs around day 120 while the annual high occurs around day 300.

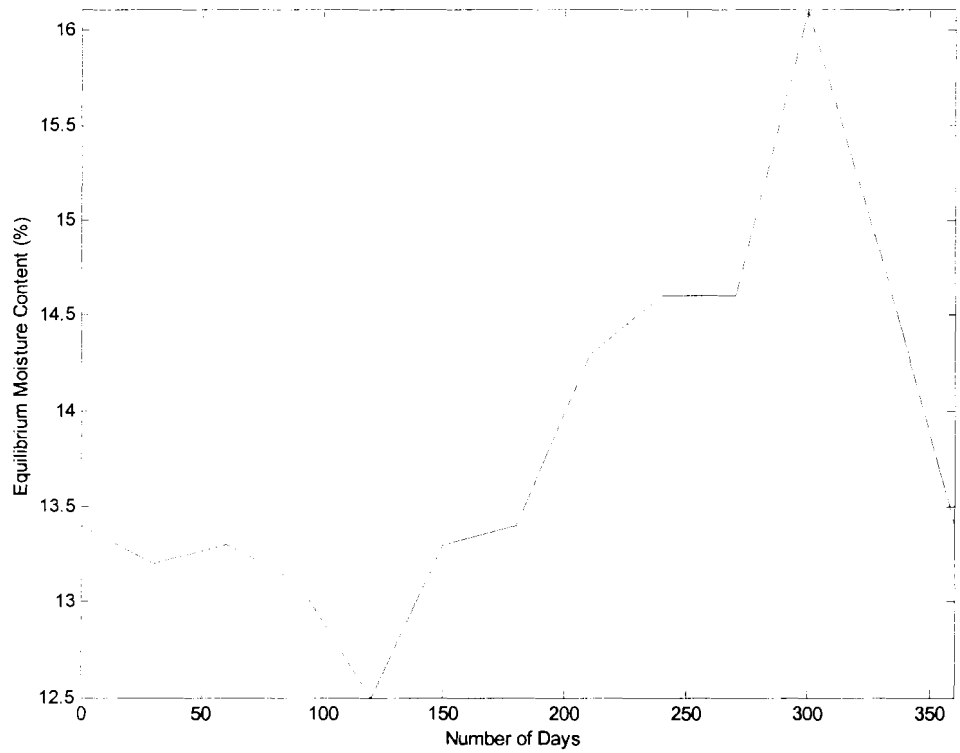

Figure 6.2 Plot of annual EMC fluctuation.

6.2.3 Convergence of Diffusion Model

To establish that the model was returning reliable results, convergence had to be established for the number of cross-sectional divisions and the number of time steps. Also, the initial conditions for the specimens needed to be determined along with the period of time necessary for the specimens to reach equilibrium with the environment.

6.2.3.1 Convergence for the Number of Cross-Sectional Divisions

In order to determine the appropriate number of divisions in the cross section and appropriate size time step, a convergence study was done. The model was run holding the time step constant and changing the number of divisions in the cross section, Δx, for

several incrementally small values until there was little evidence of change between iterations. A plot of the solutions to the model as Δx varied with changes in the number of cross sectional division can be seen below in Figure 6.3 below. The model was tested with 15, 50, 75 and 100 divisions of the cross section, and convergence was achieved after 50 divisions in the cross section. The dashed line in the plot below represents 15 divisions of the cross section. The segmented nature of the line indicates that more divisions are necessary to fill in the values between segments and smooth out the line. A smoother function is desired to give a more accurate representation of the moisture profile. The plots for 50, 75, and 100 divisions are almost coincident and therefore anything over 50 divisions was deemed acceptable for use as input for the model. These plots all show much smoother functions than the plot of 15 divisions and the difference in the shape of the plots is negligible.

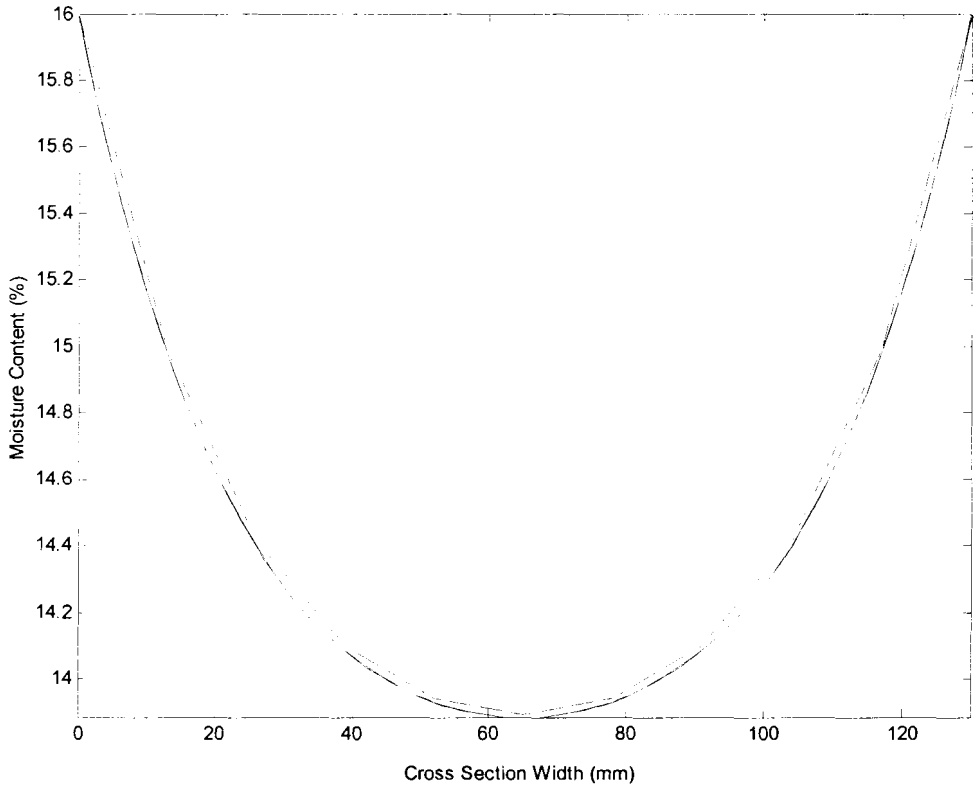

Figure 6.3 Convergence of cross-sectional divisions, Δx.

6.2.3.2 Convergence for the Number of Time Steps

Once a reliable value for the number of divisions in the width of the cross section was established, another convergence study was done for the size of the individual time steps. Holding the number of divisions constant at 50, the time step was varied and the solutions plotted. Time step values of 2 day, 1 day, ½ day, and ¼ day were used and their plots can be seen in Figure 6.4 below. As can be seen the plots of all 4 time step values are almost coincident. A time step of 1 day was convenient to work with in terms of calculation time and was found to be sufficiently small, and was thus selected.

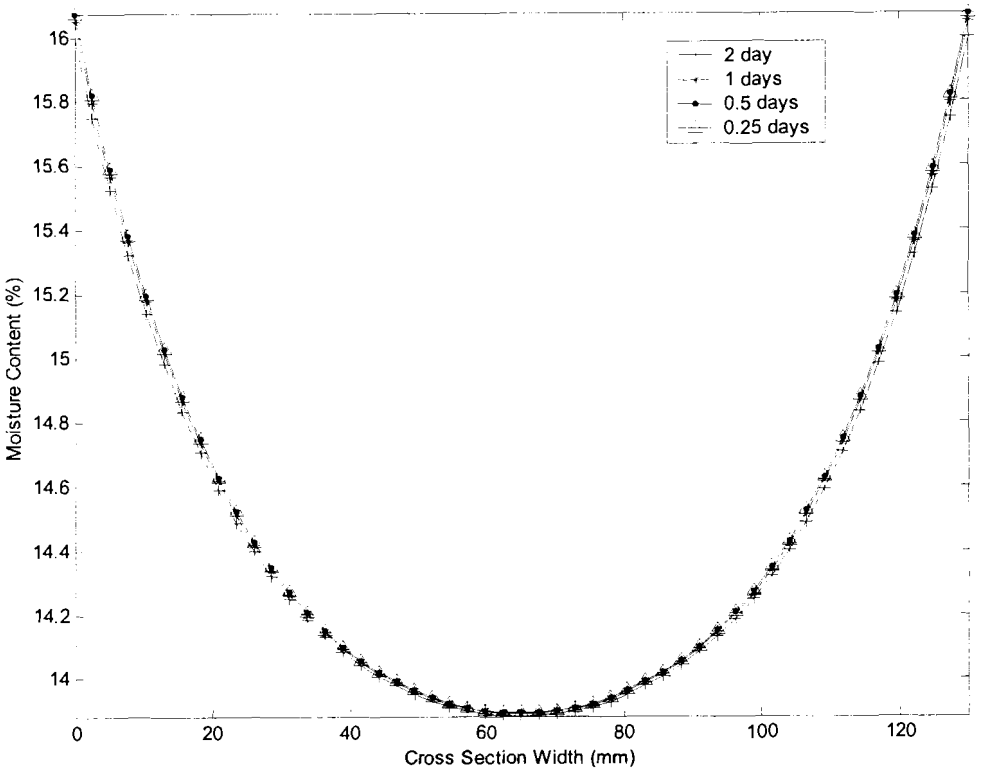

Figure 6.4 Convergence of time step value, time_step.

6.2.3.3 Initial Conditions

The next issue to be resolved was that of the initial conditions in the beam. The initial conditions were entered as an initial moisture content value for every point in the cross section. During the daily static tests of the beams tested in fatigue, moisture readings were taken using an electric moisture meter. The beams tested in the laboratory fluctuated between an average of 7% and 12% moisture content, depending on the time of year. This reading gave only an average moisture content for the outer edge of the beam. To get a more accurate reading the moisture profile throughout the cross section, an oven-dry test was conducted on several sections of a previously tested beam. This test was performed during the month of January, under relatively dry laboratory conditions.

The oven dry test followed the protocol outline in ASTM D 4442-92 and D 4933-99 (ASTM 2000). Three sections were cut from the mid span of three different beams. These were then cut into small blocks resulting in two sets of blocks; one set of the outer third of the beam and the other set from the inner third of the beam.

The oven dry test was conducted and the results showed that the average moisture content in the outer third of the beam was 7.45% and 8.23% in the inner third of the cross section. From these results, a constant moisture profile of 7% moisture content was used as the initial conditions for the model. This represents a conservative approach to the developing a hygrothermal testing procedure. The 7% is on the low end of the moisture contents observed in the beams and thus will give the greatest difference in moisture content between the manufacturing stage and environmental conditions, leading to the highest stresses due to differential shrinkage and swelling at the wood-FRP interface.

6.2.3.4 Boundary Conditions

The last variable in the model was the boundary conditions. These represented the external moisture conditions that the beam would be faced with on an annual basis. The boundary conditions were based on the Caribou, Maine data discussed earlier. This data was interpolated to give a moisture content value for every single-day time step.

6.2.3.5 Establishing an Equilibrium Point for In-Service Beams

With all of the variables established, the model was then run for several simulations to see where the annual fluctuations in moisture content reached equilibrium with the inner core of the cross section. This was done by running the model for several

annual cycles and examining the results to see when the core seemed to no longer be affected by the moisture fluctuations. The input variables discussed earlier were used in this analysis and the plots can be seen in Figure 6.5 below. Plots were generated for the January moisture profile in the cross section for a period of one year, two years, four years, five years and eight years. After a period of four years, the moisture content of the core is stable and any changes are due to the monthly changes of the boundary conditions. The line denoted by circles and the line denoted with triangles are the profiles after one annual cycle and two annual cycles, respectively. The line marked with x's at the top of the plot represents the profile after four years and is coincident with the plotted lines for five years and for eight years.

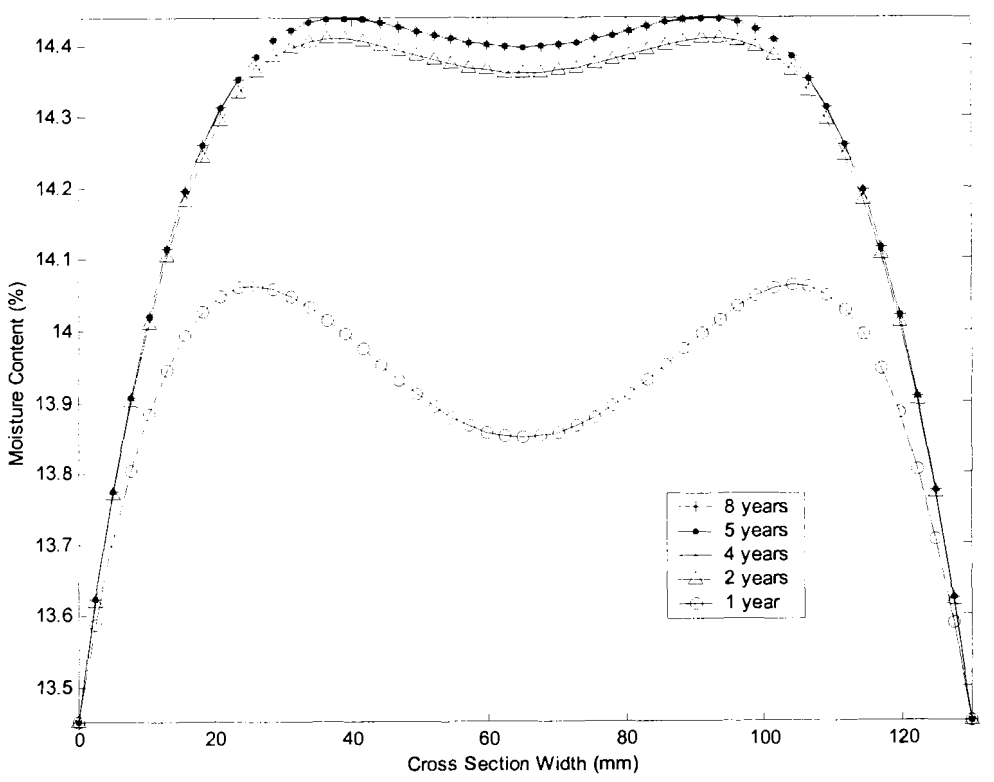

Figure 6.5 Moisture Profile for month of January after 1, 2, 4, 5, and 8 years.

Determining when the core of the beam would reach equilibrium was needed in order to determine where to start running the model for the hygrothermal stress analysis. Although initial shrinkage and swelling may cause the highest stress concentrations in the bond line of the reinforced beam, the period of time that the specimen is exposed to this higher stress level is relatively insignificant compared to the entire service life of the beam. Therefore, it was decided that the best way to model the cycling in the beam would be to try to reproduce the monthly changes a beam would see when exposed to these exterior conditions.

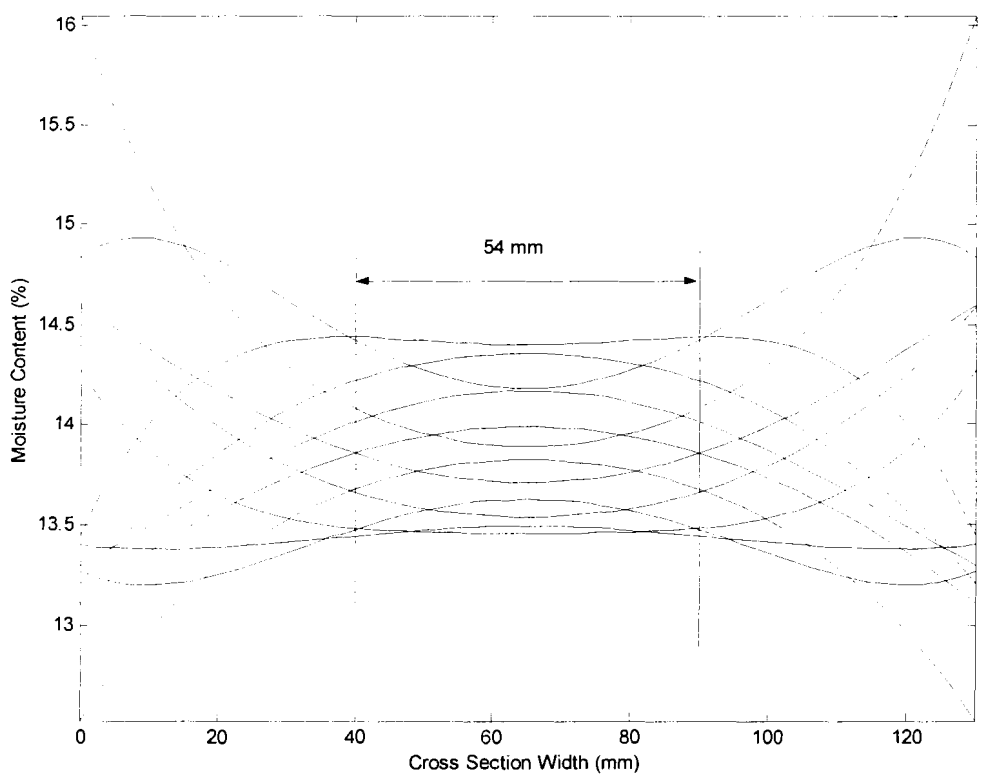

Figure 6.6 Plot of moisture profile for 12 months data after initial 4 years.

Figure 6.6 shows the variation in moisture profiles in the beam over a twelve month period, after the core has reached equilibrium. Over the middle 54 mm of the

cross section, the core moisture content changes only about 1% over the year. The stresses developed in this section due to shrinkage and swelling are less significant than the stresses developed on the outer 38 mm of either side of the beam. This outer 38 mm on either side of the cross section was identified as the "critical stress region" and was used later to help evaluate the magnitude of the cumulative stress history due to cyclic moisture change and develop a justifiable kiln schedule. The maximum range of moisture contents in this critical stress region is approximately 3.6%. This critical stress region is unique to this case and specific to this wood species and specimen dimensions. To develop the same parameter for other species of wood with different dimensions, the same technique as described above should be followed.

The moisture contents displayed in Figure 6.6 were not used directly to evaluate the stress conditions that result from the changes in moisture content. Instead, an average moisture content was determined, which was approximately 13.93%, and the change in moisture content, above or below this average, was used as input into a finite element model to evaluate the stress conditions resulting from the highest and lowest annual moisture contents.

6.3 Kiln Conditioning Limits

Ideally, the kiln conditioning would reproduce the cumulative stress history seen with the in-service beams at a highly accelerated rate, meaning the cumulative stress history occurring in one kiln cycle would be much greater than that of one cycle under in-service conditions. The most efficient way to achieve this was to cycle the equilibrium

moisture content between the upper and lower limits of the capabilities of the kiln and moisture generator.

Based on testing performed by laboratory personnel, the kiln and moisture generator were capable of producing equilibrium moisture contents ranging from 0.4% to 21.3%. The total time to needed to equilibrate from one extreme to the other was approximately five hours. Using these limits, the diffusion model was run for several different lengths of exposure time to see the degree of moisture penetration into the cross section. From the results, an exposure time of 60 hours showed reasonable penetration of moisture (about 15 mm) and was used for subsequent finite element modeling. Figure 6.7 compares the high and low moisture profiles for both the kiln conditioning limits and the in-service conditions.

Using moisture profiles from the kiln conditioning and in-service simulations, changes in moisture content were determined and finite element models using the ANSYS program were required to evaluate the stresses that develop due to the moisture changes over the year. The changes in moisture content were found in the same manner as described previously for the environmental conditions.

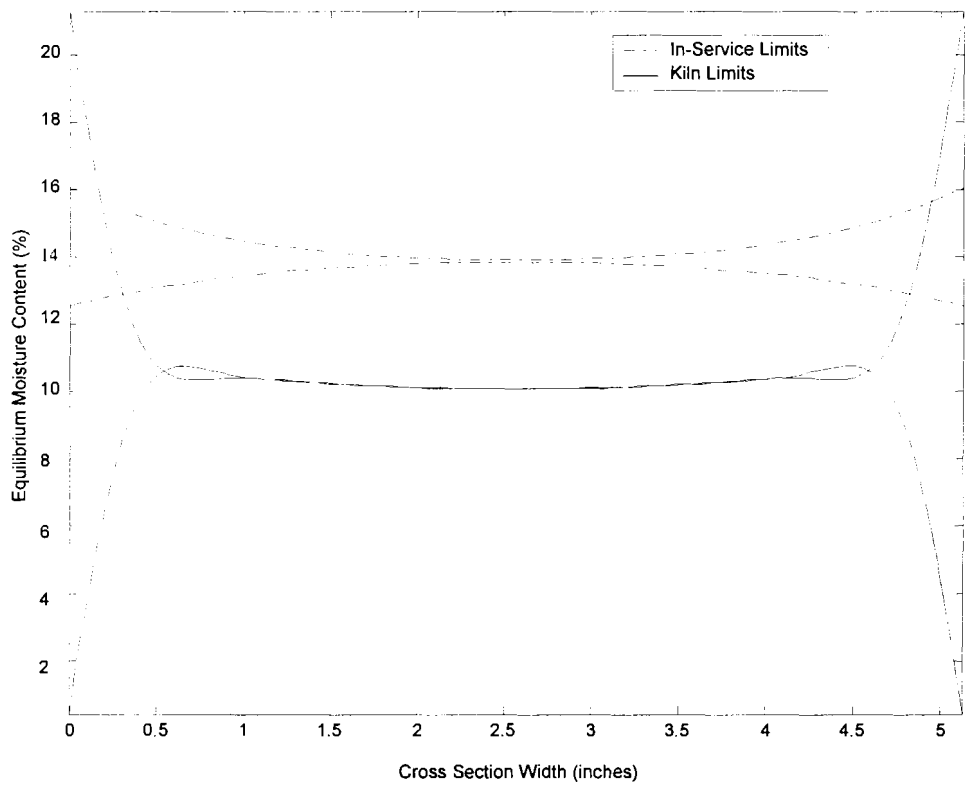

Figure 6.7 Extreme kiln limits overlaid on in-service high and low conditions

6.4 ANSYS Modeling

ANSYS, a finite element software package was used to model the stresses that develop at the wood-FRP interface. ANSYS does not have specific moisture analysis capabilities, however, the moisture profiles can be entered as temperature profiles and the thermal expansion coefficient becomes the moisture expansion coefficient. The temperature profile for this study was entered as changes in moisture content from an established average value. The modeling procedure used was performed in a similar manner to prior research done by both Gamache (2001) and Sanchez (2002). The goal of the model was to quantify the stresses that develop in the beam's cross section due to moisture fluctuations for the purpose of developing an accelerated conditioning schedule

that reproduces the effects of cumulative hygrothermal stress history over the life of a typical bridge girder.

6.4.1 Model Properties and Assumptions

A plane stress ANSYS finite element model was built using the cross-sectional properties of the 6700 mm specimens. The cross section of the glulam measured 305 mm by 130.2 mm and the FRP measured 6.35 mm by 130.2 mm. The FRP-wood interface was modeled as a completely fixed bond and the properties of the FRP were taken directly from the manufacturers published values (Gordon Composties, Inc, 2002). The properties of a glulam are often hard to characterize as radial and tangential due to the sometimes random order of the grain orientations between the different laminations. The glulam properties for the model were an average value of both radial and tangential values taken from the Wood Handbook (Forest Products Lab, 1999). The moisture expansion coefficient for the Douglas–fir glulam was calculated as outlined by Breyer, Fridley and Cobeen (1998). Table 6.2 list the properties used in the model for the FRP and glulam. The glulam beam and FRP were modeled as linear elastic, isotropic materials, which is a reasonable assumption for modeling the cross section of a beam.

Table 6.2 Model Properties for ANSYS finite element model.

Property	Glulam (Douglas-Fir)	FRP (Unidirectional E-glass)
Elastic Modulus	96170 psi	598000 psi
Poisson's Ratio	0.382	0.3
Moisture Expansion Coefficient	0.0020667	0

The element used to evaluate the model was the ANSYS PLANE42 2-D structural solid plane stress element. The four noded element has two degrees of freedom at each node (x and y translation) and has swelling capabilities (ANSYS 2000).

6.4.2 Finite Element Modeling Procedure

Significant stress concentrations occur at the interface of the FRP and wood due to the different behavior of the two materials under hygrothermal fluctuations (Gamache, 2001). To evaluate the hygrothermal shear and peeling stresses, the high and low moisture profiles from the kiln conditioning data were entered as a temperature profiles in the model. The temperature profile entered was actually a temperature change profile, taken by subtracting the temperature value at each point in the cross section from the average annual equilibrium moisture content, which was found to be approximately 14%.

Several models were built using different mesh densities in order to check for stress convergence in the model. Models were built with mesh sizes corresponding to 50, 60, 75 and 100 divisions along the width of the cross section. These divisions corresponded to a mesh density of approximately 6000, 8600, 13500 and 23900 nodes per model, respectively. Figure 6.8 shows the convergence of the model for both the tensile and shear stresses. Convergence was based on a cumulative stress history calculation, explained in more detail later, and the mesh density.

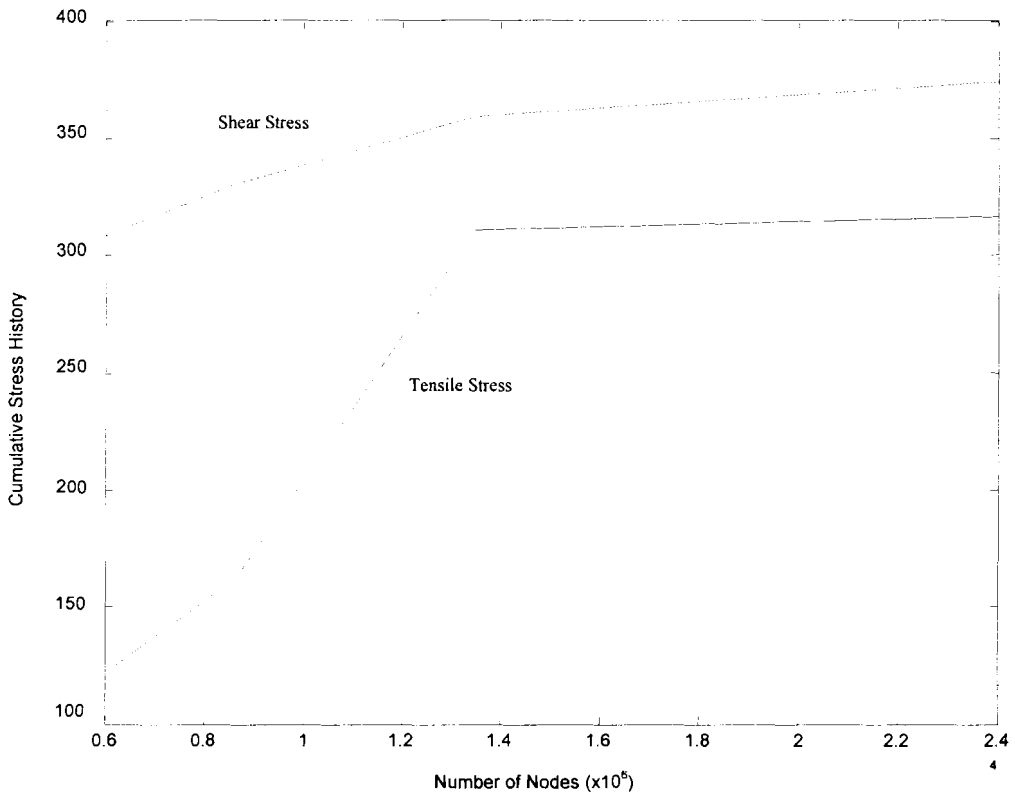

Figure 6.8 Mesh Convergence for Hygrothermal Finite Element Model

As can be seen from the above figure, the stress history is convergent with about 13500 nodes, or 75 divisions of the cross section for both tensile and shear stresses. For the purpose of evaluating the stresses that occurs at the wood-FRP interface, a mesh consisting of approximately 24000 nodes, or 100 divisions of the cross section was used in the models. This made each element a square with sides of a length of 1.3 mm. A screen image of this mesh can be seen in Figure 6.9.

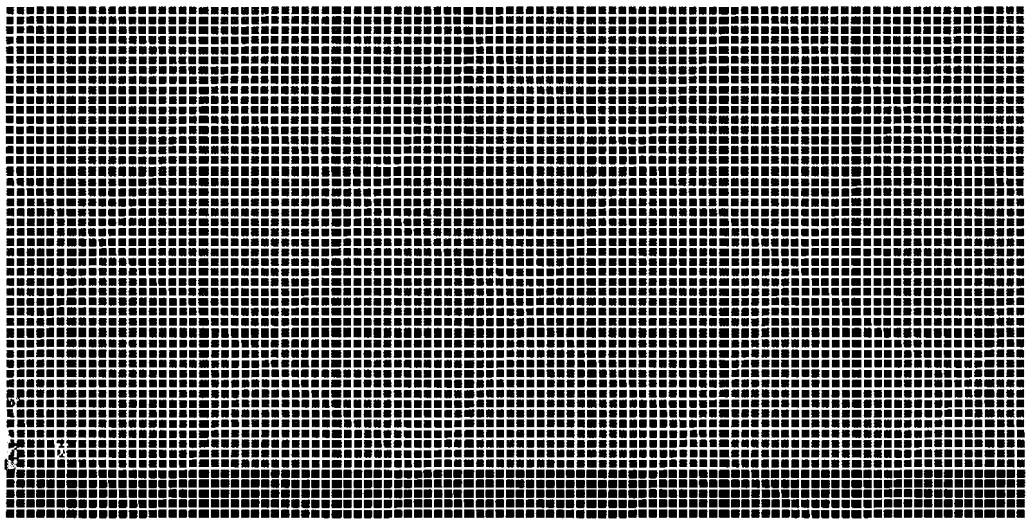

Figure 6.9 Mesh used for finite element model. The darker color on the bottom represents FRP, the lighter color represents the wood. Close-up of bottom quarter of cross section.

6.4.3 Results of ANSYS Finite Element Model

Finite element models were run for the annual high and low moisture profiles seen in a 305 mm by 130 mm FRP-reinforced glulam cross section to quantify the peeling stresses at the wood-FRP interface. Figures 6.9 through 6.12 show the contour plots of the results of the finite element models for the cyclic high point for the real-world and the kiln conditions, respectively. Figure 6.9 and 6.10 compare the normal (y-direction) tensile stresses and XY-shear stresses resulting from the cyclic high moisture profile conditions for the in-service and kiln parameters. Figure 6.11 and 6.12 shows the tensile stresses for the low moisture conditions for the in-service and kiln parameters. As expected, the highest stresses occur on the outside edge of the wood-FRP interface. ANSYS reports user specified stresses at each node and the stresses along the bond line were then used to make an estimate of the cumulative stress history occurs in one annual cycle.

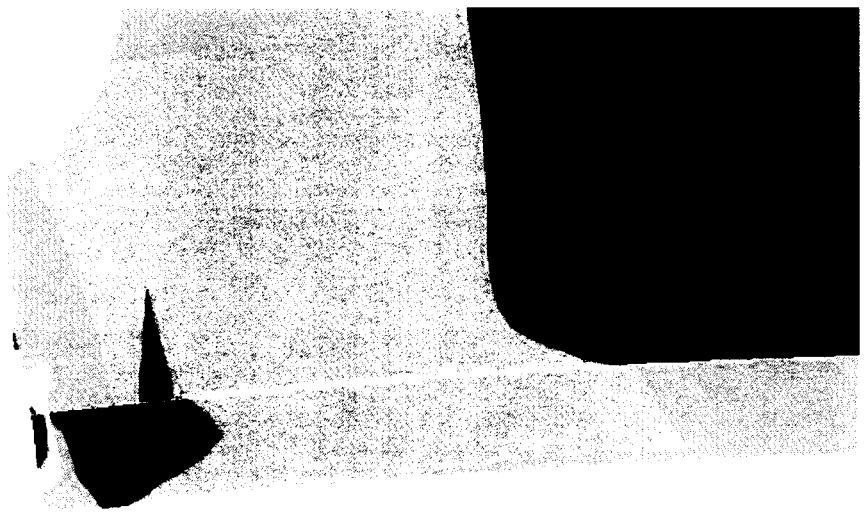

(a)

(b)

Figure 6.10 **(a)** Tensile stresses for annual high moisture profile, in-service conditions. Close-up of bottom left corner of cross section. **(b)** Tensile stresses for cyclic high moisture profile, kiln conditions. Close-up of bottom left corner of cross section.

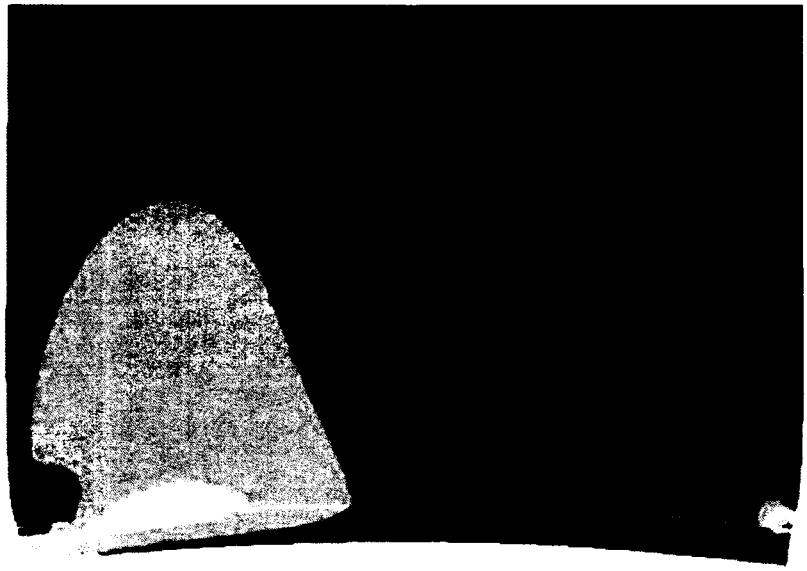

(a)

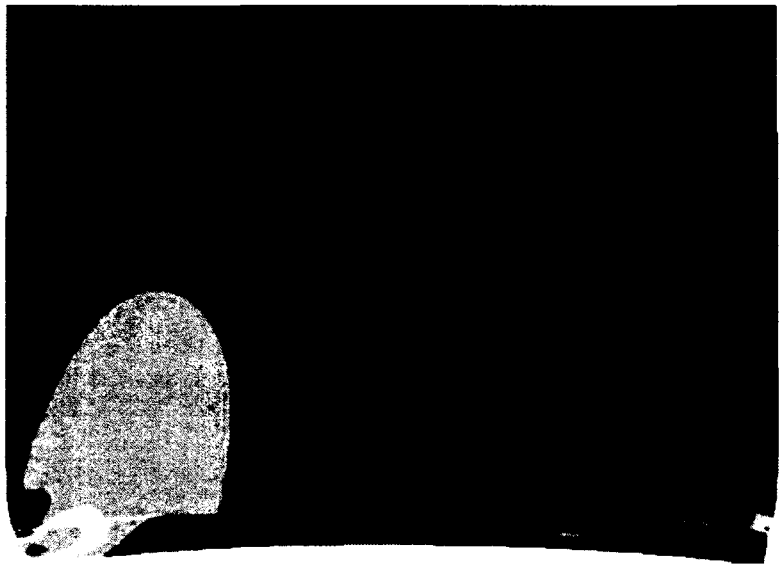

(b)

Figure 6.11 **(a)** XY-shear stresses for annual high moisture profile, in-service conditions. Close-up of bottom half of cross section. **(b)** XY-shear stresses for cyclic high moisture profile, kiln conditions. Close-up of bottom half of cross section.

(a)

(b)

Figure 6.12 **(a)** Tensile stresses for annual low moisture profile, in-service conditions. Close-up of bottom left corner of cross section. **(b)** Tensile stresses for cyclic low moisture profile, kiln conditions. Close-up of bottom left corner of cross section.

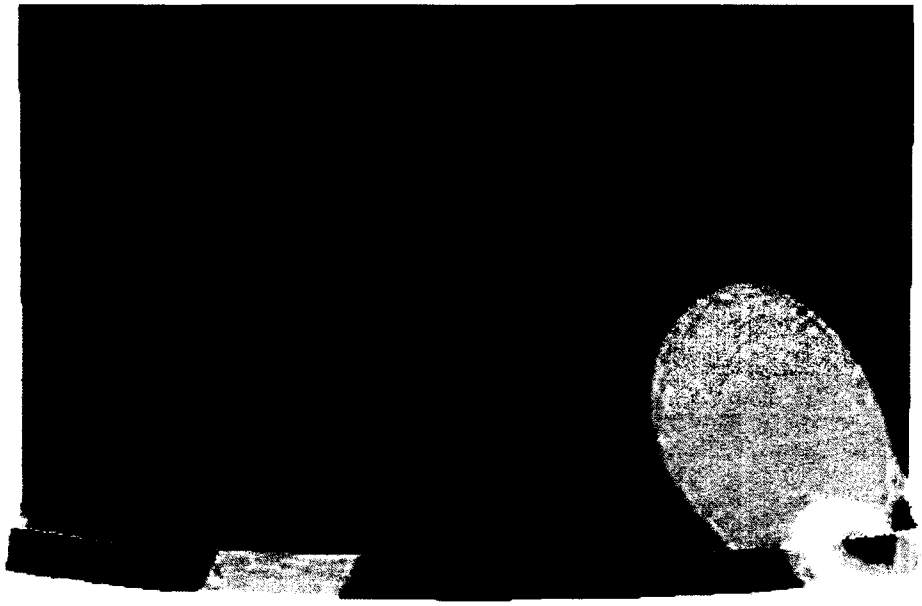

(a)

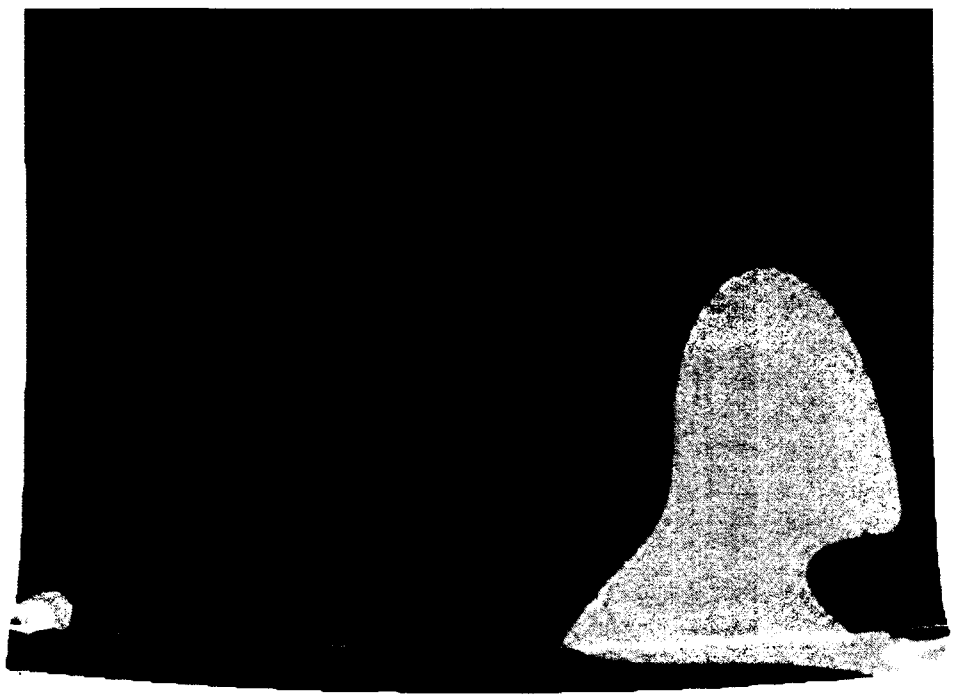

(b)

Figure 6.13 **(a)** XY-shear stresses for annual low moisture profile, in-service conditions. Close-up of bottom half of cross section. **(b)** XY-shear stresses for cyclic low moisture profile, kiln conditions. Close-up of bottom half of cross section.

6.5 Defining Cumulative Stress History

In order to compare the stress states that occur for the in-service annual high and low moisture profiles and the kiln-conditioned high and low moisture profiles, some estimate was needed to quantify the cumulative stress history that occurs during each cycle. A single cycle would consist of both a high and low moisture condition. In the case of in-service bridge girders, one cycle would represent one year of hygrothermal changes. For the kiln-conditioned beams, one cycle consists of some predetermined period of time where the beam is subjected to both a period high and low moisture contents. Making an estimate of the cumulative stress history due to one cycle established a commonality with which the kiln-conditioned beams could be compared to the real-world moisture fluctuations and a kiln schedule could be developed.

The four key assumptions made in quantifying the cumulative stress history were as follows:

1. All significant stresses occurs over the critical stress region (see section 6.1.3.5), denoted as length a in the equations to follow. Stresses in the center portion of the beam are insignificant and do not affect the performance of the reinforcing.
2. The stress history accumulates in a linear fashion, meaning the amount of cumulative stress history is directly proportional to the number of cycles.
3. The cumulative stress history is proportional to the magnitude of the stress reversal. The stress range resulting from the difference in the high and low moisture conditions is directly related to the cumulative stress history.
4. The stress history along the bond line is caused by peeling stresses (i.e. tensile stresses in the y-direction) and/or shear stresses.

Using those four assumptions, the following three methods were used to quantify the stress history occurring along the bond line of the reinforced girders:

6.5.1 Cumulative Stress History - Method 1

$$StressHistory = n\int \frac{|\sigma_{\max} - \sigma_{\min}|}{a} da \qquad \text{Eqn 6.4}$$

Method 1 for defining cumulative stress history uses Equation 6.4, above, to define stress history in terms of peeling stress. In Equation 6.4, n represents the number of total cycles, $\sigma_{\max}$ and $\sigma_{\min}$ are the peeling stresses at the respective high and low moisture conditions and a is the critical stress region as defined earlier. This calculation takes into account the magnitude of the stress range involved and integrates it over the critical stress region in order to give a more accurate, averaged stress range and a basis for comparison between the kiln and real world conditions. This equation was implemented numerically, using a trapezoidal rule to integrate the stresses over the critical zone. Equation 6.2 below shows the numerical discretization of the stress history equation that was used to evaluate the results of the ANSYS finite element models. The value of Δa in the discretized equation represents the distance between points, or in this case the distance between nodes since stress values came directly from the nodal solution to the finite element models. The value of j represents the number of points or nodes in the critical stress region.

$$StressHistory = n\frac{\sum_{i=1}^{j} |\sigma_{\max} - \sigma_{\min}|_i \Delta a}{a} \qquad \text{Eqn 6.5}$$

Using the discretized equation, the cumulative stress history was calculated for the kiln and real-world simulations, with the number of cycles, n, for the kiln conditioned beams being an unknown. Using an average service life of 50 years for the beams, the unknown number of kiln cycles needed to reproduce the stress history occurring in the in-service beams was solved for and the kiln schedule was established. The kiln schedule for Method 1, based solely on tensile stresses in the y-direction, yielded a total of 7.2 kiln cycles at 120 hours per cycle, or approximately 36 days in the kiln.

6.5.2 Cumulative Stress History - Method 2

$$StressHistory = n\int \frac{|\tau_{\max} - \tau_{\min}|}{a} da \qquad \text{Eqn 6.6}$$

Method 2, seen above in Equation 6.5, utilizes the range of shear stress as a means of defining the cumulative stress history. In the equation for Method 2, $\tau_{\max}$ and $\tau_{\min}$ represent the shear stress for the high and low moisture conditions. This equation was also implemented numerically using the results of the finite element analyses in a manner very similar to Method 1, only replacing the peeling stresses with the shear stresses. Method 2 resulted in a kiln schedule of 14.2 kiln cycles at 120 hours per cycles, or approximately 71 days in the kiln.

6.5.3 Cumulative Stress History - Method 3

$$StressHistory = n[r_1 \int \frac{|\sigma_{\max} - \sigma_{\min}|}{a} da + r_2 \int \frac{|\tau_{\max} - \tau_{\min}|}{a} da] \qquad \text{Eqn 6.7}$$

Method 3 used a weighted combination of Method 1 and Method 2. Stress History in Method 3 is defined by Equation 6.7 and takes into account the relative

contribution of both the peeling and shear stresses to the cumulative stress history. The values of r_1 and r_2 in Equation 6.7 are ratios used to define the relative contribution of peeling and shear stresses, respectively. The ratios were calculated as shown in Equations 6.8a through 6.8d. The values of R_1 and R_2 give the ratio of average maximum applied stress to allowable stress, where F_{Tperp} is the value of the tensile strength perpendicular to grain and F_{RS} is the rolling shear strength. The value for F_{Tperp} came from the National Design Specifications for Wood Construction (American Forest and Paper Association 1997) and was 2.30 MPa. The value for F_{RS} came from page 4-24 of the Wood Handbook (Forest Products Laboratory 1999) which states that there are very few test values for rolling shear, however, rolling shear strengths have averaged 18-28% of the shear parallel to grain values. From this, the rolling shear strength for the specimens was calculated as an average 23% of the shear parallel to grain, or approximately 3.01 MPa. R_1 and R_2 were calculated for both the high and low moisture conditions and the maximum values were used in the equation.

$$r_1 = \frac{R_1}{R_1 + R_2} \qquad \text{Eqn 6.8a}$$

$$r_2 = 1 - r_1 \qquad \text{Eqn 6.8b}$$

$$\text{Where } R_1 = \frac{\int \frac{|\sigma_{\max}|}{a} da}{F_{Tperp}} \qquad \text{Eqn 6.8c}$$

$$\text{and } R_2 = \frac{\int \frac{|\tau_{\max}|}{a} da}{F_{RS}} \qquad \text{Eqn 6.8d}$$

Calculating stress history using this method was also implemented numerically using a trapezoid rule, as in Methods 1 and 2. The ratios r_1 and r_2 were calculated based

on real-world conditions and were used to calculate both the stress history for the real-world conditions and the kiln conditions. The rationale behind using the peeling and shear stress ratios from the real-world conditions is to more accurately reproduce the conditions seen in beams in-service. This would give a kiln-conditioned relationship between the peeling and shear stresses that more closely reflected that seen by in-service beams.

When calculating the stress history, special note was taken to check that the stress states for both the high and low moisture conditions did not produce stresses that were both positive or negative (i.e. both high and low moisture conditions produce tension or compression). If this were the case, the value for σ_{min} or τ_{min} was taken as zero. In cycling from the low moisture condition to the high moisture condition or vice versa, the beam would, in theory, pass through the initial stress state where no hygrothermal effects are present.

Assuming the stress history affecting the bond line is a combination of the applied peeling and shear stresses, just the stress history due to peeling or shear cannot by itself quantify the cumulative stress history. Thus, Method 3 was used to develop the kiln schedule for the beams subjected to hygrothermal weathering.

6.6 Kiln Schedule

To reproduce the estimated cumulative stress history occurring over a 50 year service life for the FRP-reinforced glulam beams, the kiln had to be run at its extreme limits for a period of 60 hours at the high and low limits, giving a total cycle time of 120 hours. The cumulative stress history was calculated using Method 3 combining both the

tensile stresses and the xy-shear stresses in the wood along the bond line. A total of 11 cycles in the kiln was needed to reproduce the stress history of a 50 year service life. Eleven cycles in the kiln at 120 hours per cycle translates to a total of 54 days of hygrothermal cycling. The weighted average used in Method 3 resulted in a kiln schedule very close to that of an straight average of Method 1 and 2 which give a kiln schedule of 53.2 days. However, the results from Method 3 were used for the kiln schedule.

6.7 Summary

A procedure was developed to reproduce the cumulative stress history due to hygrothermal changes seen in the service life of bridge girders in the New England area. The climactic conditions of one of the more extreme New England environments was used to model the moisture profiles for the annual high and low moisture conditions. The profiles were then incorporated into finite element models to quantify the induced peeling and shear stresses. The peeling and shear stresses were then used to evaluate the cumulative stress history over an annual hygrothermal cycle via a method that incorporates the relative contribution of both stresses. Following this procedure, the stress history produced by one kiln cycle was determined and the total number of number of kiln cycles necessary to match the stress history of 50 years of environmental cycling was found to be 11 cycles, or 54 days of hygrothermal fatigue.

Inherent conservatism is built into this testing procedure in a number of ways. The first and most conservative aspect is that all of the hygrothermal cycling will be done prior to the specimens being fatigued. Bridge girders in-service are being fatigued at the

same time they are undergoing moisture content fluctuations. Second, the modeling done did not account for creep in the wood, which would tend to alleviate the hygrothermally induced stresses. Also, the more extreme climatic data for the New England area was used for modeling the real-world moisture fluctuations and stresses.

The kiln schedule outlined in this chapter will be implemented on six reinforced glulam bridge girders and the effects of this carefully recorded. The beams will then be fatigued at stress levels of 100% of the design strength and 130% of the design strength. The specimens will be fatigued for 2×10^6 cycles or until failure, which ever occurs first, and then broken in static bending to determine the residual strength.

Chapter 7

SUMMARY AND CONCLUSIONS

7.1 Introduction

The objective of the completed research was to evaluate the fatigue durability of FRP-reinforced glued laminated bridge girders and to help determine the effectiveness of FRP as a reinforcing material. Preliminary research on this matter had been conducted which provided a good basis to form a plan of action for conducting the fatigue tests. The following chapter provides summaries of the work completed, as well as the conclusions drawn from the test results and recommendations for topics of future research.

7.2 Summary of Testing Program

A testing program was developed to evaluate the fatigue durability of structural scale FRP-reinforced glulam beams. The test involved cycling specimens in four-point bending for a total of two million cycles, or until failure. Specimens were sinusoidally cycled between a minimum and maximum load to produce two different flexural stress levels: $1.0F_b$ and $1.3F_b$, where F_b is the allowable bending stress. Loading at $1.0F_b$ fatigued the specimens at a stress ratio of R=0.333, which was based on a design of a typical 14,630 mm timber bridge girder. For the stress level of $1.3F_b$, the minimum load was held constant while the maximum load was increased to produce 130% of the allowable flexural stress. This produced a stress ratio of R=0.255.

Load heads were spaced to produce a shear stress to flexural stress ratio consistent with that seen in in-service timber bridge girders. Using this spacing, the peak loads produced 81% of the allowable shear stress simultaneously with $1.0F_b$ and 104% at $1.3F_b$.

The cycling frequency was limited by the capacity of the hydraulic system and actuators used to apply the loads and was found to be 2.0 Hz for the 6,700 mm long beams and 1.0 Hz for the 11,278 mm long beams.

An important note in the design of the testing program is that the lamstock data used to generate an estimate of the allowable flexural stress of the reinforced specimens was significantly higher than that of the lamstock used in the glulam specimens tested. Also, the transformed section properties of the specimens were erroneously used in place of the wood section properties to calculate flexural stress. The cumulative effect of these inconsistencies resulted in a conservative testing program, where the specimens fatigued at $1.0F_b$ were in reality being stressed at 1.52Fb, while the specimens fatigued at $1.3F_b$ were being stress at 1.98Fb.

7.3 Summary of Specimen Construction

A total of eighteen glulam beams were reinforced on the flexural tension side with an E-glass fiber reinforced polymer (FRP) for the purpose of fatigue testing. The glulam beams were purchased from a manufacturer and reinforced at the AEWC laboratory. Full length reinforcing was used on twelve beams while the remaining six were partially reinforced. Partial-length reinforcing was designed with and without restraints at the FRP terminations.

For both the full-length and partial length reinforcing, the FRP was bonded to the glulam beams using the same procedure. Three of the partially reinforced specimens had unrestrained FRP terminations with a 30 degree bevel on the FRP to alleviate peeling stress that occur at the end of partial length reinforcing. The other set of six partially reinforced specimens utilized steel plates and lag screws to mechanically confine the terminations and prevent the FRP from peeling off the glulam.

7.4 Summary of Mechanical Fatigue Testing

To evaluate the fatigue durability of FRP as a reinforcing for glulam bridge girders, eighteen structural-scale specimens were tested with varying stress levels and reinforcing lengths. Beams were fatigued at stress levels corresponding to 100% and 130% of the design flexural strength. Twelve beams were tested at $1.0F_b$ with full length reinforcing and six were tested with partial length reinforcing. Of the six beams tested at $1.3F_b$, three were fully reinforced and three were partially reinforced. Table 5.1, located in Chapter 5, gives a summary of the results of all of the fatigue tests performed.

The six specimens that were fatigued at $1.0F_b$ with full-length reinforcing showed good fatigue durability. Three of the specimens tested were 6,700 mm in length (6,400 mm span) and the other three were 11,278 mm long (10,970 mm span). All six specimens were fatigued for the full 2 million cycle regimen with no significant stiffness loss or visible signs of damage. The average modulus of rupture for the three 11,278 mm long specimens was approximately 18% less than the 6,700 mm specimens. However, the average MOR of the 6,700 mm specimens was significantly higher due to

the very high failure load of specimen S1. All six specimens failed in tension at a knot or finger joint near midspan.

The six partially reinforced 6,700 mm long beams were tested at $1.0F_b$, three of which had unrestrained FRP terminations and three had mechanically restrained terminations. Only one of the unrestrained specimens lasted the full 2 million cycles and failed at a load almost 28% less than the average capacity of the fully reinforced specimens of the same size. Problems arose with the unrestrained FRP terminations and it was found that the terminations needed to be otherwise confined. The two specimens that failed during fatigue failed due to a loss of bond at the FRP termination which caused a subsequent tensile failure in the beam. The mechanical restraints seemed to solve this problem by adequately confining the terminations during fatigue. All three of the mechanically restrained partially, reinforced specimens lasted the full 2 million cycles and broke at a load on average 17% less than the fully reinforced specimens of the same size. Compression failures during fatigue were seen in one specimen from each of the unrestrained and restrained groups. In each case the compression failure caused a significant loss of stiffness which worsened with fatigue.

A group of six specimens were tested at a higher stress level of $1.3F_b$ to evaluate the effects of vehicular traffic overloading the bridge girders. Three of the six were fully reinforced and three were partially reinforced beams with mechanically restrained FRP terminations. The three fully reinforced beams failed in fatigue at an average of 800,000 cycles. Two of the specimens exhibited compression failures during fatigue but ultimately failed in tension, and one failed in horizontal shear. The three partially reinforced specimens fared similarly to their fully reinforced counterparts, but failed

during fatigue at 360,000 cycles on average, about half as many cycles as the fully reinforced specimens loaded to the same level. The three partially reinforced specimens failed in tension with one failing in a combination of shear and then a subsequent tension failure.

7.5 Summary of Hygrothermal Fatigue Evaluation

A procedure was developed to reproduce the cumulative damage due to hygrothermal changes seen in the service life of bridge girders in the New England area. The climatic conditions of one of the more extreme New England environments was used to develop the moisture profiles across the glulam width corresponding to the annual high and low moisture conditions. The profiles were then incorporated into finite element models to quantify the induced peeling and shear stresses. The peeling and shear stresses were then used to evaluate the cumulative damage over an annual hygrothermal cycle via a method that incorporates the relative contribution of both stresses. Following this procedure, the damage produced by one kiln cycle was determined and the total number of number of kiln cycles necessary to match the damage of 50 years of environmental cycling was found to be 11 cycles, or 54 days of hygrothermal fatigue.

Inherent conservatism is built into this testing procedure in a number of ways. The first conservative aspect is that all of the hygrothermal cycling will be done before any mechanical fatigue cycling, which will maximize damage due to hygrothermal effects prior to fatigue. Bridge girders in-service are being fatigued at the same time they are undergoing moisture content fluctuations. Second, the modeling done did not account for creep in the wood, which would tend to alleviate the hygrothermally induced stresses.

Also, the more extreme climatic data for the New England area was used as input for modeling the real-world moisture fluctuations and stresses.

The kiln schedule will be implemented on six reinforced glulam bridge girders and the effects of this carefully recorded. The beams will then be fatigued at stress levels of $1.0F_b$ and $1.3F_b$ in the same manner as those specimens tested to date, and will be fatigued for 2 x 10^6 cycles or until failure, which ever occurs first, and then broken in static bending to determine the residual strength.

7.6 Conclusions

The results of this research provided valuable insight into fatigue durability of FRP-reinforced glulam bridge girders. Failure modes and durability issues have been better identified which provide insight into the long-term in-service behavior of reinforced glulam.

The full length reinforcing yielded good durability results under the administered testing program. One of the main conclusions drawn from full length reinforcing testing is that glulam beams with approximately 2% full length GFRP reinforcing do not seem to be prone to fatigue failures. Given the fact that the full length reinforced specimens were able to withstand two million fatigue cycles at 152% of the allowable design bending strength with no significant stiffness or strength losses indicates that there are no significant fatigue durability issues with the reinforced beams regarding their use in structural applications. This conclusion is exclusively with respect to the mechanical fatigue of the reinforced glulam and does not consider hygrothermal effects. Additionally, the study did not include the testing of preservative-treated girders, and

prior research has shown that preservatives may have detrimental effects on the reinforcing and/or the FRP-wood bond line.

The partial length reinforcing was a more complicated issue than the full length reinforcing. The necessity of restraints on the FRP terminations is the one definitive conclusion that can be drawn from the results of the testing performed. The poor performance of the partial length reinforced specimens with unrestrained terminations gave little confidence in their practicality in construction uses in bridges, or any application where the member would be subject to repeated loading and unloading. The specimens with mechanical restraints far outperformed the unrestrained specimens. The added material and labor costs may prohibit the use of partial length reinforced girders in new construction, however, this does not exclude their use in retrofitting applications. The results showed positive strength benefits from the reinforcing, which indicates the possibility for their use in reinforcing damaged or otherwise compromised members. Retrofitting with the same materials used in this research would require clamping the FRP to the existing structure, which could be a significant hindrance, therefore other methods of confining the reinforcing should be explored.

7.7 Design Recommendations

With regard to AASHTO design specifications, recommendations for untreated FRP-reinforced glulam beams stemming from this study include the following:

1. Full length reinforcing does not appear to be prone to fatigue failures.
2. For partial length reinforcing, adequate end restraints must be used to mechanically confine the FRP termination.

3. Knots should not be present near FRP termination of partial length reinforced beams (this study used a distance of 150 mm either side of the FRP termination).
4. The applied shear stress should be limited to 80% of the allowable design shear stress, F_v.

7.8 Recommendations for Future Work

The research presented in this thesis has helped provide justification for the use of FRP-reinforced glulam beams. There are several areas of research that would further justify their use and clarify lingering concerns. Future work in the area of fatigue durability of FRP-reinforced glulam beams should focus on better establishing the effects of hygrothermal fluctuations in the environment, the effects of fractures, delaminations and crack propagation, improving reinforcing techniques, and also the effect of common preservative treatments.

The potential for delaminations exists both in the manufacturing process and while the beam is in service. Many factors like knots in the wood and improper quality control contribute to delaminations in the manufacturing process while environmental factors such as hygrothermal stresses and ice flows can cause debonding in the field. A delamination can compromise the ability of the reinforcing to properly strengthen the beam and increases the likelihood of premature failure. A particularly important issue is the propensity of these delaminations to propagate under repeated loading and the effect this will have on the strength and life span of the beam.

Aside from the behavioral concerns, the reinforcing process holds much room for improvement. The process of bonding the FRP to the wood, while relatively simple, can be time consuming and labor intensive. The FPL 1A epoxy used to bond the FRP to the glulam required a minimum of eight hours under pressure for proper curing and strength. This process could be improved upon by integrating the reinforcing step into the manufacturing process of the glulam beams. If the FRP and bonding agent were compatible with the wood laminating process, it would save time and money.

In addition, the steel plate and lag screw method of confining the FRP termination served its purpose for the testing conducted here but is clearly not a viable option for construction. Testing showed that creep and hygrothermal fluctuations caused significant tension loss in the lag screws. Therefore, an improved method of confinement is necessary for commercial use of partial length reinforcement. More research could be done to better evaluate the stress condition at the FRP termination.

Further, in-service bridge girders are almost always preservative-treated, and the potentially detrimental effects of treatment on fatigue life should be considered in future studies.

Finally, this study considered only a single FRP-adhesive combination, while many such combinations exist. Future research should examine the effectiveness of a variety of commercially viable FRP reinforcing systems.

REFERENCES

AASHTO (1996). *Standard Specifications for Highway Bridges*, 16th Edition. American Association of State Highway and Transportation Officials, Washington, D.C.

American Concrete Institute. (1999). *Building Code Requirements for Structural Concrete (318-99) and Commentary (318R-99)* (Second Printing). Farmington Hills, MI.

American Forest & Paper Association. (1997) National Design Specifications for Wood Construction. Washington, DC: American Wood Council.

American Laminators. (2003). "Fiber Reinforced Glulam Beams." Available: www.americanlaminators.com.

ANSYS. (2000). *ANSYS 5.6.2 University high option.* [CD-ROM] SAS IP, Inc. Available: ANSYS, Inc.

APA: The Engineered Wood Association. (2003). *The Leading Resource for Information about Engineered Wood Products.* [Online] Available: http://www.apawood.org/.

APA: Engineered Wood Systems. (1996). *Glued Laminated Timber Appearance Classifications for Construction Applications.* [Pamphlet]. Tacoma, WA.

APA: The Engineered Wood Association. (1998, April). *FRP Plywood.* Available: http://www.apawood.org/pdfs/managed/G215-E.pdf

ASTM E1150/87. (1987). *Standard Definitions of Terms Relating to Fatigue.* American Society for Testing Materials. W. Conshohocken, PA: ASTM, 1-10.

Bagdahn, J., Sharpe, W., and Jadaan, O. (2003). "Fracture Strength of Polysilicon at Stress Concentrations." *Journal of Microelectromechanical Systems.* 12(3), 302-313.

Bodig, J., and Jayne, B. (1982). *Mechanics of wood and wood composites.* New York, NY: Van Nostrand Reinhold Inc.

Breyer, D.E., Fridley, K.J., and Cobeen, K.E. (1998). *Design of Wood Structures, Fourth Edition.* New York: McGraw-Hill.

Chawla, K.K. (1987). *Composites Materials: Science and Engineering.* New York, NY: Springer-Verlag.

Cheng, S., Chen, D., and Shi, Y. (1991). "Analysis of Adhesive-Bonded Joints with Non-identical Adherents." *Journal of Engineering Mechanics.* 117(3), 605-623.

Christiansen, A.W., and Okkonen E. (2003). "Improvements to Hydroxymethylated Resorcinol Coupling Agent for Durable Bonding to Wood." *Forest Products Journal.* 53(4), 81-84.

Christiansen, A.W., and Vick, C.B. (1991). "Hydroxymethylated Resorcinol Coupling Agent for Wood Surfaces to Produce Exterior Durable Bonds. In K.L. Mittal (Ed.), *Proceedings of the Symposium on Silanes and Other Coupling Agents* (pp. 193-208). Midland, MI.

Coffey, D. (1962). "Effects of knots and holes on the fatigue strength of quarter-scale timber bridge stringers." MS Thesis, University of Wisconsin.

Coger, T. (1997, November). "World's First FRP-Glulam Ocean Pier; Bar Harbor Maine." *Crossings: Newsletter of the Wood in Transportation Program* 28, 1-6.

Conway, H.M. and Liston, L.L. (Eds.). *The Weather handbook : A Summary of Climatic Conditions and Weather Phenomena for Selected Cities in the United States and around the World.* Norcross, Ga., USA: Conway Data, 1990.

Dagher, H. J., and Bragdon M. (2001). "Composites Enhance Timber Bridges." *Civil Engineering.* 71(8), A2-A10.

Dagher, H.J., and R. Lindyberg. (2003, Jan 12-16). "Development of AASHTO Specifications for FRP-Reinforced Glulam Beams." In *Proceeding of the Annual Meeting of the Transportation Research Board Compendium of Papers CD-ROM* Transportation Research Board: Washington, DC.

Dagher, H.J., and Lindyberg, R. (1999). "West Seboeis Stream FRP-Glulam Highway Bridge." *Proceedings of the 1999 International Composites Expo.* Cincinnati, OH; Session 25-D.

Dagher, H.J., Abdel-Magid, B., Lindyberg, R., Poulin, J., and Shaler, S. (1998). "Static Bending Test Results of Douglas-Fir and Western Hemlock FRP-Reinforced Glulam Beams." *AEWC Report No. 98-4*, Orono, ME: University of Maine Advanced Engineered Wood Composites Laboratory.

Dagher, H.J., Kimball, T., Shaler, S., and Abdel-Magid, B. (1996). "Effect of FRP Reinforcement on Low Grade Eastern Hemlock Glulams." In M.A. Ritter, S.R. Duwadi and P.D. H. Lee (Eds.), *Proceeding of the National Conference on Wood Transportation Structures.* (pp. 207-214) Madison. WI: US Dept of Agriculture, Forest Products Service, Forest Products Laboratory.

Davids, W.G. (2000). "Modeling Response of FRP-Reinforced Glulam Concrete Beams with Partial Composite Action." *AEWC Report No. 00-06*, Orono, ME: University of Maine Advanced Engineered Wood Composites Laboratory.

Davids, W.G. (2001). "Nonlinear Analysis of FRP-Glulam-Concrete Beams with Partial Composite Action." *Journal of Structural Engineering.* 127, 967-970.

Dickson, B.W. (1996). "Engineered Wood Products for Transportation Structures-An Overview of the Obstacles and Opportunities." In M.A. Ritter, S.R. Duwadi and P.D.H. Lee (Eds.), *Proceeding of the National Conference on Wood Transportation Structures* (pp. 490-494). Madison, WI: USDA, Forest Products Service, Forest Products Laboratory.

Elmendorf, A. (1918). "Fatigue Tests on Sitka Spruce, Douglas Fir and Southern White Oak." *U.S. Forest Products Laboratory Progress Report*, L-229.

Falk, R.H., and Colling, F. (1995). "Laminating Effects in Glued-Laminated Timber Beams." *Journal of Structural Engineering* 121, 1857-63.

Forest Products Laboratory (1999). *Wood handbook: wood as an engineering material.* Madison, WI: USDA, Forest Products Service, Forest Products Laboratory.

Frieder, S., Vistap, M, and Gilbert, H. (2003). "Carbon Shell Advanced Composite Bridge Test." UCSD – Department of Structural Engineering. Available: http://www.structures.uscd.edu/Research/CarbonShell.shtml

Galloway, T.L. (1996a). "Initial Tests of Kevlar Prestressed Timber Beams." In M.A. Ritter, S.R. Duwadi and P.D.H. Lee (Eds.), *Proceeding of the National Conference on Wood Transportation Structures* (pp. 215-224). Madison, WI: US Dept of Agriculture, Forest Products Service, Forest Products Laboratory.

Galloway, T.L. (1996b). "Performance of Kevlar Prestressed Glued Laminated Timber Beams." MS Thesis, Department of Civil Engineering, University of Wyoming, Laramie, WY.

Gamache, C. (2001). Preliminary investigation on the durability of FRP-reinforced glulam bridge girders. MS Thesis, Department of Civil and Environmental Engineering, University of Maine, Orono, ME.

Gere, J.M. and Timoshenko, S.P. (1997). Mechanics of Materials. Boston: PWS Publishing Company.

Gong, M., and Smith, I. (2000). "Failure mechanism of softwood under low-cycle fatigue load in compression parallel to grain." Washington State University. Available: http://timber.ce.wsu.edu/Resources/papers/7-6-5.pdf

Gordon Composites Inc. (2002). Material Properties for GC67-UB. Available: http://www.gordoncomposites.com.

Hansen, L.P. (1991). "Experimental Investigation of Fatigue Properties of Laminated Wood Beams." In *Proceeding of the Timber Engineering Conference* (pp. 374-382). London, England.

Hoffmeyer, P. (1993). "Non-Linear Creep by Slip Plane Formation." *Wood Science and Technology.* 27, 321-335.

Hong, Y. (2003). "Fatigue of wood-FRP interface: Experimental Characterization and Performance Limits." MS Thesis, Department of Civil and Environmental Engineering, University of Maine, Orono, ME.

Kimball, T. (1995). "Feasibility of Glulam Beams Reinforced with FRP Sheets." MS Thesis, Department of Civil and Environmental Engineering, University of Maine Orono, ME.

Leggett, J. L. (1953). "Investigation of Fatigue Strength of Large Timber Beams." Doctoral Thesis, Purdue University.

Lewis, W. C. (1960). "Design considerations for fatigue in timber structures." In *Proceedings of the Committee on Timber, No ST5.* ASCE, 86.

Lewis, W. C. (1962). "Fatigue resistance of quarter-scale bridge stringers in flexure and shear." *U.S. Forest Products Laboratory Report* No. 2236.

Lindyberg, R.F., and Dagher, H.J. (2000). "Probabilistic Nonlinear Model for Reinforced Glulam Beams." In *Proceeding of the World Conference on Timber Engineering*; Vancouver, BC, Canada.

Lindyberg, R.F. Personal Communication. May 5, 2003.

Lindyberg, R.F. Personal Communication. September 17, 2001.

Lindyberg, R.F.. (2000). "ReLAM: A Nonlinear Stochastic Model for the Analysis of Reinforced Glulam Beams in Bending." Doctoral Thesis, Department of Civil and Environmental Engineering, University of Maine, Orono, ME.

Liu, J. and Ross, R. (1996). "Energy Criterion for Fatigue Strength of Wood Structural Members." *Journal of Engineering Materials and Technology.* 118, 375-378.

Liu, J. and Simpson, W. (1996). Mathematical Relationship Between Surface Emission and Diffusion Coefficients. Drying Technology 14, 677-699.

Liu, J.Y., Zahn, J.J., and Schaffer, E.L. (1994) "Reaction Rate Model for the Fatigue Strength of Wood." *Wood and Fiber Science.* 21(1), 3-10.

Lopez-Anido, R., Michael, A.P., and Sandford, T.C. (2003) "Experimental Characterization of FRP-Composite-Wood Pile Structural Response by Bending Tests." *Marine Structures.* 16, 257–274.

Lopez-Anido, R., and Xu, H. (2002). "Structural Characterization of Hybrid Fiber-Reinforced Polymer-Glulam Panels for Bridge Decks." *Journal of Composites for Construction.* 6(3), 194-203.

Martinez, M.E. and Calil, C.J. (2002). "Statistical Design and Orthogonal Polynomial Model to Estimate the Tensile Fatigue Strength of Wooden Finger Joints." *International Journal of Fatigue.* (25) 237-243.

MDA: Marketing Development Alliance of the FRP Composite Industry. (2003). Harrison, NY. Available at: http://www.mdacomposites.org/

Meierhofer, U.A. (1995). "Fiber Reinforced Plastic Splices for Joints in Timber Structures." *Material and Structures.* 176(28), 106-107.

MSC Fatigue 2003 User's Manual. (2003). MSC Software Corporation. Santa Ana, CA.

Paepegem, W.V., and Degrieck, J. (2002). "Tensile and Compressive Damage Coupling for Fully-Reversed Bending Fatigue of Fiber-Reinforced Composites." *Fatigue and Fracture of Engineering Materials & Structures.* 25(6), 547-562.

Petersen, K. and Solberg, B. (2002). "Greenhouse Gas Emissions, Life-cycle Inventory and Cost-Efficiency of Using Laminated Wood Instead of Steel Construction. Case: Beams at Gardermoen Airport." *Environmental Science & Policy.* 5, 169-182.

Plevris, N., and Triantafillou, T. (1992). "FRP-Reinforced Wood as Structural Material." *Journal of Materials in Civil Engineering, ASCE* 4(3), 300-317.

Ritter, M.A. (1990). *Timber Bridges: Design, Construction, Inspection, and Maintenance.* United States Department of Agriculture Forest Service Washington, DC

Romani, M. and H.J. Blaß. (2001). "Design Model for FRP Reinforced Glulam Beams." In *Proceeding of the International Council for Research and Innovation in Building and Construction, Working Commission W18 – Timber Structures* (pp. 1-10). Venice, Italy.

Sanchez, O. (2002). *Performance Study of In-service FRP reinforced glulam bridge girders.* MS Thesis. Department of Civil and Environmental Engineering, University of Maine, Orono, ME.

Scurfiled, G., Silva, S.R., and Wold, M.B. (1972). "Failure of Wood Under Load Applied Parallel to Grain: A Study Using Scanning Electron Microscopy." *Micron*. 3, 160-184.

Senthilnath, P., Belarbi, A., and Myers, J. (2001). "Performance of CFRP Strengthened Reinforced Concrete (RC) Beams in the Presence of Delaminations and Lap Splices under Fatigue Loading." In *Proceeding of the International Conference in Construction* (pp. 323-328). Porto, Portugal.

Serrano, E. (1997). "Finger-joints for laminated beam. Experimental and Numerical Studies of Mechanical Behavior." *Report TVSM-3021*. Lund Institute of Technology, Division of Structural Mechanics. Lund, Sweden. Licentiate thesis.

Serrano, E., and Larsen, H.J. (1999). "Numerical Investigations of the Laminating Effect in Laminated Beams." *Journal of Structural Engineering*. 125, 740-745.

Siau, J.F. (1995). *Wood: Influence of moisture on physical properties*. Department of Wood Science and Forest Products. Virginia Polytechnic Institute and State University, Blacksburg, VA

Singh, N., Khelawan, R., and Mathur, G.N. (2001). "Effect of Stress Ratio and Frequency on Fatigue Crack Growth Rate of 2618 Aluminum Alloy Silicon Carbide Metal Matrix Composite." *Bulletin of Material Science*. 24(2), 169-171.

Tascioglu, C., Goodell, B., and Lopez, R. (2003). "Bond durability characterization of preservative treated wood and E-glass/phenolic composite interfaces." *Composite Science and Technology*. 63, 979-991.

Tascioglu, C., Goodell B., and Lopez-Anido, R. (2002). Effects of Wood Preservative Treatments on Mechanical Properties of E-glass / phenolic pultruded reinforcement for wood." In press. *Forest Products Journal* 52(11/12).

Tascioglu, C. Personal Communication. July 25, 2001.

Tingley, D.A., Gilham, P.C., and Kent, S.M. (1996). "Long Term Performance of FRP Reinforced Glulam Bridge Girders." In M. A. Ritter, S. R. Duwadi and P. D. H. Lee (Eds.) *Proceeding of the National Conference on Wood Transportation Structures* (pp. 201-206). Madison, WI: USDA, Forest Products Service, Forest Products Laboratory.

Toratti, T. (1992). Creep of timber beams in a variable environment. Doctoral Thesis, Helsinki University of Technology, 40-42.

Triantafillou, T., and Deskovic, N. (1992). "Prestressed Sheets as External Reinforcement of Wood Members." *Journal of Structural Engineering*. 118(5), 1270-1284.

Tsai, K. T. and Ansell, M. P. (1990). "The fatigue properties of wood in flexure." *Journal of Materials Science.* 22, 865-878.

Vaddadi, P., Nakamura, T., and Singh, R. (2003). Transient hygrothermal stresses in fiber reinforced composites: a heterogenous characterization approach. *Composites Part A: Applied Science and Manufacturing.* 34, 689-799.

Vick, C.B., Christiansen, A.W., and Okkonen, E.A. (1998). "Reactivity of Hydroxymethylated Resorcinol Coupling Agent as it Affects Durability if Epoxy Bonds to Douglas-Fir." *Wood and Fiber Science* 30(3), 312-322.

Vick, C.B. and Okkonen, E.A. (1997) "Structurally Durable Epoxy Bonds to Aircraft Woods." *Forest Products Journal.* 47(3), 71-77.

Youngquist, John. (1995). "Unlikely Partners? The Marriage of Wood and Non-wood Materials." *Forest Products Journal.* 45(10), 25-30.

Appendix A

DATA SHEETS FROM PERIODIC STATIC TESTS

Specimen S1

Day #	Relative Humidity	Ambient Temp (F)	Moisture Content (6 readings, 3 from each side)						Cycle Number
1	20%	71.9	6.9	7	7.2	7.3	6.9	7.5	0
2	20%	71.8	7.4	7.7	7.3	7.2	6.9	7.6	38002
3	20%	71.2	6.4	6.8	7	7	6.5	6.8	76185
4	20%	72	6.8	6.9	7.1	7	6.7	7.1	183238
5	39%	71.9	6.7	6.7	6.9	6.8	6.7	6.9	209532
6	20%	66.5	7.1	7.6	7	7.3	7.8	7.3	275964
7	21%	70.3	7.6	7.7	7.6	7.7	7.8	7.4	394422
8	20%	70.8	6.9	7	7.5	7.7	7.2	7.1	556518
9	20%	71.8	7.5	8.1	7.3	7.6	7.2	7.4	728745
10	20%	73.1	6.8	7.4	7.6	7.8	7.1	7.6	910146
11	20%	72.9	7.4	8.1	7.2	7.5	7	7.5	1061602
12	20%	70.5	7.1	7.6	7.4	6.9	8	7.1	1210750
13	25%	70.2	7.5	8	7.6	8.1	6.5	6.9	1263054
14	28%	72	7.6	8.2	7.7	8.1	6.6	7.4	1397444
15	20%	71.9	7.5	8.1	7.3	8	7.2	7.3	1567447
16	22%	69.2	7.4	7.8	7.4	7.9	7.3	6.9	1762898
17	21%	70.7	7.1	7.6	8	7.8	7.6	7.2	1929030

Specimen S2

Day #	Relative Humidity	Ambient Temp (F)	Moisture Content (6 readings, 3 from each side)						Cycle Number
1	44%	79.5	10.2	10.4	10.6	10.2	10.5	10.6	0
2	49%	75	10.3	10.2	10.5	10.7	10.4	10.4	151213
3	62%	75.9	10.4	10.6	10.4	10.7	10.2	10.7	332574
4	61%	82	10.5	10.6	10.4	10.7	10.2	10.4	602324
5	63%	84.1	10.6	10.7	10.8	10.6	10.1	10.4	789372
6	39%	83.1	10.7	10.5	10.7	10.5	10.7	10.1	961997
7	48%	78.3	11.1	10.9	10.8	10.7	10.6	11.3	1092717
8	64%	75.2	11.3	11.2	11	11.4	10.7	10.9	1266120
9	48%	76.6	11.2	11.4	10.8	11.1	11.1	10.7	1459399
10	37%	75.6	11.3	11.3	11.5	10.8	11.2	11.3	1686024
11	45%	71.1	11.4	11.2	11.4	11.3	11.3	11.5	1839133
12	72%	71.6	11.5	11.3	10.9	10.9	11.2	11.1	2000000

Specimen S3

Day #	Relative Humidity	Ambient Temp (F)	Moisture Content (6 readings, 3 from each side)						Cycle Number
1	29%	62.6	11.5	11.8	12	12.1	11.5	10.8	0
2	28%	72.1	11.2	11.7	11.9	12	11.5	11	152034
3	26%	69.8	11	10.8	11.4	11.1	11.6	11	336722
4	28%	68.7	11	10.9	11.8	11.8	11.6	11.5	491114
5	28%	68.9	11	10.2	11.7	10.3	10.4	10.5	662118
6	29%	72.1	12.5	11.8	11	11.2	11.2	10.9	837998
7	26%	70.3	12.1	9.6	10.5	10.6	9.7	11.5	1006498
8	26%	71.6	11.7	10.6	10.4	11	10.5	10.7	1164147
9	26%	70.8	11.4	10.9	11.1	10.6	10.9	11.2	1329215
10	23%	70.3	11	11	11	11	12	10	1489564
11	24%	71.1	12	12	10	10	9.9	9.7	1614001
12	24%	70.7	11	12	11	10	10	10	1760019
13	21%	71	12	11	11	10	10	9.7	2000000

Specimen S4

Day #	Relative Humidity	Ambient Temp (F)	Moisture Content (6 readings, 3 from each side)						Cycle Number
1	20%	73.7	7.3	7.4	7.4	6.7	7.5	7.5	0
2	21%	72.1	7.2	7.4	7.4	6.9	7.2	7.7	231525
3	18%	74	7.1	7.4	7.5	6.8	7.6	7.6	464500
4	18%	73.8	6.8	7.2	7	7.1	6.6	6.4	622760
5	18%	73.4	6.7	6.9	6.7	6.5	6.9	7	799099
6	20%	72.2	6.8	6.7	6.7	6.4	7.1	7	974215
7	19%	72.7	6.9	7.1	6.8	6.7	6.7	6.5	7277576
8	18%	73.6	6.7	7	6.9	6.4	7.3	7.1	1437506
9	21%	74.5	7.2	7.1	6.8	6.8	7	6.7	1609405
10	19%	72.7	6	6.1	6.3	6.2	6.2	6.4	1751864
11	19%	72.2	6.2	6.4	6.4	6.6	6	6.1	2000000

Specimen S5

Day #	Relative Humidity	Ambient Temp (F)	Moisture Content (6 readings, 3 from each side)						Cycle Number
1	23%	71.3F	6.8	7.1	6.8	7.3	7.3	6.9	0
2	26%	75.1F	7.2	6.8	7.3	7.3	7.3	7	86754
3	26%	72.5F	7	7.1	7.4	6.8	7.1	6.9	179732
4	28%	73.2F	7.2	7.4	6.8	7.3	7.3	7.1	437289
5	34%	73.1F	7.6	6.8	7.1	6.8	6.9	7	762351
6	25%	70.1F	7.3	7.4	6.8	7.2	7.2	7.1	1057684
7	24%	74.1F	7.5	6.8	7.5	7.1	7.5	7.5	1325298
8	26%	68.7F	7.6	7.1	7.2	7.2	6.8	7.5	1653275
9	26%	72.1F	7.2	7	7.4	7.1	7.4	7.6	1938257
10	25%	74.0F	7.3	6.9	7.4	7.3	8.1	7.6	2000000

Specimen S6

Day #	Relative Humidity	Ambient Temp (F)	Moisture Content (6 readings, 3 from each side)						Cycle Number
1	30%	70.9	7.1	7	7.3	6.7	6.8	7.1	0
2	28%	71.3	7.6	7.4	7.5	7.8	7.7	7.4	104010
3	31%	30.6	7.8	7.4	7.6	7.5	7.3	7.7	2876124
4	38%	73.4	7.6	7.8	7.3	7.6	7.6	7.7	469657
5	43%	74.8	7.8	8.1	7.9	7.7	7.9	7.4	609553
6	61%	75.2	7.7	7.8	8	7.9	7.7	7.8	825610
7	63%	74.7	8	8.2	8.3	8.2	8.4	8.3	987258
8	63%	73.6	8.1	8	7.8	7.7	8	8.1	1217327
9	75%	72.5	8	8.3	8.1	7.6	7.8	7.9	1422792
10	64%	78.8	8.2	8.4	8.4	8.5	8.3	8.1	1627933
11	66%	79	8.7	8.9	8.9	9.1	9.2	8.5	1824271
12	64%	80.6	8.8	8.8	8.7	8.9	9.2	9.1	2000000

Specimen S7

Day #	Relative Humidity	Ambient Temp (F)	Moisture Content (6 readings, 3 from each side)						Cycle Number
1	56%	86	9.8	9.8	9.9	9.6	10.3	10.5	0
2	56%	80.6	10	10.1	11	10.4	9.4	9.9	186466
3	40%	79.9	9.5	9.6	11	10.4	9.3	9.8	301705
4	27%	80.8	9.7	9.4	10.6	9.6	9.7	10	505988
5	40%	76	9.7	9.4	10.6	9.7	9.5	9.8	654742
6	43%	81.6	9.8	9.6	9.9	10.1	9.6	9.7	816523

Failure at 1061377

Specimen S8

Day #	Relative Humidity	Ambient Temp (F)	Moisture Content (6 readings, 3 from each side)						Cycle Number
1	29%	79.7	9.8	10.7	10.3	10.9	10.7	11.2	0
2	40%	76.1	9.8	10.4	10	10.3	10.5	11	81390
3	44%	92.3	9.9	10.5	10	10.6	10.3	11.3	156314
4	45%	78.7	9.6	10.3	10.2	10.7	10.7	11.1	236932
5	58%	79.6	10.3	10.6	10.5	10.4	10.3	11.6	337962
6	44%	80.8	10.5	10.9	10.6	10.3	10.7	11.2	413977
7	52%	78.7	10.5	10.4	10.6	10.5	10.6	10.7	496134
8	62%	77.4	10.1	10.6	10.6	10.3	10.7	11.5	613839
9	28%	80.1	9.8	11.3	10.3	10.2	10.5	11.2	792555
10	30%	79.4	9.7	10.3	10	10.1	9.8	10.3	851045
11	67%	78.3	10.5	10.4	10.2	10	10.2	10.5	1074345
12	62%	81.5	11.9	11.4	11.5	11.6	11.4	11.7	1150555
13	45%	81.7	10.3	10.9	11.6	11.2	11	11.1	1318635
14	65%	79.9	10.4	11.4	11.2	11.3	11.2	11.4	1665849
15	45%	88.4	10.3	11.2	10.5	10.3	10.6	10.4	1847200
16	25%	90.7	10.4	10.8	10.2	10.3	10.2	10.7	2000000

Specimen S9

Day #	Relative Humidity	Ambient Temp (F)	Moisture Content (6 readings, 3 from each side)						Cycle Number
1	52%	79.2	10.3	11	11.2	11.5	11.4	11.6	0
2	44%	81.3	10.2	10.8	10.7	10.6	11.1	11.4	177335
3	62%	77.2	10.6	11.4	11.7	11.8	11.1	11.5	210022
4	53%	90	11.2	11.9	11.5	12.1	12.5	12.3	360157
5	36%	76	10.8	11.6	11.4	11.7	11.7	11.6	505079

Failure at 592311

Specimen S10

Day #	Relative Humidity	Ambient Temp (F)	Moisture Content (6 readings, 3 from each side)						Cycle Number
1	42%	82.1	11.6	11.7	11.3	10.9	11.4	11.3	0
2	35%	81.2	10.5	10.8	11.2	10.3	11.2	11.1	159708
3	38%	78.3	10.7	10.6	10.4	10.2	10.7	10.6	307324
4	49%	86.2	10.3	10.6	10.8	10.4	11.2	11.4	489065
5	43%	88.1	10.6	10.8	10.7	10.3	11.1	11.2	651247
6	40%	76	10.4	10.3	10.5	10.2	10.8	10.7	824037
7	41%	77.8	10.2	10.4	10.1	10.1	10.6	10.8	1174268
8	39%	77.8	10.3	10.1	9.8	10	10.5	10.7	1359026
9	39%	78.5	10.1	10.5	10.6	9.7	9.9	10.8	1526889
10	36%	75.1	10.3	10.2	9.3	9.8	9.2	10.5	1689270
11	41%	77	10.3	10	9.7	9.6	10.4	10.6	18677945
12	56%	75.1	10.4	9.7	9.8	10.1	10.6	10.8	2000000

Specimen S11

Day #	Relative Humidity	Ambient Temp (F)	Moisture Content (6 readings, 3 from each side)						Cycle Number
1	41%	77.4	10.6	10.1	10.6	10.9	10.5	11.8	0
2	41%	83.7	10.5	10.2	10.5	10.9	10.7	11.1	99763
3	36%	79.2	10.6	9.8	10.3	10.9	10.8	11.4	269323
4	36%	75.1	9.8	10.2	9.8	10.3	10.1	10.2	446336
5	66%	74.3	9.9	10.3	9.7	10.5	10.3	9.8	696436
6	50%	75.4	10.5	10.7	10.7	10.8	11.5	10.7	866069
7	45%	84.1	10.5	10.6	10.8	10.7	11	10.5	1045720
8	52%	72.7	10.4	10.2	10.6	10.5	11.1	10.7	1210164
9	41%	83.2	9.7	9.8	10.4	10.6	10.9	11	1397210
10	49%	72.7	9.5	9.5	9.8	9.9	10	9.7	1564382
11	44%	75.8	9.4	9.6	9.7	9.9	9.8	9.9	1636926
12	41%	76.3	9.3	9.5	9.9	9.7	9.6	9.7	1876322
13	56%	75.1	9.2	9.2	9.6	9.4	9.3	9.6	2000000

Specimen S12

Day #	Relative Humidity	Ambient Temp (F)	Moisture Content (6 readings, 3 from each side)						Cycle Number
1	58%	77.4	11.2	11.4	11.4	11.2	9.6	10.8	0
2	72%	77.6	11.1	11.5	11.4	11.3	9.5	1.7	149137
3	50%	75.4	10.9	11.6	11.2	11.1	9.7	10.5	360305
4	32%	77.2	10.7	11.5	11.1	10.9	9.8	10.6	411325
5	45%	84.1	10.6	11.1	10.8	10.9	9.9	10.8	747645
6	27%	77.6	10.5	11.1	10.8	10.8	9.6	10.5	940308
7	52%	72.7	10.4	10.9	10.9	10.9	10.1	10.9	1076957
8	35%	73.6	10.3	10.8	10.8	10.7	10.3	10.8	1258785
9	46%	82.4	10.4	10.2	9.8	9.8	9.7	9.8	1450079
10	20%	78.3	10.8	11.5	11.1	10.4	10.6	9.9	1610846
11	49%	72.7	10.8	10.6	10.4	10.4	9.9	9.7	1778567
12	44%	75.8	10.5	10.7	10.5	9.9	10.1	9.8	1926014
13	51%	73.1	9.6	9.7	9.8	9.7	9.4	9.5	2000000

Specimen S13

Day #	Relative Humidity	Ambient Temp (F)	Moisture Content (6 readings, 3 from each side)						Cycle Number
1	30	72.8	8.4	8.5	8.4	7.9	8.2	8.2	0

Failure at 31487

Specimen S14

Day #	Relative Humidity	Ambient Temp (F)	Moisture Content (6 readings, 3 from each side)						Cycle Number
1	21%	72.1	9.6	9.5	9.3	9.2	8.9	9.5	0
2	21%	73.4	9.8	9.1	9.6	9.4	9.3	9.4	84405
3	20%	71.3	9.8	9.1	9.6	9.4	9.3	9.4	126798
4	20%	72.4	9.4	9.8	9.3	9.9	9.6	9.2	319021
5	40%	71.6	9.5	9.3	9.1	9.6	9.6	9.5	485020
6	41%	71.4	8.8	8.1	9.4	9.2	9.9	9.1	602035
7	45%	71.1	9.2	9.5	9.6	9	9.1	9.7	754522
8	45%	71.3	9.1	9.6	10	9.6	10	9.6	932088
9	51%	71.5	9.3	9.1	9.7	9.5	9.4	9.2	1061950
10	38%	79.7	8.7	8.3	8.7	9.1	9.8	10	1182039

Failure at 1272585

Specimen S15

Day #	Relative Humidity	Ambient Temp (F)	Moisture Content readings, 3 from each side)					(6	Cycle Number
1	44%	76.5	10.5	9	9.3	9.4	9.5	9.7	0
2	43%	71.6	9.3	8.3	9.6	9.7	9.6	8.9	152955
3	45%	70.8	9.6	9.1	8.9	10.1	9.4	9.6	205129
4	41%	71.3	9.3	9.5	8.7	9.4	9.7	9.7	281457
5	45%	71.1	10.1	10	9.2	10	8.2	9.8	310802
6	50%	71.5	9.7	9.2	9.8	9.5	8.6	8.2	394171
7	29%	84.4	9	8.8	9.7	9.7	10.3	9.7	585014
8	49%	75.4	9.3	8.7	9.7	8.6	9.8	7.9	645584
9	40%	81.7	9.2	9.2	9.5	9	9.1	9.3	784867
10	56%	80.6	10.3	10.3	10	10.1	10.2	9.1	974359

Failure at 1109229

Specimen S16

Day #	Relative Humidity	Ambient Temp (F)	Moisture Content readings, 3 from each side)					(6	Cycle Number
1	57%	81.2	9.5	9.6	9.2	9.2	9.3	9	0
2	38%	74.3	9.4	9.7	9.3	9.2	9.2	8.8	172437
3	24%	71.3	9.3	9.5	9.2	9	9.1	9.1	270878
4	38%	70.2	9.1	9.4	9.3	9.1	8.8	9	398003
5	40%	73.1	8.8	9.4	9.1	8.9	9.2	9.1	477552
6	26%	73.8	8.7	8.8	9.1	8.8	8.8	8.9	751430
7	21%	74.5	8.6	8.7	8.9	8.9	8.1	8.9	828733
8	22%	76	8.6	8.7	8.8	8.8	8.9	8.6	889890
9	24%	74	8.7	8.9	8.6	8.9	8.7	8.9	952545

Failure at 953845

Specimen S17

Day #	Relative Humidity	Ambient Temp (F)	Moisture Content readings, 3 from each side)					(6	Cycle Number
1	70%	9.6	9.7	9.9	9.8	9.7	9.7	0	70

Failure at 101647

Specimen S18

Day #	Relative Humidity	Ambient Temp (F)	Moisture Content readings, 3 from each side)					(6	Cycle Number
1	38%	70.2	9.3	9.5	9.1	9.7	9	9.2	0

Failure at 19722

Appendix B

CALCULATIONS

B.1 Calculation for Design of Test Protocol

Example followed from pages 7-26 – 7-40 of:
Ritter, M.A. (1990) *Timber Bridges: Design, Construction, Inspection, and Maintenance.* United States Department of Agriculture Forest Service Washington, DC
Units are in English System to be consistent with those given in design example.

For Unreinforced Glulam Section

Example from TImber Bridge Manual using 48 foot long glulam bridge girder:

HS-25 Loading $M_{LL} := 245ft \cdot kip$ $V_{LL} := 13.4kip$

$F_b := 1558psi$ $F_v := 190psi$ $F'_b := \left(\frac{1630}{2400}\right) \cdot F_b$ $F'_b = 1058.1psi$

24F-V4

Try 8-1/2" x 55"

$b := 8.5in$ $h := 55in$ $L := 48ft$

$w_{DL} := 269\frac{lbf}{ft} + (b \cdot h) \cdot \left(50\frac{lbf}{ft^3}\right)$ $w_{DL} = 431.33\frac{lbf}{ft}$

$M_{DL} := \frac{w_{DL} \cdot L^2}{8}$ $M_{DL} = 124.22kip \cdot ft$

$V_{DL} := w_{DL} \cdot \left(\frac{L}{2} - \frac{L}{12}\right)$ $V_{DL} = 8.63kip$

Check Shear

$f_v := \frac{3 \cdot (V_{DL} + V_{LL})}{2 \cdot b \cdot h}$ $f_v = 70.67psi$

Check Bending

$S := \frac{b \cdot h^2}{6}$ $S = 4285.42in^3$

$f_b := \frac{(M_{DL} + M_{LL})}{S}$ $f_b = 1034psi$ less than F'b=1058 psi... OK

Ratios:

$\frac{M_{LL}}{M_{DL}} = 1.97$ $\frac{V_{LL}}{V_{DL}} = 1.55$ $\frac{f_b}{F_b} = 0.66$ $\frac{f_v}{F_v} = 0.37$ $\frac{\frac{f_v}{F_v}}{\frac{f_b}{F_b}} = 0.56$

For Reinforced Glulam Section

Example from TImber Bridge Manual using 48 foot long glulam bridge girder:

HS-25 Loading $M_{LL} := 245ft \cdot kip$ $V_{LL} := 13.4kip$

$F_b := 3422psi$ $F_v := 190psi$ $F'_b := \left(\frac{1630}{2400}\right) \cdot F_b$ $F'_b = 2324.1psi$

24F-V4

Try 8-1/2" x 36"

$b := 8.5in$ $h := 36in$ $L := 48ft$

$w_{DL} := 269\frac{lbf}{ft} + (b \cdot h) \cdot \left(50\frac{lbf}{ft^3}\right)$ $w_{DL} = 375.25\frac{lbf}{ft}$

$M_{DL} := \frac{w_{DL} \cdot L^2}{8}$ $M_{DL} = 108.07kip \cdot ft$

$V_{DL} := w_{DL} \cdot \left(\frac{L}{2} - \frac{L}{12}\right)$ $V_{DL} = 7.5kip$

Check Shear

$f_v := \frac{3 \cdot (V_{DL} + V_{LL})}{2 \cdot b \cdot h}$ $f_v = 102.48psi$

Check Bending

$S := \frac{b \cdot h^2}{6}$ $S = 1836in^3$

$f_b := \frac{(M_{DL} + M_{LL})}{S}$ $f_b = 2308psi$ less than F'b=2324 psi... OK

Ratios:

$\frac{M_{LL}}{M_{DL}} = 2.27$ $\frac{V_{LL}}{V_{DL}} = 1.79$ $\frac{f_b}{F_b} = 0.67$ $\frac{f_v}{F_v} = 0.54$ $\frac{\frac{f_v}{F_v}}{\frac{f_b}{F_b}} = 0.8$

B.2 Calculations for 6700 mm Specimens – Untransformed Section

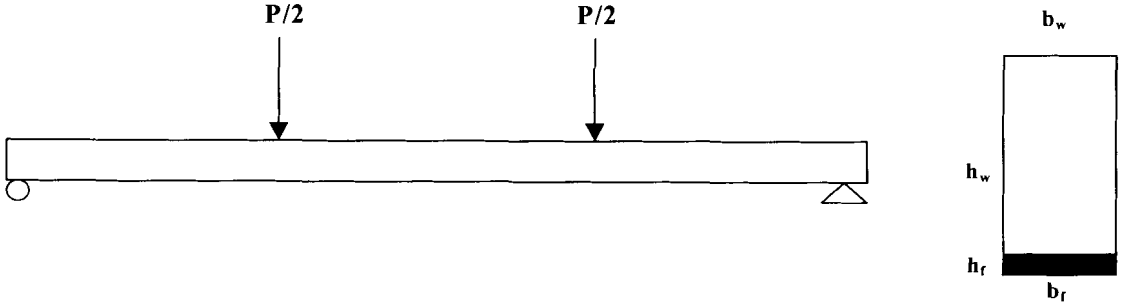

Figure B.1 Specimen with boundary conditions

APPLIED LOADS & LOAD HEAD SPACING

Cross-Sectional Properties

Wood (Glulam Beam)

$b_w := 130.175mm$ $\quad L := 6705.6mm$ $\quad span := 6400.8mm$

$h_w := 304.8mm$ $\quad area_w := b_w \cdot h_w$ $\quad area_w = 3.968 \times 10^4 mm^2$

Fiber Reinforcing (Gordon E-Glass)

$b_f := 120.65mm$

$h_f := 6.35mm$ $\quad area_f := b_f \cdot h_f$ $\quad area_f = 766.128mm^2$

Material Properties

$F_b := 23.594MPa$ (from ReLAM)

$F_v := 1.31MPa$ (from NDS)

$E_w := 1.10310^4 MPa$

$E_f := 4.12310^4 MPa$

Neutral Axis (NA) Location from Top

$$NA := \frac{h_w}{2}$$

Reinforced (Glulam beam with FRP)

moment of inertia of untranformed section

$$I := \frac{b_w \cdot h_w^3}{12} \qquad I = 3.072 \times 10^8 mm^4$$

For 1.0*F_b Fatigue Testing

Want $f_b := F_b$ $\qquad f_b = 23.594MPa$

Want $f_v := 0.8 \cdot F_v$ (based on typical Timber Bridge ratios) $\qquad f_v = 1.048MPa$

1.0*Moment capacity of Reinforced Beam

$y := NA$

$M_{max} := \frac{f_b \cdot I}{y}$ $\qquad M_{max} = 47.6kN \cdot m$

Determine Load P (P is load from actuator)

$Q := \frac{b_w \cdot (NA)^2}{2}$

$V_{max} := \frac{f_v \cdot I \cdot b_w}{Q}$ $\qquad V_{max} = 28kN$

$P := 2 \cdot V_{max}$ $\qquad P = 55.4kN$

Determine Load Head Spacing a (distance from support to loadhead)

$a := \frac{2 \cdot M_{max}}{P}$ $\qquad a = 1.7 \times 10^3 mm$

Distance from end of beam $\qquad distance := a + 152.4mm$ $\qquad distance = 1.9 \times 10^3 mm$

Typical 4-point bending a=l/3 (for comparison only)

$\frac{span}{3} = 2.134 \times 10^3 mm$

Instron Fatigue Cycling Data (LL:DL = 2:1) set to cycle from DL to LL

$LL := P$ $\qquad LL = 55.44kN$

$DL := \frac{1}{3} \cdot LL$ $\qquad DL = 18.48kN$

$Amplitude := \frac{LL + DL}{2}$ $\qquad Amplitude = 36.962kN$

For 1.3*F_b Fatigue Testing

Using same loadhead spacing as 1.0*Fb:

Want $f_{b1.3} := 1.3 \cdot F_b$ $\qquad a = 67.54in$ $\qquad f_b = 23.594MPa$

1.3*Moment capacity of Reinforced Beam

$M_{max1.3} := \frac{f_{b1.3} \cdot I}{y}$ $\qquad M_{max1.3} = 61.8kN \cdot m$

$P_{1.3} := 2 \cdot \frac{M_{max1.3}}{a}$ $\qquad P_{1.3} = 72.08kN$

Applied Shear Stress, fv

$V_{max1.3} := \frac{P_{1.3}}{2}$ $\qquad V_{max} = 27.721kN$

$f_{v1.3} := \frac{V_{max1.3} \cdot Q}{I \cdot b_w}$ $\qquad f_{v1.3} = 1.36MPa$

$\frac{f_{v1.3}}{F_v} = 104\%$

PARTIAL LENGTH REINFORCING
DEVELOPMENT LENGTH OF FRP REINFORCING

Moment Capacities of Reinforced and Unreinfrced Sections

Unreinforced (Glulam beam only)
moment of inertia of unreinforced beams

$I := \frac{b_w \cdot h_w^3}{12}$

$I = 3.072 \times 10^8 \, mm^4$

$F_{b.un} := 1558 psi$ unreinforced allowable bending stress

$c := \frac{h_w}{2}$

$M_{un} := \frac{F_{b.un} \cdot I}{c}$ $M_{un} = 21.7 kN \cdot m$

Reinforced (Glulam beam with FRP)

$F_{b.re} := 23.594 MPa$ reinforced allowable bending stress

$M_{re} := \frac{F_{b.re} \cdot I}{y}$ $M_{re} = 47.6 kN \cdot m$

Theoretical Cut-Off Point (TCOP) for FRP measured from support

$\frac{P}{2} = 27.721 kN$

$a = 1.7 \times 10^3 \, mm$

$M_{un} = \left(\frac{P}{2}\right) \cdot TCOP$

$TCOP := 2 \cdot \frac{M_{un}}{P}$ $TCOP = 781.052 mm$

$CutOff := TCOP$ $CutOff = 781.052 mm$

Total Length of FRP Reinforcing

$L_{FRP} := span - 2 \cdot CutOff$ $L_{FRP} = 4.8 \times 10^3 \, mm$

$L_{dl.theoretical} := \frac{L_{FRP}}{2}$ $L_{dl.theoretical} = 2419.3 mm$

Stress in Wood-FRP Interface at Cut-Off

$M_{cutoff} := \left(\frac{P}{2}\right) \cdot CutOff$ $M_{cutoff} = 21.7 kN \cdot m$

$y_{interface} := h_w - NA$ $y_{interface} = 152.4 mm$

$f_{cutoff} := \frac{M_{cutoff} \cdot y_{interface}}{I}$ $f_{cutoff} = 10.7 MPa$

Shear Stress in Wood-FRP Interface at Cut-Off

shear force at Cut-Off

$V := \frac{P}{2}$ $\qquad V = 27.7kN$

first moment Q of area above interface

$Q := h_w \cdot b_w \cdot \left(\frac{h_w}{2}\right)$ $\qquad Q = 6 \times 10^6 mm^3$

shear stress at interface in wood

$\tau_{wood} := \frac{V \cdot Q}{I \cdot b_w}$ $\qquad \tau_{wood} = 4.2MPa$

shear stress at interface in FRP

$\tau_{FRP} := \frac{V \cdot Q}{I \cdot b_f}$ $\qquad \tau_{FRP} = 4.5MPa$

bending stress in Wood-FRP Interface at maximum moment

$y := h_w - NA \qquad n := 3.738$

$f_{FRP} := \frac{M_{re} \cdot y}{I} \cdot n$ $\qquad f_{FRP} = 88MPa$

Tension in FRP at Maximum Moment

$A_{FRP} := b_f \cdot h_f$

$T_{FRP} := f_{FRP} \cdot A_{FRP}$ $\qquad T_{FRP} = 68kN$

Allowable Shear Stresses (shear parallel to grain)

$F_v := 1.31MPa$ based on ReLAM

$L_{dl.req} := \frac{T_{FRP}}{F_v \cdot b_f}$ $\qquad L_{dl.req} = 427.51mm$

$L_{dl} := \max(L_{dl.req}, L_{dl.theoretical})$ $\qquad L_{dl} = 2.4 \times 10^3 mm$

$\%FRPsaved := \frac{|2 \cdot L_{dl} - L|}{L}$ $\qquad \%FRPsaved = 27.8\%$

LOADS FOR FATIGUE CYCLING WITH 55k ACTUATOR

Load from Actuator

$P = 55.442kN$

Load from each Loadhead

$\frac{P}{2} = 27.721kN$

Cycle Minimum (Design Dead Load, LL:DL = 2:1)

$P_{min} := \frac{P}{3}$ $\qquad P_{min} = 18.48kN$

Cycle Maximum (Design Live Load)

$P_{max} := P$ $\qquad P_{max} = 55.442kN$

Test Amplitude (Instron measures Amplitude as 1/2 distance from trough to peak of wave)

$Amp := \frac{P_{max} - P_{min}}{2}$ $\qquad Amp = 18.481kN$

B.3 Calculations for 6700 mm Specimens – Transformed Section

APPLIED LOADS & LOAD HEAD SPACING

Cross-Sectional Properties

Wood (Glulam Beam)

$b_w := 130.175mm$ $L := 6705.6mm$ $span := 6400.8mm$

$h_w := 304.8mm$ $area_w := b_w \cdot h_w$ $area_w = 3.968 \times 10^4 mm^2$

Fiber Reinforcing (Gordon E-Glass)

$b_f := 120.65mm$

$h_f := 6.35mm$ $area_f := b_f \cdot h_f$ $area_f = 766.128mm^2$

Material Properties

$F_b := 23.594MPa$ (from ReLAM)

$F_v := 1.31MPa$ (from NDS)

$E_w := 1.10310^4 MPa$

$E_f := 4.12310^4 MPa$

$n := \frac{E_f}{E_w}$ $n = 3.738$

Transformed Section (subscript "tf" signifies "transformed fiber")

$b_{tf} := n \cdot b_f$ $b_{tf} = 451mm$

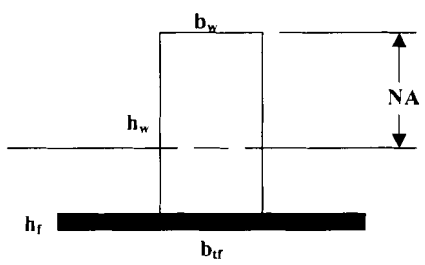

Figure B.2 Transformed section

Neutral Axis (NA) Location from Top

$$\Sigma yA := (b_w \cdot h_w) \cdot \frac{h_w}{2} + (b_{tf} \cdot h_f) \cdot \left(h_w + \frac{h_f}{2}\right)$$

$$\Sigma A := area_w + n \cdot area_f$$

$$NA := \frac{\Sigma yA}{\Sigma A}$$ $NA = 162.87mm$

Reinforced (Glulam beam with FRP)
moment of inertia of tranformed section

$$I_t := \frac{b_w \cdot h_w^3}{12} + b_w \cdot h_w \cdot \left(\frac{h_w}{2} - NA\right)^2 + \frac{n \cdot b_f \cdot h_f^3}{12} + n \cdot b_f \cdot h_f \cdot \left[\left(h_w + \frac{h_f}{2}\right) - NA\right]^2$$

$$I_t = 3.72 \times 10^8 mm^4$$

<u>For 1.0*F_b Fatigue Testing</u>

Want $f_b := F_b$ $f_b = 23.594MPa$

Want $f_v := 0.8 \cdot F_v$ (based on typical Timber Bridge ratios) $f_v = 1.048MPa$

1.0*Moment capacity of Reinforced Beam

$y := NA$

$$M_{max} := \frac{f_b \cdot I_t}{y}$$ $M_{max} = 53.9kN \cdot m$

Determine Load P (P is load from actuator)

$$Q := \frac{b_w \cdot (NA)^2}{2}$$

$$V_{max} := \frac{f_v \cdot I_t \cdot b_w}{Q}$$ $V_{max} = 29kN$

$P := 2 \cdot V_{max}$ $P = 58.8kN$

Determine Load Head Spacing a (distance from support to loadhead)

$$a := \frac{2 \cdot M_{max}}{P}$$ $a = 1833.4mm$

Distance from end of beam $distance := a + 152.4mm$ $distance = 1985.8mm$

Typical 4-point bending a=l/3 (for comparison only)

$$\frac{span}{3} = 2.134 \times 10^3 mm$$

Instron Fatigue Cycling Data (LL:DL = 2:1) set to cycle from DL to LL

$LL := P$ $LL = 58.759kN$

$DL := \frac{1}{3} \cdot LL$ $DL = 19.586kN$

$$Amplitude := \frac{LL + DL}{2}$$ $Amplitude = 39.17kN$

For 1.3*F_b Fatigue Testing

Using same loadhead spacing as 1.0*Fb:

Want $f_{b1.3} := 1.3 \cdot F_b$ $a = 1.833 \times 10^3 \text{ mm}$ $f_b = 23.594\text{MPa}$

1.3*Moment capacity of Reinforced Beam

$$M_{max1.3} := \frac{f_{b1.3} \cdot I_t}{y}$$ $M_{max1.3} = 70\text{kN} \cdot \text{m}$

$$P_{1.3} := 2 \cdot \frac{M_{max1.3}}{a}$$ $P_{1.3} = 76.39\text{kN}$

Applied Shear Stress, fv

$$V_{max1.3} := \frac{P_{1.3}}{2}$$ $V_{max} = 29.38\text{kN}$

$$f_{v1.3} := \frac{V_{max1.3} \cdot Q}{I_t \cdot b_w}$$ $f_{v1.3} = 1.36\text{MPa}$

$$\frac{f_{v1.3}}{F_v} = 104\%$$

PARTIAL LENGTH REINFORCING
DEVELOPMENT LENGTH OF FRP REINFORCING

Moment Capacities of Reinforced and Unreinfrced Sections

Unreinforced (Glulam beam only)
moment of inertia of unreinforced beams

$$I := \frac{b_w \cdot h_w^3}{12}$$

$$I = 3.072 \times 10^8 \, mm^4$$

$F_{b.un} := 10.742 MPa$ unreinforced allowable bending stress

$$c := \frac{h_w}{2}$$

$$M_{un} := \frac{F_{b.un} \cdot I}{c} \qquad M_{un} = 21.7 kN \cdot m$$

Reinforced (Glulam beam with FRP)

$F_{b.re} := 23.594 MPa$ reinforced allowable bending stress

$$M_{re} := \frac{F_{b.re} \cdot I_t}{y} \qquad M_{re} = 53.9 kN \cdot m$$

Theoretical Cut-Off Point (TCOP) for FRP measured from support

$$\frac{P}{2} = 29.38 kN$$

$$a = 1.8 \times 10^3 \, mm$$

$$M_{un} = \left(\frac{P}{2}\right) \cdot TCOP$$

$$TCOP := 2 \cdot \frac{M_{un}}{P} \qquad TCOP = 736.965 mm$$

$$CutOff := TCOP \qquad CutOff = 736.965 mm$$

Total Length of FRP Reinforcing

$$L_{FRP} := span - 2 \cdot CutOff \qquad L_{FRP} = 4.9 \times 10^3 \, mm$$

$$L_{dl.theoretical} := \frac{L_{FRP}}{2} \qquad L_{dl.theoretical} = 2463 mm$$

Stress in Wood-FRP Interface at Cut-Off

$$M_{cutoff} := \left(\frac{P}{2}\right) \cdot CutOff \qquad M_{cutoff} = 21.7 kN \cdot m$$

$$y_{interface} := h_w - NA \qquad y_{interface} = 141.93 mm$$

$$f_{cutoff} := \frac{M_{cutoff} \cdot y_{interface}}{I_t} \qquad f_{cutoff} = 8.3 MPa$$

shear force at Cut-Off

$V := \frac{P}{2}$ $\qquad V = 29.4kN$

first moment Q of area above interface

$Q := h_w \cdot b_w \cdot \left(\frac{h_w}{2}\right)$ $\qquad Q = 6 \times 10^6 mm^3$

shear stress at interface in wood

$\tau_{wood} := \frac{V \cdot Q}{I_t \cdot b_w}$ $\qquad \tau_{wood} = 3.7MPa$

shear stress at interface in FRP

$\tau_{FRP} := \frac{V \cdot Q}{I_t \cdot b_f}$ $\qquad \tau_{FRP} = 4MPa$

bending stress in Wood-FRP Interface at maximum moment

$y := h_w - NA$

$f_{FRP} := \frac{M_{re} \cdot y}{I_t} \cdot n$ $\qquad f_{FRP} = 77MPa$

Tension in FRP at Maximum Moment

$A_{FRP} := b_f \cdot h_f$

$T_{FRP} := f_{FRP} \cdot A_{FRP}$ $\qquad T_{FRP} = 59kN$

Allowable Shear Stresses (shear parallel to grain)

$F_v := 190psi$ based on Relam (Lindyberg)

$L_{dl.req} := \frac{T_{FRP}}{F_v \cdot b_f}$ $\qquad L_{dl.req} = 372.52mm$

$L_{dl} := max(L_{dl.req}, L_{dl.theoretical})$ $\qquad L_{dl} = 2.5 \times 10^3 mm$

$\%FRPsaved := \frac{|2 \cdot L_{dl} - L|}{L}$ $\qquad \%FRPsaved = 26.5\%$

LOADS FOR FATIGUE CYCLING WITH 110k ACTUATOR

Load from Actuator

$P = 58.759kN$

Load from each Loadhead

$\frac{P}{2} = 29.38kN$

Cycle Minimum (Design Dead Load, LL:DL = 2:1)

$P_{min} := \frac{P}{3}$ $\qquad P_{min} = 19.59kN$

Cycle Maximum (Design Live Load)

$P_{max} := P$ $\qquad P_{max} = 58.759kN$

Test Amplitude (Instron measures Amplitude as 1/2 distance from trough to peak of wave)

$Amp := \frac{P_{max} - P_{min}}{2}$ $\qquad Amp = 19.586kN$

BEAM LAY-UP

Total Area of Glueline	$A_{glue} := b_w \cdot L$	$A_{glue} = 9 \times 10^5 mm^2$
Clamping Pressure Desired	$F_{clamp} := 0.345MPa$	
Number of Frames	$N_{frames} := 12$	
Total Number of Rods	$N_{rods} := 2N_{frames}$	$N_{rods} = 24$
Total Clamping Load	$P_{total} := A_{glue} \cdot F_{clamp}$	$P_{total} = 301.151kN$
Load Per Rod	$P_{rod} := \frac{P_{total}}{N_{rods}}$	$P_{rod} = 13kN$
Torque Coefficient	$k := 0.2$	
Nominal Rod Diameter	$d := 19.05mm$	
Tightening Torque Per Rod	$T := k \cdot d \cdot P_{rod}$	$T = 47.81kN \cdot mm$

MOR CALCULATION
All calculations for MOR based on wood section only

$h_w = 0.305m \quad b_w = 0.13m \quad a = 1.8m$

$I := \frac{b_w \cdot h_w^3}{12} \qquad y := \frac{h_w}{2}$

Failure load for 6700 mm beams

$$Actuator_load := \begin{pmatrix} 149.6 \\ 121.4 \\ 121.6 \\ 96.0 \\ 112.3 \\ 101.4 \\ 110.3 \end{pmatrix} kN \quad \begin{pmatrix} S1 \\ S2 \\ S3 \\ S9 \\ S10 \\ S11 \\ S12 \end{pmatrix} \qquad P := \frac{Actuator_load}{2} \qquad P = \begin{pmatrix} 74.8 \\ 60.7 \\ 60.8 \\ 48 \\ 56.15 \\ 50.7 \\ 55.15 \end{pmatrix} kN$$

Maximum Applied Moment at Failure

$$M := a \cdot P \qquad M = \begin{pmatrix} 137.1 \\ 111.3 \\ 111.5 \\ 88 \\ 102.9 \\ 93 \\ 101.1 \end{pmatrix} kN \cdot m$$

Modulus of Rupture

$$MOR := \frac{M \cdot y}{I} \qquad MOR = \begin{pmatrix} 68 \\ 55.2 \\ 55.3 \\ 43.7 \\ 51.1 \\ 46.1 \\ 50.2 \end{pmatrix} MPa \quad \begin{pmatrix} S1 \\ S2 \\ S3 \\ S9 \\ S10 \\ S11 \\ S12 \end{pmatrix}$$

Percent difference in MOR - ReLAM prediction compared to test results

$$MOR_{6700} := 45.6MPa \qquad A := \begin{pmatrix} 68 \\ 55.2 \\ 55.3 \\ 43.7 \\ 51.1 \\ 46.1 \\ 50.2 \end{pmatrix} MPa \quad \begin{pmatrix} S1 \\ S2 \\ S3 \\ S9 \\ S10 \\ S11 \\ S12 \end{pmatrix} := \begin{pmatrix} 68 \\ 55.2 \\ 55.3 \\ 43.7 \\ 51.1 \\ 46.1 \\ 50.2 \end{pmatrix} MPa \qquad \frac{A - MOR_{6700}}{MOR_{6700}} = \begin{pmatrix} 49.123 \\ 21.053 \\ 21.272 \\ -4.167 \\ 12.061 \\ 1.096 \\ 10.088 \end{pmatrix} \%$$

B.4 Calculations for 11,278 mm Specimens –Transformed Section

APPLIED LOADS & LOAD HEAD SPACING

Cross-Sectional Properties

Wood (Glulam Beam)

$b_w := 130.175mm$ $L := 11277.6mm$ $span := 10972.8mm$

$h_w := 533.4mm$ $area_w := b_w \cdot h_w$ $area_w = 6.944 \times 10^4 mm^2$

Fiber Reinforcing (Gordon E-Glass)

$b_f := 130.175mm$

$h_f := 11.43mm$ $area_f := b_f \cdot h_f$ $area_f = 1.488 \times 10^3 mm^2$

Material Properties

$F_b := 24.849MPa$ (from ReLAMt)

$F_v := 1.31MPa$ (from ReLAM)

$E_w := 1.10310^4 MPa$

$E_f := 4.123 \times 10^4 MPa$

$n := \frac{E_f}{E_w}$ $n = 3.738$

Transformed Section (subscript "tf" signifies "transformed fiber")

$b_{tf} := n \cdot b_f$ $b_{tf} = 486.6mm$

Neutral Axis (NA) Location from Top

$$\Sigma yA := (b_w \cdot h_w) \cdot \frac{h_w}{2} + (b_{tf} \cdot h_f) \cdot \left(h_w + \frac{h_f}{2}\right)$$

$\Sigma A := area_w + n \cdot area_f$

$NA := \frac{\Sigma yA}{\Sigma A}$ $NA = 286.9mm$

Reinforced (Glulam beam with FRP)

moment of inertia of tranformed section

$$I_t := \frac{b_w \cdot h_w^3}{12} + b_w \cdot h_w \cdot \left(\frac{h_w}{2} - NA\right)^2 + \frac{n \cdot b_f \cdot h_f^3}{12} + n \cdot b_f \cdot h_f \cdot \left[\left(h_w + \frac{h_f}{2}\right) - NA\right]^2$$

$I_t = 2.03 \times 10^9 mm^4$

For 1.0*F_b Fatigue Testing

Want $f_b := F_b$ $f_b = 24.849MPa$

Want $f_v := 0.8 \cdot F_v$ (based on typical Timber Bridge ratios) $f_v = 1.048MPa$

1.0*Moment capacity of Reinforced Beam

$y := NA$

$$M_{max} := \frac{f_b \cdot I_t}{y}$$ $M_{max} = 175.7kN \cdot m$

Determine Load P (P is load from actuator)

$$Q := \frac{b_w \cdot (NA)^2}{2}$$

$$V_{max} := \frac{f_v \cdot I_t \cdot b_w}{Q}$$ $V_{max} = 52kN$

$P := 2 \cdot V_{max}$ $P = 103.3kN$

Determine Load Head Spacing a (distance from support to loadhead)

$$a := \frac{2 \cdot M_{max}}{P}$$ $a = 3401.4mm$

Distance from end of beam $distance := a + 152.4mm$ $distance = 3553.8mm$

For 1.3*F_b Fatigue Testing

Using same loadhead spacing as 1.0*Fb:

Want $f_{b1.3} := 1.3 \cdot F_b$ $a = 3.401 \times 10^3 mm$ $f_b = 24.849MPa$

1.3*Moment capacity of Reinforced Beam

$$M_{max1.3} := \frac{f_{b1.3} \cdot I_t}{y}$$ $M_{max1.3} = 228.4kN \cdot m$

$$P_{1.3} := 2 \cdot \frac{M_{max1.3}}{a}$$ $P_{1.3} = 134.3kN$

Applied Shear Stress, fv

$$V_{max1.3} := \frac{P_{1.3}}{2}$$ $V_{max} = 51.653kN$

$$f_{v1.3} := \frac{V_{max1.3} \cdot Q}{I_t \cdot b_w}$$ $f_{v1.3} = 1.36MPa$

$$\frac{f_{v1.3}}{F_v} = 104\%$$

LOADS FOR FATIGUE CYCLING WITH 110k ACTUATOR

Load from Actuator

$P = 103.305kN$

Load from each Loadhead

$\frac{P}{2} = 51.653kN$

Cycle Minimum (Design Dead Load, LL:DL = 2:1)

$P_{min} := \frac{P}{3}$ $\qquad P_{min} = 34.44kN$

Cycle Maximum (Design Live Load)

$P_{max} := P$ $\qquad P_{max} = 103.305kN$

Test Amplitude (Instron measures Amplitude as 1/2 distance from trough to peak of wave)

$Amp := \frac{P_{max} - P_{min}}{2}$ $\qquad Amp = 34.435kN$

MOR CALCULATION
All calculations for MOR based on wood section only

$h_W = 21\,in \qquad b_W = 5.125in \qquad a = 133.9in$

$$I := \frac{b_W \cdot h_W^3}{12} \qquad y := \frac{h_W}{2}$$

Failure load for 6700 mm beams

$$Actuator_load := \begin{pmatrix} 199.3 \\ 169.2 \\ 176.1 \end{pmatrix} kN \quad \begin{pmatrix} S4 \\ S5 \\ S6 \end{pmatrix} \qquad P := \frac{Actuator_load}{2} \qquad P = \begin{pmatrix} 99.7 \\ 84.6 \\ 88 \end{pmatrix} kN$$

Maximum Applied Moment at Failure

$$M := a \cdot P \qquad M = \begin{pmatrix} 338.9 \\ 287.8 \\ 299.5 \end{pmatrix} kN \cdot m$$

Modulus of Rupture

$$MOR := \frac{M \cdot y}{I} \qquad MOR = \begin{pmatrix} 54.9 \\ 46.6 \\ 48.5 \end{pmatrix} MPa \quad \begin{pmatrix} S4 \\ S5 \\ S6 \end{pmatrix}$$

Percent difference in MOR - ReLAM prediction compared to test results

$$MOR_{11278} := 44.2MPa \qquad B := \begin{pmatrix} 54.9 \\ 46.6 \\ 48.5 \end{pmatrix} MPa \quad \begin{pmatrix} S4 \\ S5 \\ S6 \end{pmatrix} := \begin{pmatrix} 54.9 \\ 46.6 \\ 48.5 \end{pmatrix} MPa \qquad \frac{B - MOR_{11278}}{MOR_{11278}} = \begin{pmatrix} 24.208 \\ 5.43 \\ 9.729 \end{pmatrix} \%$$

B.5 Hygrothermal Study Calculations

EQUILIBRIUM MOISTURE CONTENT CALCULATIONS

**Equation taken from FPL Wood Handbook

INPUT
Relative Humidity (%)

$RH := 93\%$

Temperature (Degrees F)

$T := 100$

COEFFICIENTS

$W := 330 + 0.452 \cdot T + 0.00415 T^2$

$K := 0.791 + 0.000463 T - 0.000000844 T^2$

$K_1 := 6.34 + 0.000775 T - 0.0000935 T^2$

$K_2 := 1.09 + 0.0284 T - 0.0000904 T^2$

OUTPUT
Equilibrium Moisture Content

$$EMC := \frac{1800}{W} \cdot \left[\frac{K \cdot RH}{(1 - K \cdot RH)} + \frac{\left(K_1 \cdot K \cdot RH + 2K_1 \cdot K_2 \cdot K^2 \cdot RH^2\right)}{\left(1 + K_1 \cdot K \cdot RH + K_1 \cdot K_2 \cdot K^2 \cdot RH^2\right)} \right]$$

$EMC = 21.39$

DIFFUSION COEFFICIENT

D is linear for 5% to 15% MC - - assume 10% initial MC

$C := 10$

$D := 0.01607 \cdot (\exp(0.0228 C))$

$D = 0.02$ in^2/day

$$0.02 \frac{in^2}{day} = 12.9032 \frac{mm^2}{day}$$

HYGROTHERMAL CUMULATIVE STRESS HISTORY CALCULATIONS

Method 1

Stress History based on peeling stress (tension in the y-direction)

$$D\sigma yy = n \cdot \frac{\int \left|\sigma yy_{max} - \sigma yy_{min}\right| da}{a}$$

$D\sigma yy_{kiln} := 310.82$

$D\sigma yy_{real_world} := 44.58$

Number of cycles

$n_{real_world} := 50$

$$n_{kiln} := \frac{n_{real_world} \cdot D\sigma yy_{real_world}}{D\sigma yy_{kiln}} \qquad n_{kiln} = 7.171$$

Total time in kiln

$T_{kiln} := n_{kiln} \cdot 60hr \cdot 2 \qquad T_{kiln} = 35.857day$

Method 2

Stress History based on shear stress in radial-tangential plane

$$D\tau xy = n \cdot \frac{\int \left|\tau xy_{max} - \tau xy_{min}\right| da}{a}$$

$D\tau xy_{kiln} := 373.83$

$D\tau xy_{real_world} := 105.62$

Number of cycles

$n_{real_world} := 50$

$$n_{kiln} := \frac{n_{real_world} \cdot D\tau xy_{real_world}}{D\tau xy_{kiln}} \qquad n_{kiln} = 14.127$$

Total time in kiln

$T_{kiln} := n_{kiln} \cdot 60hr \cdot 2 \qquad T_{kiln} = 70.634day$

Method 3

Stress History based on ratios of contributions of peeling and shear stresses

$$R_1 = \frac{\dfrac{\int \left|\sigma yy_{max}\right| da}{a}}{F_{Tperp}} \qquad R_2 = \frac{\dfrac{\int \left|\tau xy_{max}\right| da}{a}}{F_{RS}}$$

$$r_1 = \frac{R_1}{R_1 + R_2} \qquad r_2 = 1 - r_1$$

$$\text{Damage} = n \cdot \left(r_1 \cdot \frac{\int \left|\sigma yy_{max} - \sigma yy_{min}\right| da}{a} + r_2 \cdot \frac{\int \left|\tau xy_{max} - \tau xy_{min}\right| da}{a} \right)$$

$F_{Tperp} := 2.3 \times 10^6 \cdot Pa$ $\qquad$ $F_{RS} := 3.261 \times 10^5 \cdot Pa$

$R_{1_real_world_max} := \dfrac{28.929}{F_{Tperp}}$ $\qquad$ $R_{2_real_world_max} := \dfrac{2.989}{F_{RS}}$

$R_{1_real_world_min} := \dfrac{23.099}{F_{Tperp}}$ $\qquad$ $R_{2_real_world_min} := \dfrac{2.742}{F_{RS}}$

$R_1 := \max\left(\begin{vmatrix} R_{1_real_world_max} \\ R_{1_real_world_min} \end{vmatrix} \right)$ $\qquad$ $R_2 := \max\left(\begin{vmatrix} R_{2_real_world_max} \\ R_{2_real_world_min} \end{vmatrix} \right)$

$r_1 := \dfrac{R_1}{R_1 + R_2}$ $\qquad$ $r_2 := 1 - r_1$

$D_{real_world} := n_{real_world} \cdot \left(r_1 \cdot D\sigma yy_{real_world} + r_2 \cdot D\tau xy_{real_world} \right)$

$D_{real_world} = 3.62 \times 10^3$

Want to reproduce real-world damage in kiln therefore:

$D_{kiln} := D_{real_world}$

$n_{kiln} := \dfrac{D_{kiln}}{\left(r_1 \cdot D\sigma yy_{kiln} + r_2 \cdot D\tau xy_{kiln} \right)}$ $\qquad$ $n_{kiln} = 10.661$

Total time in kiln

$T_{kiln} := n_{kiln} \cdot 60hr \cdot 2$ $\qquad$ $T_{kiln} = 53.306day$

Appendix C

MATLAB CODE FOR 1D MOISTURE DIFFUSION MODEL

```
function moisture = time_stepper_1D(width, x_div, time, num_time_steps,
D, IC, BC);

% This function calculates the variation in moisture content in 1D with
time assuming
%       Fickian diffusion
%
% "width" is the beam width
% "x_div" is the number of divisions across the beam width
% "time" is the total simulation time
% "num_time_steps" is the number of divisions of time
% "D" is the diffusion coefficient
% "IC" is a row vector with the initial MC at each point across the
section
% "BC" is a nx2 array of boundary conditions, with the first column
containing
%       discrete times from 0 to time and the second column containing
corresponding
%       MC values
%
% "result" is an array with x_div+1 columns and num_time_steps+1 rows.
Each row contains
%       MC at every x location in the cross-section, and each column
corresponds to a
%       discrete solution time from "0" to "time".
%
% All units MUST be consistent

tic;
pts_x = x_div + 1;
del_x = width/x_div;
del_t = time/num_time_steps;

moisture(1,:) = IC;

% loop over time
for (i = 2:num_time_steps+1)
   % interpolate boundary value
   current_bc = interp1(BC(:,1), BC(:,2), (i-1)*del_t);
   % generate RHS vector
   F = generate_F_1D(moisture(i-1,:), del_x, del_t, D, pts_x,
current_bc);
   % generate coefficient matrix with current mc
   K = generate_K_1D(del_x, del_t, D, pts_x);
   moisture(i,:) = (K\F)';
   i;
end

%Save moisture data to separate text file
%save  file.txt -ascii moisture
```

```
%Plot Moisture Profile in cross section of beam at last time step

figure(1);
%clf
hold on
x=[0:del_x:width];
plot(x,moisture(num_time_steps-1,:))%,'--');
title('Moisture Profile')
xlabel('Cross Section Width (inches)')
ylabel('Moisture Content (%)')
```

```
function F = generate_F_1D(mc, del_x, del_t, D, pts_x, bc)

r = D*del_t/(2*del_x^2);
for (i = 2:pts_x-1)
   F(i,1) = r*mc(i-1) + (1-2*r)*mc(i) + r*mc(i+1);
end

% now, boundaries
F(1,1) = bc;
F(pts_x,1) = bc;
```

```
function K = generate_K_1D(del_x, del_t, D, pts_x)

% set K to be sparse
K = sparse(pts_x, pts_x);
K(1,1) = 1;
K(pts_x, pts_x) = 1;

r = D*del_t/(2*del_x^2);

% loop by rows
for (i = 2:pts_x-1)
   K(i,i-1) = -r;
   K(i,i) = 1 + 2*r;
   K(i,i+1) = -r;
end
```

BIOGRAPHY OF THE AUTHOR

Matthew Richie was born in Columbus, OH on February 27, 1979. He moved to Bangor, ME at the age of three, where he graduated from Bangor High School in 1997. He attended the University of Maine and graduated in 2001 with a Bachelor's degree in Civil and Environmental Engineering. He continued his studies at the University of Maine in the graduate program in Civil Engineering. Matthew is a candidate for the Master of Science degree in Civil Engineering from The University of Maine in December, 2003.